Sedimentological and petrophysical analysis of the Monte Sant'Angelo Megabreccias (Cenomanian), Gargano, Southern Italy

BY

PER OLAV EIDE SVENDSEN

DEPARTMENT OF EARTH SCIENCE
UNIVERSITY OF BERGEN
2008

SUBMITTED TO THE DEPARTMENT OF EARTH SCIENCE, UNIVERSITY OF BERGEN, IN PARTIAL FULFILMENT OF THE REQUIREMENTS TO OBTAIN THE DEGREE OF MASTER OF SCIENCE IN PETROLEUM GEOLOGY/SEDIMENTOLOGY

ABSTRACT

The Monte Sant'Angelo Megabreccias (Cenomanian) is one of three distinct and impressive Cretaceous megabreccias exposed on the flank of the Apulian platform, Gargano Promontory, southern Italy. This thesis describes and interprets stratigraphic and petrophysical data collected from two successions on the northern and southern Gargano peninsula, respectively.

The northern succession displays a prograding (outcrop scale) package of clast-supported and matrix-supported megabreccias which grade upwards into proximal calciturbidites. The southern succession displays an aggrading (outcrop scale) package of stacked, matrix-supported megabreccias. Sedimentological mapping led to the recognition of subfacies which suggest that marginal platform areas were source of these allochthonous debrites. Sediments were lithified prior to erosion and re-sedimentation. Data support previous speculations on synsedimentary tectonics as a controlling factor for the repeated collapse of these marginal areas. Changes in accommodation space controlled the depositional patterns.

One hundred and seventeen plug samples with corresponding thin-sections, permeability- and porosity measurements are classified according to three porosity classification systems. All three systems fail to produce adequate correlations of permeability and porosity for their respective groupings. Poroperm distributions also form the basis for petrophysical interpretations in terms of stratigraphic impact, and correlations between poroperm signatures and stratigraphic properties of the Monte Sant'Angelo Megabreccias are discussed.

Stratigraphic and petrophysical analysis supports the subdivision of the mapped megabreccias into 4 distinct flow-units, which display important differences in terms of depositional pattern, internal fabric and petrophysical properties. Important differences are also mapped in the comparison of the northern and southern succession. These differences are underpinned by statistical analysis of petrophysical data, and coincide with the stratigraphic data. The diagenetic history and its impact on reservoir properties is described and discussed.

ACKNOWLEDGEMENTS

I express my sincere gratitude to my main supervisor, Prof. Michael R. Talbot (Department of Earth Science, UiB), for valuable guidance and advices throughout the period of this research. Co-supervisor Dr. Gunnar Sælen (SB) (IRIS) provided constructive criticism, valuable encouragement, extensive guiding and valuable advices. He is especially recognized for the assistance on the statistical analysis. My sincere gratitude is also expressed to co-supervisor Dr. Luigi Spalluto (University of Bari) for the sharing of some of his encyclopaedic knowledge on carbonate sedimentology, and for the constructive criticism and suggestions that significantly improved this thesis.

Ivar Grunnaleite (IRIS) and Nils Bo Jensen (IRIS) are recognized for their valuable assistance and support.

Atle Sande has carried out the work for his master thesis parallel to the present study and in the same field area, and is thanked for the many useful discussions through the period of this study as well as through the years at the Department of Earth Science, University of Bergen.

Prof. Arne Graue and PhD. Martin Fernø (Reservoir Physics Group, Department of Physics and Technology, University of Bergen) made available for me their laboratory facilities, and are also thanked for the valuable help and support they provided during in-house measuring of petrophysical properties.

Nino Osso (Studi & Ricerche Geologiche, Italy) is recognized for his valuable assistance during field work, which we would not have managed without.

Henrik Horsås (Roxar) is thanked for his support on the IRAP RMS™ software.

The owners and workers at the Vico del Gargano quarry are acknowledged for generously allowing us to enter their premises.

I would especially like to thank my good friends at 'lunsjrommet', UiB, for the useful (and the not so useful) discussions, the advices and suggestions, the early mornings, the late nights and the long lunches. I look forward to seeing you again on various occasions in the future as we all enter the same industry.

Finally, Tonje Folkvang is thanked for the personal support and patience.

Bergen, June 1st 2008

Per Olav Eide Svendsen

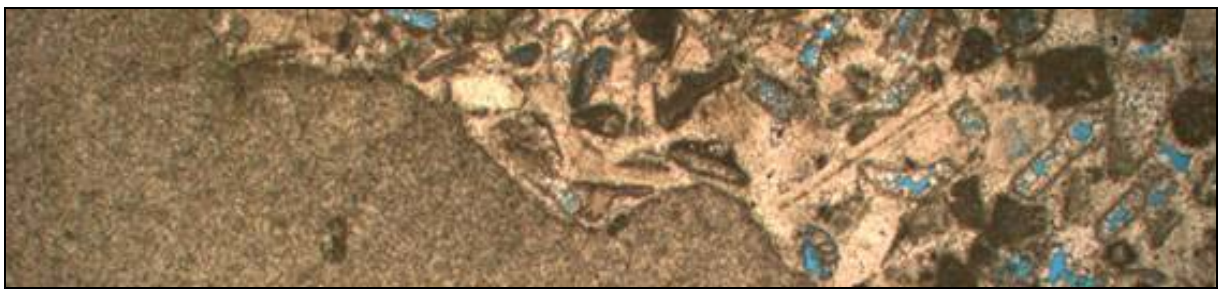

CONTENTS

1 Introduction 1
2 Geological Framework 3
3 Data 11
4 Stratigraphic analysis 47
5 Petrophysical analysis 57
6 Implications for reservoir characterization 81
7 Summary and conclusion 87
8 References cited 93

Appendix 1 – Methods
Appendix 2 – In-house measurements
Appendix 3 – Limitations and suggestions for future contributions

1 INTRODUCTION

This study presents a stratigraphic and petrophysical investigation of the Monte Sant'Angelo Megabreccias (Cenomanian), exposed on the slope of the Cretaceous Apulian carbonate platform, on the Gargano Promontory, southern Italy. The study is based on field observations and the petrophysical and stratigraphic analysis of representative samples.

This thesis is submitted as part of the Petromaks project "Carbonate Reservoir Geomodels", in co-operation with the International Research Institute of Stavanger (IRIS) and funded by NFR, ConocoPhillips Norway, StatoilHydro and DNO. Supervisors have been Professor Michael R. Talbot (University of Bergen), Dr. Gunnar Sælen (IRIS) and Dr. Luigi Spalluto (University of Bari).

Figure 1.1 – Italy

Arrow: Gargano peninsula.

PURPOSE AND GOALS

The goal of this thesis is to describe and interpret the collected petrophysical and stratigraphic data with special emphasis on the relations between permeability and porosity. The study further aims to address methods for measuring and estimating porosity and permeability. The integration of petrophysics and stratigraphy, and the combination of elements of sedimentology and petroleum engineering, seek to add to our understanding of poroperm signatures in carbonate slope deposits.

METHODS

Two successions were studied and a total of 117 plug samples (mini-drill cores) were collected from two localities on the Gargano Peninsula, Italy. Among these, 52 were collected from an 11x5 m grid of samples while the remaining 65 samples were representative for selected fabrics, established stratigraphic units and lithologies. Thin-sections were obtained for the samples along with permeability and porosity measurements for 107 and 113 samples, respectively. Effectively, poroperm measurements were available for a total of 107 samples.

Porosity and permeability of 28 samples were measured in-house, while 115 were measured externally by Reslab AS. Among these, 26 samples were measured both in-house and externally.

Standard laboratory methods were used. In-house measurements were measured using brine, while external measurements were performed using gas. Porosity was estimated from epoxy-stained thin-sections using image-analysis methods. Samples and corresponding poroperm datapoints were classified according to the systems developed by Choquette & Pray (1970), Lucia (1983, 1995, 1999, 2007) and Lønøy (2006).

A 'Nikon Alpaphot-2 YS2' polarization microscope was used for studies of fossil content, mineralogy, textural composition and diagenetic relations and a 'Spot RT3' digital camera was used to produce digital images of thin-sections.

A digital topographic model of the Vico del Gargano quarry was developed using Irap RMS™ based on portable GPS measurements in the field.

Image enhancement methods were developed and applied on high-resolution images of the Malpasso Valley outcrop.

Snedecor's F-test (*e.g.* Davies, 2002) and Student's t-test (*e.g.* Davies, 2002) was applied on the normally distributed porosity (φ) and permeability (ln k/log k) datasets.

Cathodoluminescence (i.e. Richter *et.al.*, 2003) were performed on selected thin-sections. Staining of thin-sections using Alizarinrot S and Kaliumhexa-cyanoferrat (III) (Dickson, 1966; Lindholm & Finkleman, 1972; James & Choquette, 1990) were subsequently performed with only minor results.

For extended description of selected methods, see appendix 1.

2 GEOLOGICAL FRAMEWORK

The Gargano Promontory belongs to the northern sector of the Apulian foreland, which forms a broad, low-elevation region east of the Apennines (fig 2.1). An approximately 6 km thick accumulation of shallow-water, Mesozoic carbonates (Apulian Platform) (*e.g.* Ciaranfi *et.al.,* 1988; Ricchetti *et.al.*, 1988; Schlüter, 2008) now constitute the bulk of the Apulian foreland. The lowermost ~ 1 km of this succession is made up of Triassic anhydrite-dolomite deposits (Butler *et.al.*, 2004) and a few wells have found fluvial-deltaic terrigenous facies of Permo-Triassic age (Ricchetti *et.al.*, 1988; Bosellini *et.al.*, 1993; Butler *et.al.*, 2004; Di Bucci *et.al.*, 2006). Based on magnetic and gravimetric data, an igneous/metamorphic Paleozoic basement is hypothesized (*i.e.* Mostardini & Merlini, 1986; Chiappini *et.al.*, 2000; Tiberti *et.al.*, 2005; Di Bucci *et.al.*, 2006).

The area primarily shows extensional deformation and NW-SE striking normal faults divides the region into a series of fault blocks (Funiciello *et.al.*, 1991; Marsella *et.al.*, 1995, Brankman & Aydin, 2004). The grade of deformation is, however, very little compared to the interior of the Apennine chain (fig 2.1). The 1000 km^2 region is uplifted some 900 meters above the adjacent foreland, related to contractional step-over between two sinistral, E-W-trending faults, among which the Mattinata fault is the most prominent (*e.g.* Tondi *et.al.*,

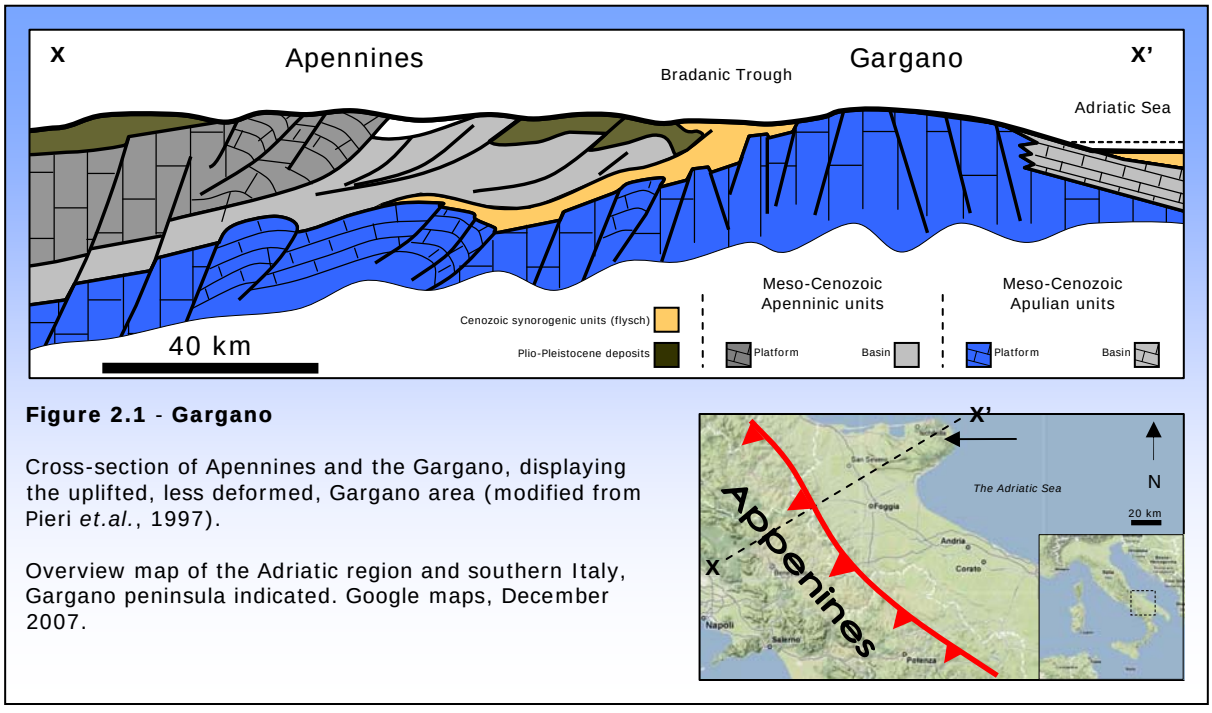

Figure 2.1 - **Gargano**

Cross-section of Apennines and the Gargano, displaying the uplifted, less deformed, Gargano area (modified from Pieri *et.al.*, 1997).

Overview map of the Adriatic region and southern Italy, Gargano peninsula indicated. Google maps, December 2007.

2005; Billi *et.al.* 2007). The Apennine Thrust belt initiated during the latest Cretaceous to Pleistocene (*e.g.* Dewey *et.al.,* 1989; Boccaletti *et.al.*, 1990; Monaco *et.al.*, 1998; Ghisetti & Vezzani, 1999; Menardi Noguera & Rea, 2000; Patacca & Scandone, 2001) and emplaced a series of thick Mesozoic and early Cenozoic carbonate platform (*Apenninic platform* units) and deep-water basinal units onto the western margin of the Apulian platform (Brankman & Aydin, 2004) during Tertiary times (fig 2.1). The Cretaceous platform-to-basin transition in the Gargano has long been a topic of contrasting interpretations (*e.g.* Sinni & Masse, 1987; Borgomano & Philip, 1987; Graziano, 1992, 1994, 1999, 2000, 2001; Bosellini *et.al.* 1993, 1994, 1999; Sinni & Borgomano 1994; Morsilli & Bosellini 1997; Borgomano, 2000) in terms of age assignments, correlation patterns, facies analysis and genetic interpretation.

Authors have stated that the Apulian Platform was affected by syn-sedimentary tectonics during the Early Cretaceous, that down-faulted the platform margin and produced thick toe-of-slope megabreccia intervals (*e.g.* Masse & Borgomano, 1987; Graziano 1994, 2000, 2001). These same deposits are considered by Bosellini *et.al.* (1993, 1994, 1999) and Bosellini & Neri (1993) to be Albian-

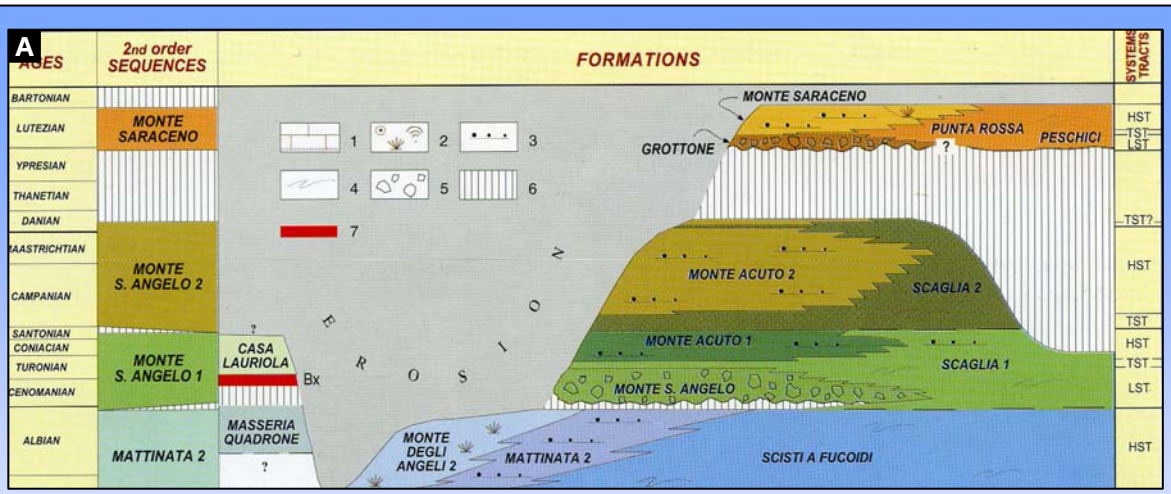

Figure 2.2 – Bosellini *et.al.* (2000)

A) Upper Cretaceous stratigraphy of Gargano, modified from Bosellini *et.al.*, 2000. Note the occurrence of one single Cenomanian megabreccia level labelled "Monte S. Angelo".

B) Cretaceous platform margin scallops on the Gargano Promontory. Localities in the present study is indicated by red dots (from Bosellini *et.al.*, 2000).

Cenomanian in age and these authors physically correlate them to other Cenomanian megabreccias exposed elsewhere in the Gargano area. The resulting huge lithosome, termed the *Monte S. Angelo Megabreccia* (figure 2.2A) is viewed by these latter authors as the product of repeated gravity collapses of the scalloped platform margin during a late Albian-Cenomanian low-stand that has been linked to the bauxitiferous unconformity of the Apulia Platform (*e.g.* Bosellini *et.al.,* 1993, 1994, 1999).

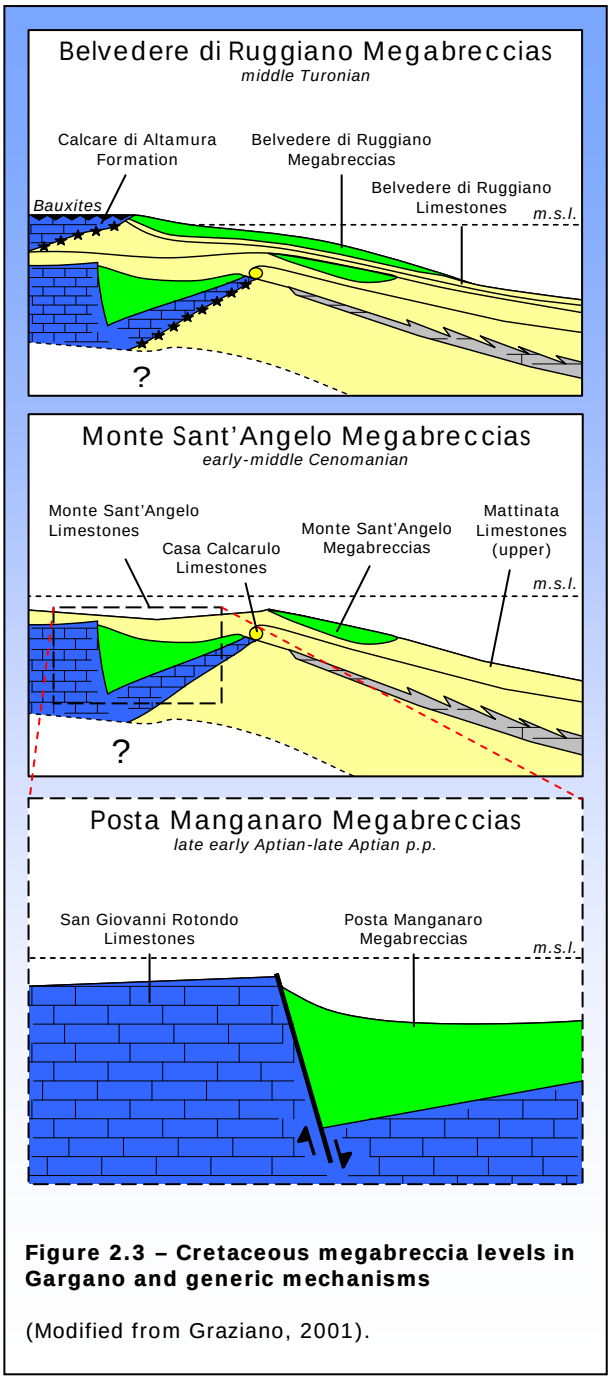

Figure 2.3 – Cretaceous megabreccia levels in Gargano and generic mechanisms

(Modified from Graziano, 2001).

Bosellini & Morsilli (1994) reported the identification of two scallop features on the Cretaceous Apulian margin, interpreted as margin collapses during a Cenomanian low-stand of the relative sea-level (figure 2.2B) and in part occupied by megabreccias and by a thick Miocene succession (Bosellini, 1999).

The reported occurrence of one single and unique megabreccia unit has been questioned by Graziano (1999, 2000) who states that the huge single megabreccia body (Monte S. Angelo Megabreccia, *sensu* Bosellini *et.al.* (1993, 1994, 1999) is actually composed of three distinct megabreccias that were deposited during the Aptian-Albian (Posta *Manganaro Megabreccias*), Cenomanian (*Monte Sant'Angelo Megabreccias, sensu stricto*) and Turonian (*Belvedere di Ruggiano Megabreccias*). These megabreccia levels were deposited, respectively, during distinct episodes of drowning, progradation and continental exposures of the Apulia platform (Graziano, 2001) (fig 2.4). The megabreccia levels sharply overlie tectonically enhanced

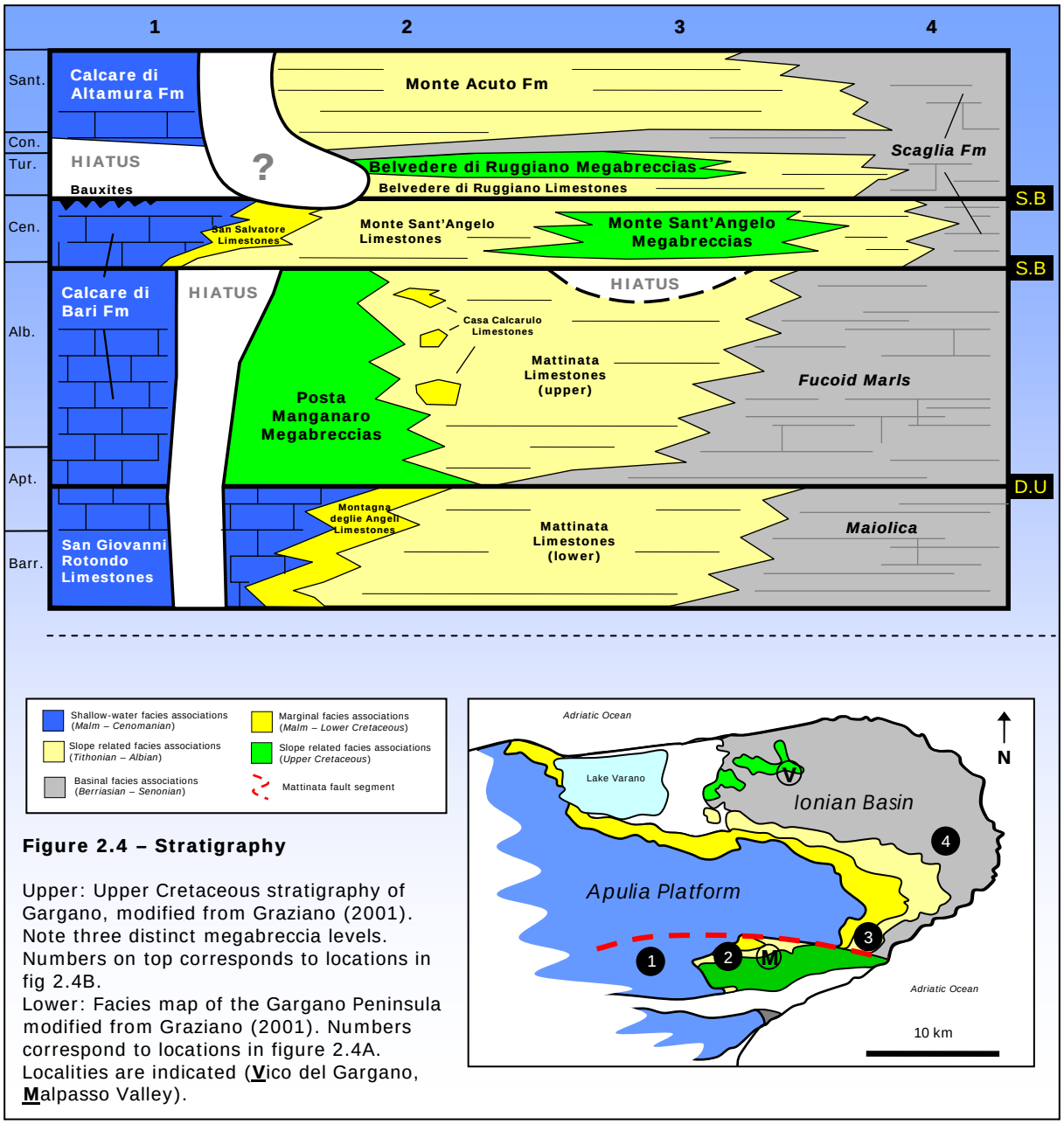

Figure 2.4 – Stratigraphy

Upper: Upper Cretaceous stratigraphy of Gargano, modified from Graziano (2001). Note three distinct megabreccia levels. Numbers on top corresponds to locations in fig 2.4B.
Lower: Facies map of the Gargano Peninsula modified from Graziano (2001). Numbers correspond to locations in figure 2.4A. Localities are indicated (**V**ico del Gargano, **M**alpasso Valley).

unconformities of late early Aptian, late Albian and late Cenomanian ages (Graziano 2001) connected to a bulge-related deformation induced by the distant collision-tectonics at the eastern margin of the Adriatic plate (Graziano, 1992, 1994, 2001) and eustatic sea-level changes played only a minor role in controlling their formation. The scope of the present study is the megabreccias pertaining to the Monte Sant'Angelo Megabreccias (*sensu* Graziano, 2001) (figs 2.3 and 2.4).

Carbonate megabreccias formed by major platform margin gravitational instability events were first identified as such in the geological record around fifty years ago (*e.g.* Rigby, 1958) but have commonly been misinterpreted as patch

reefs or in-situ bioherms (*e.g.* Pray & Stehli, 1962; Cook *et.al.*, 1972; Conaghan *et.al.*, 1976; Read & Pfeil, 1983; Spence & Tucker, 1997). The term *megabreccia* (Cook *et.al.*, 1972; Mountjoy *et.al.*, 1972; Wright & Burchette, 1996; Spence & Tucker, 1997) has been most widely adopted among many other proposed and used terms for such deposits. Carbonate megabreccias are found on many platform margins (*i.e.* the Mid-Cretaceous Pyrenean Basin (Spain) (Drzewiecki & Simó, 2002), the mid-Cretaceous Gorbea Platform (Spain) (Garcia-Mondéjar, 1990; Garcia-Mondéjar & Fernández-Mendiola, 1993; Fernández-Mendiola, *et.al.,* 1993, Rosales *et.al.,* 1994), the Late Jurassic Lusitanian Basin (Portugal) (Ellis *et.al.,* 1990), the Upper Cretaceous Maiella Platform (Italy) (Mutti *et.al.,* 1996) along with numerous others spanning from the Late Permian to recent platforms of Bahamas and the Nicaraguan Rise (for extensive lists, see Drzewiecki & Simó, 2002, table 1; Spence & Tucker, 1997, table 1).

The Monte Sant'Angelo Megabreccias are situated within the Monte Sant'Angelo Limestones Formation (fig 2.4A) and constitute a stacked pile of amalgamated megabeds up to 20 meters thick, which is uniquely made up of intraclastic gravels and boulders up to 3 m across, composed of rudists (Caprinids and Radiolitids), gastropods and *Orbitolina* grainstones-to-rudstones (Graziano, 2001). The maximum thickness of the Monte Sant'Angelo megabreccia is reported by Graziano (2001) to be around 200 meters near the village of Monte Sant'Angelo, where large-scale channel geometry and an erosive lower boundary occur. Graziano (2001) further reports that the intraclasts of the Monte Sant'Angelo Megabreccias are often subrounded and float in a locally abundant matrix which shows similar composition and texture but different diagenetic features. The clasts and matrix of these deposits are of the same age. Grains of the intraclasts are reported to be well rounded and sorted, but lack any internal sedimentary structures (Graziano, 2001).

The Apulian Platform is limited to the north (Marche-Umbria), to the east (Adriatic Sea) and to the west (Molise-Lagonegro) by Jurassic and Cretaceous deep-marine deposits (*e.g.* Eberli *et.al.*, 1993; Zappaterra, 1994). According to geophysical data, wells and sub-sea observations, several authors suggest that the platform probably also stretched over the Otranto-strait to the Greek islands of Cephalonia and Zante towards the Cephalonia-fault where it terminates

abruptly and is shifted toward the southwest (Rossi & Borsetti, 1974; Auroux *et.al.*, 1985; Finetti *et.al.*, 1996; Sachpazi *et.al.*, 2000).

The Apulian platform is considered an isolated type carbonate platform by several authors (*e.g.* Eberli *et.al.*, 1993; Simo *et.al.*, 1993; Bosellini *et.al.*, 1999; Philip *et.al.*, 2003; Schlüter *et.al.*, 2008). Bosellini (2002) states that the Apulia Platform should be considered an attached type platform, connected, at least during Jurassic-early Cretaceous times, to a wider continental area (North Africa) (figure 2.5B). Vlahovic *et.al.* (2005) indicated that the Apulian Platform area represented parts of the Gondwana margin until the Middle Triassic. Intense tectonic activity that culminated during the Middle Triassic led to the formation of a huge shallow-marine isolated carbonate platform within the southern Tethys realm (the name *Southern Tethyan Megaplatform (STM)* is proposed by Vlahovic *et.al.* (2005) for this paleogeographic entity). Disintegration of the STM led to the separation of the Apulian platform from the *Apenninic platform* and the *Adriatic platform* and took place during Toarcian times (Bernoulli, 1971; Jelaska, 1973; Zappaterra, 1990, 1994; Grandic *et.al.*, 1999; Vlahovic *et.al.*, 2005).

Nicosia *et.al.* (2007) states that the main periadriatic carbonate platforms were probably connected during most of the Cretaceous. This scenario results in a shallow-water area of some 600 000 km^2 – or nearly twice the size of present-

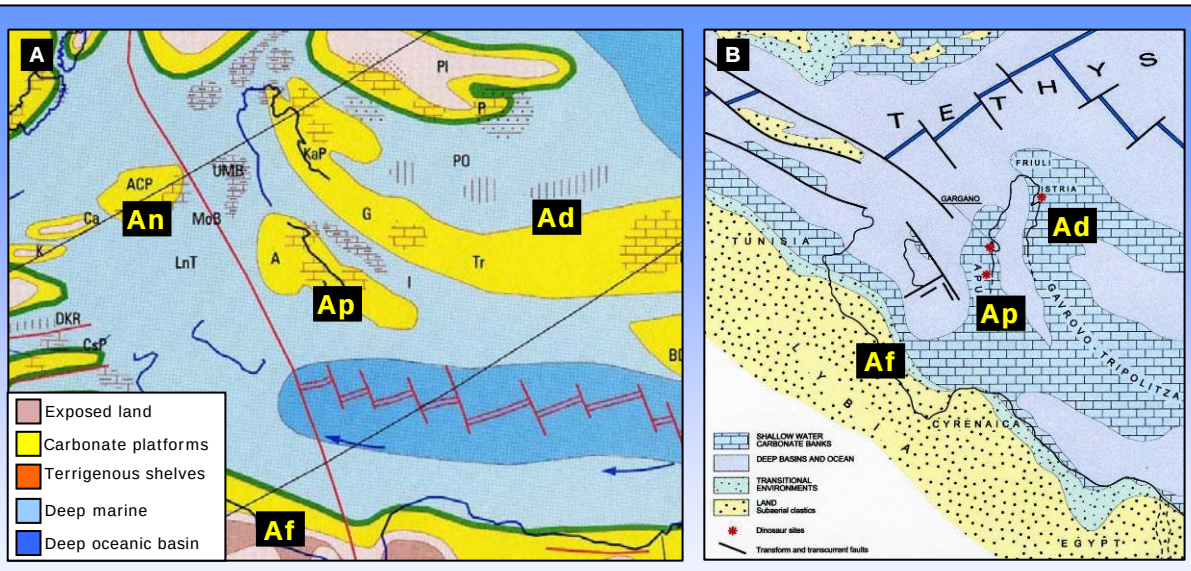

Figure 2.5 – Cenomanian paleogeography of the Periadriatic region

A) Aptian (107-114 Ma) paleogeography of the western Tethys Ocean and the Peri-adriatic domain (Simo *et.al.*, 1993).
B) Jurassic-Early Cretaceous paleogeographic reconstruction (Bosellini, 2002).

Ap: Apulian Platform, An: Apennine Platform, Ad: Adriatic Platform, Af: Africa

day Norway. Considering the small percentage of emergent areas within platforms, such dimensions are necessary in order to fit the needs for a large land animal population indicated from paleontological evidence (Nicosia *et.al.* 2007). These authors also conclude that carbonate platforms of the Neotethys domain may have been connected to Gondwana mainland in the south and, from Coniacian times, to the Laurasian mainland in the north, during periods of low sea-level, where inter-platform areas have emerged and bridged the oceanic area between these platforms and the African mainland.

A number of carbonate platforms existed within the favorable conditions of the Tethys realm. On the northern and southern margins, on the passive margins of the Eurasian and African plates, attached-type platforms developed while isolated-type platforms developed in the central parts (e.g. Philip, 2003). According to paleoclimatic reconstructions, these carbonate platforms were, during the late Cretaceous, located at lower latitudes on the northern hemisphere (Barron & Washington, 1982; Lloyd, 1982). While the northern platforms were mainly influenced by wet temperate climatic conditions (*e.g.* Parrish *et.al.*, 1982, Philip *et.al.*, 1991), the southern platforms developed in an arid climate (Philip, 1982). Among the platforms of the central Tethys, strong paleobiogeographic similarities with the southern Tethyan province exists (Philip, 2003).

On all the carbonate platform domains of the southern Tethyan belt, repeated variations of sea-level were superimposed on tectonic-related substrata contributing to a complex depositional pattern in which the Cenomanian rudist-bearing carbonate facies accumulated (*e.g.* Vlahovic *et.al.*, 1994; Csoma *et.al.*, 2004; Vlahovic *et.al.*, 2005; Carannante *et.al.*, 2007).

3 DATA

This chapter presents the data which form the basis for the subsequent stratigraphic and petrophysical discussion and conclusions. The data are here presented accordingly.

STRATIGRAPHIC DATA

The stratigraphic information is divided according to informal and descriptive stratigraphic entities termed *units*. They reflect mainly major differences in rock fabric, but are also confined by important surfaces. Lithofacies and corresponding subfacies are described for each unit, and a tabulated overview is presented in table 3.1.

For the classification of carbonates, the Dunham (1962) classification with modifications by Embry & Klovan (1971) is mostly used. Classifications based on grain sizes (*e.g.* Scholle & Ulmer-Scholle, 2003) and the classification by Folk (1959, 1962) are also utilized.

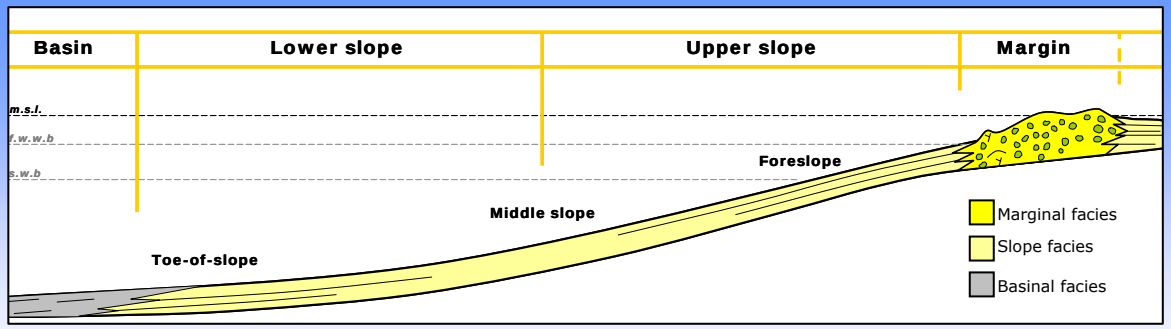

Figure 3.1 – Carbonate slope: Terms and zones

Carbonate slope nomenclature used in the presentation of data. Based largely on James & Mountjoy (1983) and Heath & Mullins (1984). This sketch is not to scale.

Figure 3.1 displays a generalized cross-section of the carbonate slope environment, and introduces terms that are used throughout the presentation of data and the subsequent discussion of data. Similar divisions of the platform-to-basin transition have been published by numerous authors (e.g. Flügel, 2004) and a variety of terms and opinions exist.

Logged sections are presented in figure 3.2 which introduces stratigraphic units and lithofacies which will be further elaborated. Localities are further introduced in relations to description of lithofacies.

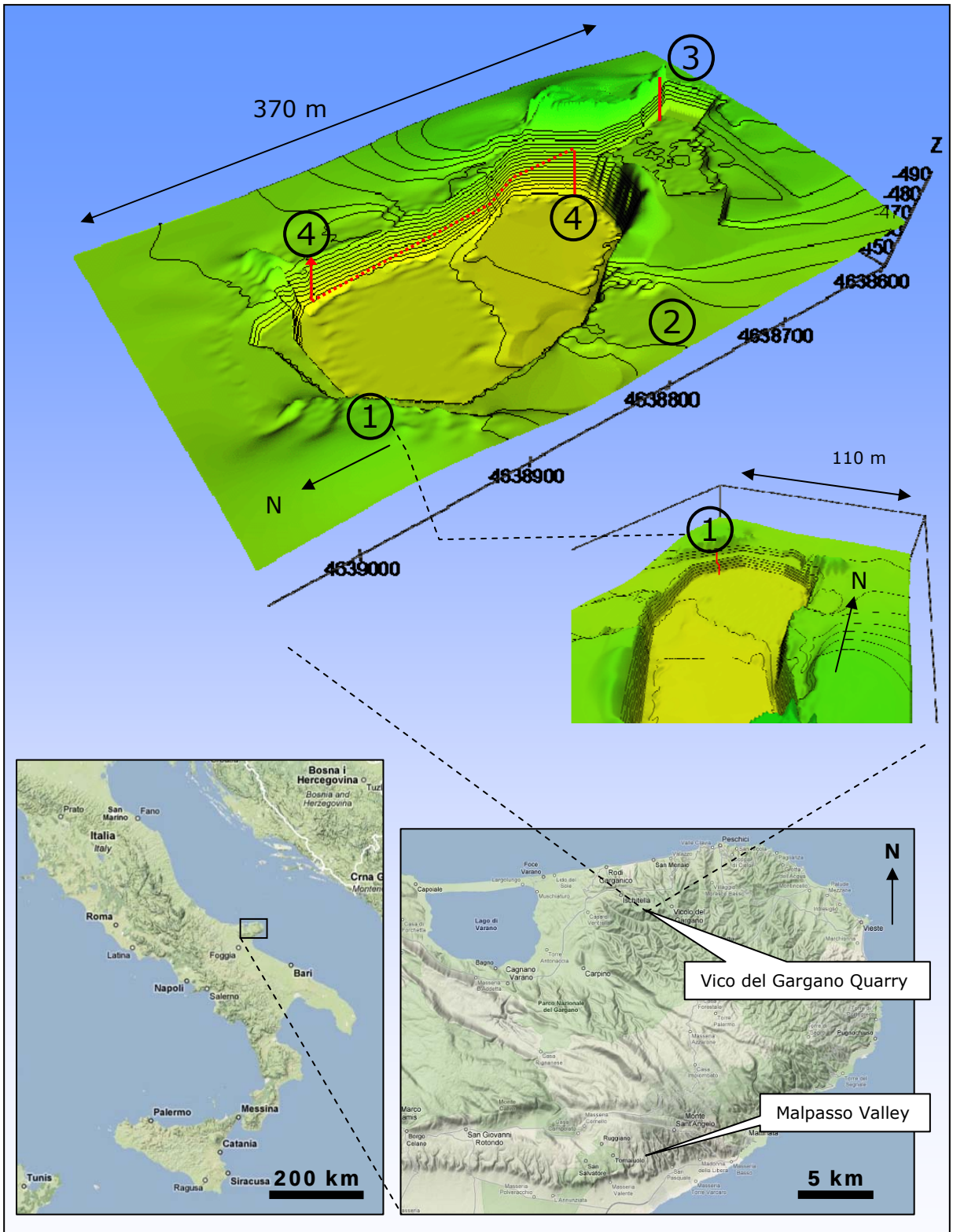

Figure 3.2 – Logged sections

↑ Position of logs. Vico del Gargano logs are positioned on topographic model of the quarry.

→ Logs and legend. Numbers on Vico del Gargano logs correspond to topographic model.

This figure spans two pages. Subfacies are derived from thin-section analysis and not included on logs. Lithofacies are indicated. Localities are further introduced later in this chapter.

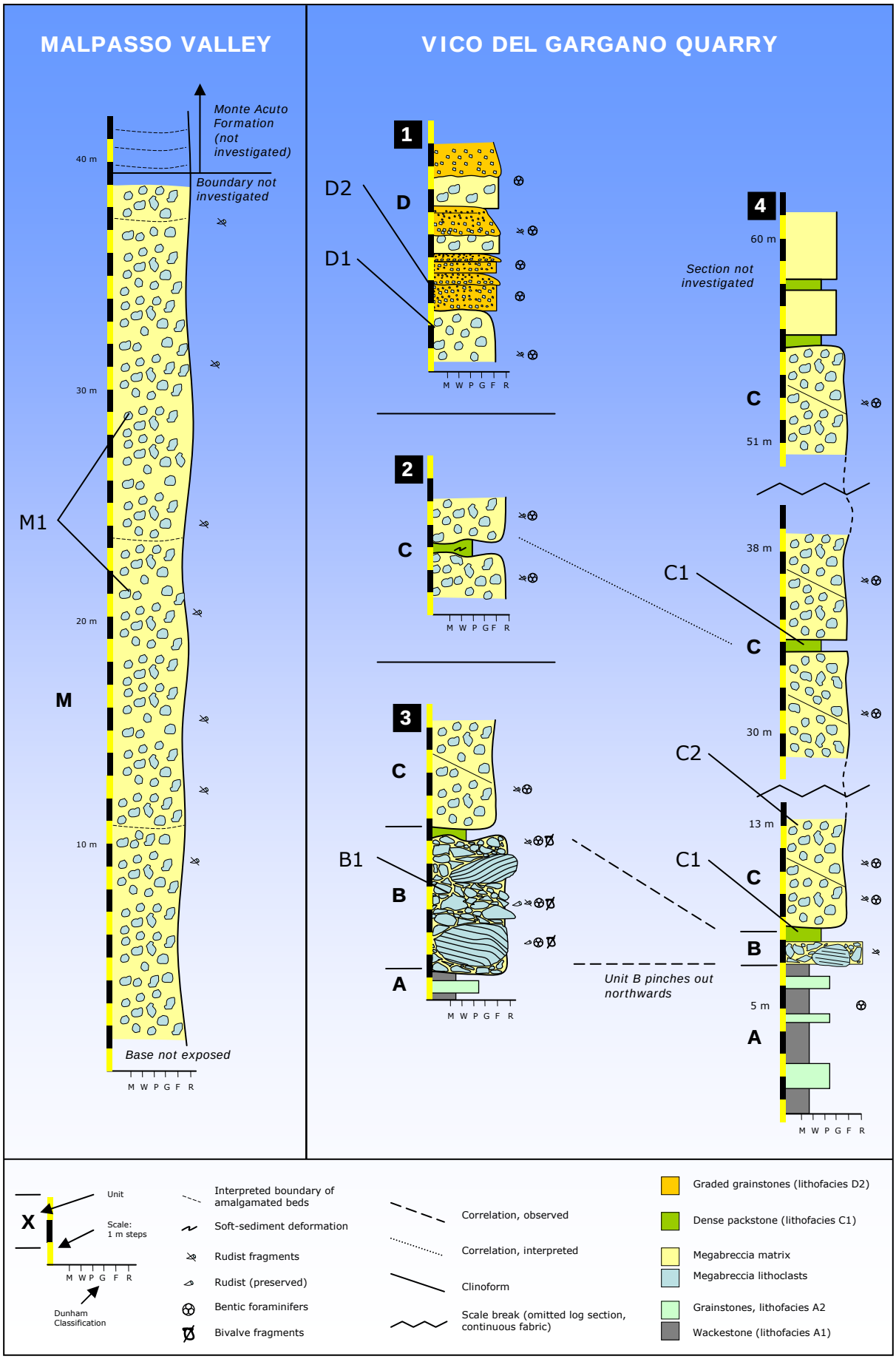
MALPASSO VALLEY
Monte Acuto Formation (not investigated)
Boundary not investigated
40 m
30 m
20 m
10 m
M1
M
Base not exposed
M W P G F R
VICO DEL GARGANO QUARRY
1
D2
D
D1
2
C
3
C
B1
B
A
4
60 m
Section not investigated
C
51 m
C1
38 m
C
30 m
C2
13 m
C1
C
B
5 m
A
Unit B pinches out northwards
Unit
Scale: 1 m steps
Dunham Classification
Interpreted boundary of amalgamated beds
Soft-sediment deformation
Rudist fragments
Rudist (preserved)
Bentic foraminifers
Bivalve fragments
Correlation, observed
Correlation, interpreted
Clinoform
Scale break (omitted log section, continuous fabric)
Graded grainstones (lithofacies D2)
Dense packstone (lithofacies C1)
Megabreccia matrix
Megabreccia lithoclasts
Grainstones, lithofacies A2
Wackestone (lithofacies A1)

Table 3.1 – Units, lithofacies and subfacies

Locality	Unit ID	Litho-facies ID	Sub-facies ID	Name/description	Boundaries	Sedimentary structures	Biota	Important diagenetic features	Interpretation
Malpasso Valley	M			Matrix-supported rudist megabreccias	See lithofacies M1	See lithofacies M1	See lithofacies M1	See lithofacies M1	See lithofacies M1
		M1		Matrix-supported rudist megabreccia 1	Sharp upper boundary. Base is not exposed.	Sub-horizontal bedded, thick 10-15 m amalgamated beds. Poorly sorted, matrix-supported. Clasts from few cm to ~1-2 m across.	See subfacies M1	See subfacies M1	Debris-flows originating from the marginal areas of the platform.
			M1a	Grainstone			Benthic foraminifers, rudist- and bivalve fragments	Grain-dissolution, micrite envelopes early marine-phreatic isopachous cement and meteoric-phreatic cement, nonfabric-selective dissolution. M1d and M1e micrite matrix also have rhombohedra shaped selective dissolved pores.	Marginal platform environment
			M1b	Grain-dominated extraclastic packstone					Marginal platform-to-foreslope environment
			M1c	Mud-dominated extraclastic packstone					Marginal platform-to-foreslope environment
			M1d	Mud-dominated skeletal rudstone					Foreslope-to-platform margin environment
			M1e	Wackestone					Low-energy foreslope environment
Vico del Gargano Quarry	A			Wacketones and graded calcarenite packstones	Sharp upper boundary. Lower not exposed.	See lithofacies A1/A2	See lithofacies A1/A2	See lithofacies A1/A2	Distal slope-to-proximal basin deposits
		A1		Lime mudstones/ wackestones	Sharp upper and lower boundaries	Horizontal, thin bedding	*Thalassanoid* trace fossils	Stylolites	Hemipelagic highstand-shedding deposits
		A2		Graded calcarenite grainstone	Sharp lower-, gradient upper boundaries.	Graded, horizonal bedding. Bouma-divisions DE.		Sparite cements	Distal low-density calciturbidites
	B			Clast-supported rudist megabreccias	See lithofacies B1	See lithofacies B1	See lithofacies B1	See lithofacies B1	See lithofacies B1
		B1		Clast-supported rudist megabreccia with bouldersized clasts ranging from cm to m scale.	Sharp	Matrix-supported, poorly sorted, cm to several m lithoclasts. Some clasts have internal sedimentary structures (bedding)	See subfacies	See subfacies	Single-event submarine landslide (grain flow) originating from the upper-slope, margin and platform interior areas.
			B1a	Grainstone with bimodal distributed grains. Well rounded lime pellets and moderately rounded skeletal fragments.				Early isopachous sparite cement. Dominance of moldic porosity. Micrite envelopes preserve grain shapes and sizes.	High-energy marginal platform environment
			B1b	Grain-dominated packstone			*Orbitolina sp.*	Micrite envelopes, early isopachous marine-phreatic cement. Later equant meteoric-phreatic cement.	Moderate energy marginal platform-to-foreslope environment
			B1c	Mud-dominated packstone with skeletal fragments and pellets.					Low-energy foreslope-to-marginal platform environment
	C			Matrix-supported rudist megabreccias separated by packstone clinoforms.	Sharp base. Top not exposed.	Stacked megabreccia beds, separated by northwards dipping packstone clinoforms.	See lithofacies C1 and C2	See lithofacies C1 and C2	Debris-flow deposits originating from upper-slope and marginal areas. Prograde northwards.
		C1		Dense, 20-40 cm packstone layers separating units B and C, and segments of facies C2	Sharp top and base. Local undulations.	Local soft-sediment deformations	Benthic foraminifers, bivalve- and rudist fragments		High-stand shedding of platform-derived skeletal materials.
		C2		Matrix-supported rudist megabreccias 2	Sharp base and top, local undulations.	Matrix-supported, poorly sorted, few cm to < 1 m lithoclasts.			Middle-to-lower slope debris-flow deposits
	D			Graded grainstones alternating with matrix-supported megabreccias	Not exposed	Large-scale syncline shaped. Stacked channelled beds of 1-2 m.	See lithofacies D1 and D2	See lithofacies D1 and D2	Stacked channelled proximal high-density calciturbidites and megabreccia debris-flows
		D1		Matrix-supported rudist megabreccias 3	Undulating, locally channelled	Matrix-supported, poorly sorted < 1 m clasts, < 2 m beds.	See subfacies	See subfacies	Multiple debris-flows interbedded with proximal calciturbidites.
			D1a	*Orbitolina* grainstone			Benthic foraminifers, bivalve- and rudist fragments	Early isopachous marine-phreatic cement, later equant meteoric-phreatic cement, grain-dissolution, rare nonfabric-selective porosity.	High-energy, platform margin environment.
			D1b	Grain-dominated packstone					High-energy, platform margin environment.
			D1c	Mud-dominated packstone					Lower-energy, platform margin-to-foreslope environment
		D2		Graded grainstones	Erosive based, channelled.	Bouma-divisions T(abc)	*Orbitolina sp.*		Proximal high-density turbidites on proximal-to-middle slope

Colours are for visualization purposes only. Boundaries and sedimentary structures are not included for subfacies, which are derived from thin-sections.

MALPASSO VALLEY

The Malpasso Valley is situated approximately 4 km SSE of the village of Monte Sant'Angelo and cuts through Cretaceous slope strata (fig 3.3). Weathering is a major problem on this locality, which limits the detailed stratigraphic analysis.

81 mini-drill cores were collected from the Malpasso Valley, including 52 from a 10 x 5 m grid on the west wall and 29 representative clast- and matrix samples from the eastern wall. The petrophysical parameters results from analysis of these samples are presented in chapter 4 and discussed in chapter 5. A total of 4 days were spent on this locality during August 2006, collecting plug samples.

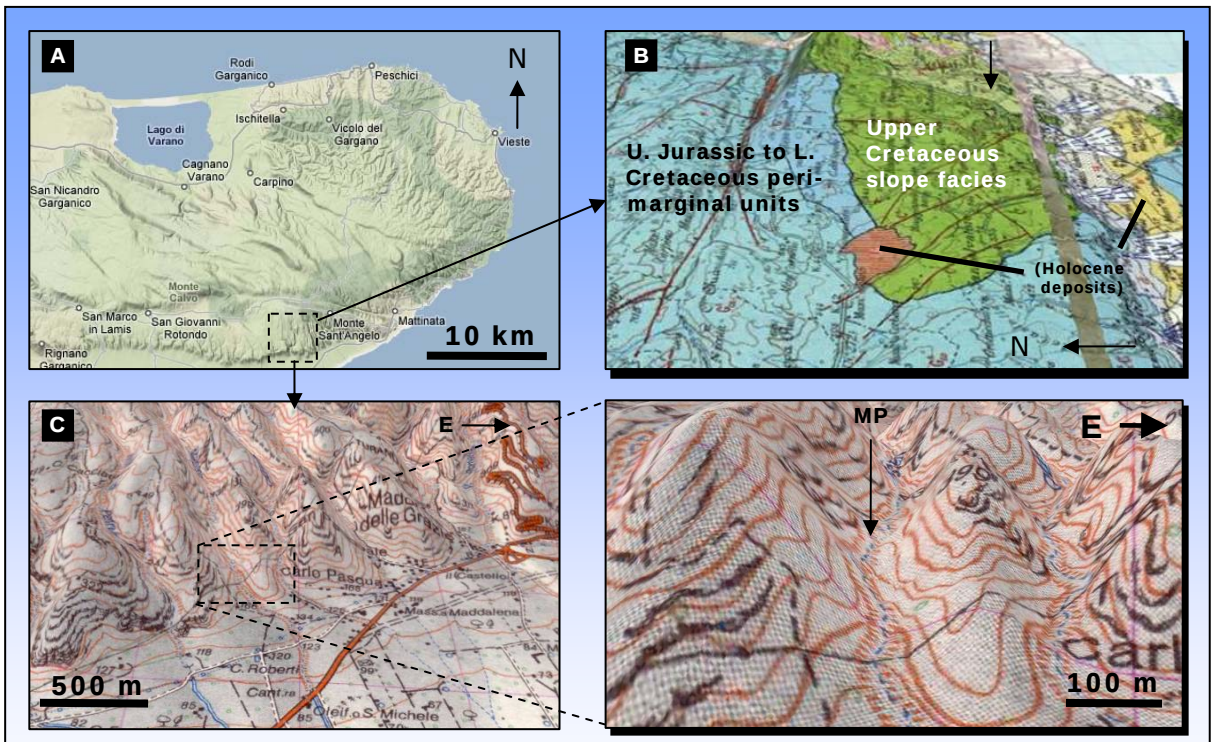

Figure 3.3 – Malpasso Valley

A) Southern Gargano overview (Google maps as of December 2007). Arrow points to location of the Malpasso Valley.
B) Topography from Google Earth as of April 2008 draped with geological map 1:000 000 by R. Selli. MP = Malpasso Valley.
C) Topographic map draped on topography from Google Earth™ as of April 2008.

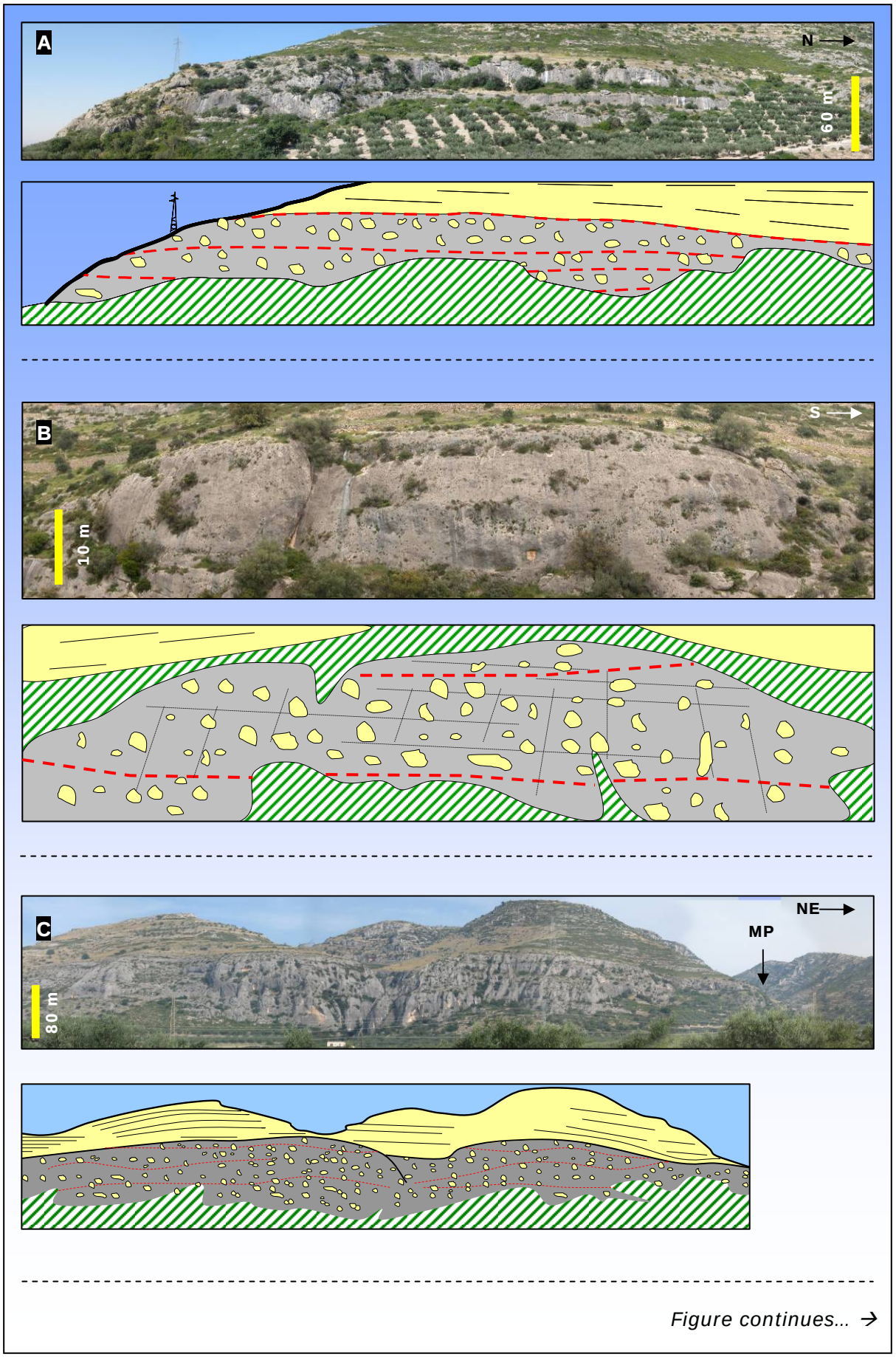

Figure continues... →

DESCRIPTION OF UNIT M AND CORRESPONDING LITHOFACIES

Unit M and lithofacies M1 are the same entity. The term unit M is introduced for implementation with the units of the Vico del Gargano succession. See table 3.1 for a graphical view of this issue.

Unit M/lithofacies M1 consists of matrix-supported rudist megabreccias, that are confined to sub-horizontal, amalgamated 5-15 m beds (figure 3.4). The upper boundary of this unit/lithofacies is sharp towards overlying slope deposits of the Monte Acuto Limestone Formation. Lower boundary is not exposed. Mapped thickness is some 40 meters. Lithoclasts are poorly rounded, and the deposit is poorly sorted. Image enhancement methods were utilized in the visualisation of lithoclasts (figure 3.5). Investigated lithoclasts consists of grainstones that are dominated by moldic porosity. The lithoclast/matrix contacts are sharp and distinct, and related to abrupt changes in fabric (figure 3.6).

DESCRIPTION AND INTERPRETATION OF SUBFACIES TO LITHOFACIES M1

Subfacies M1a is a well sorted, moderately rounded grainstone dominated by moldic and interparticle porosity. Some samples display in extraclasts. Grains display micrite envelopes (Bathurst, 1966), and dissolution have frequently removed the entire grain leaving an inverted porosity fabric that is overgrown with calcite cement. Two distinct generations of calcite cements are recognized. An inner rim of isopachous, bladed cement has precipitated directly onto the rounded grains preserved through micrite envelopes. Equant calcite cement has precipitated onto the marine cement.

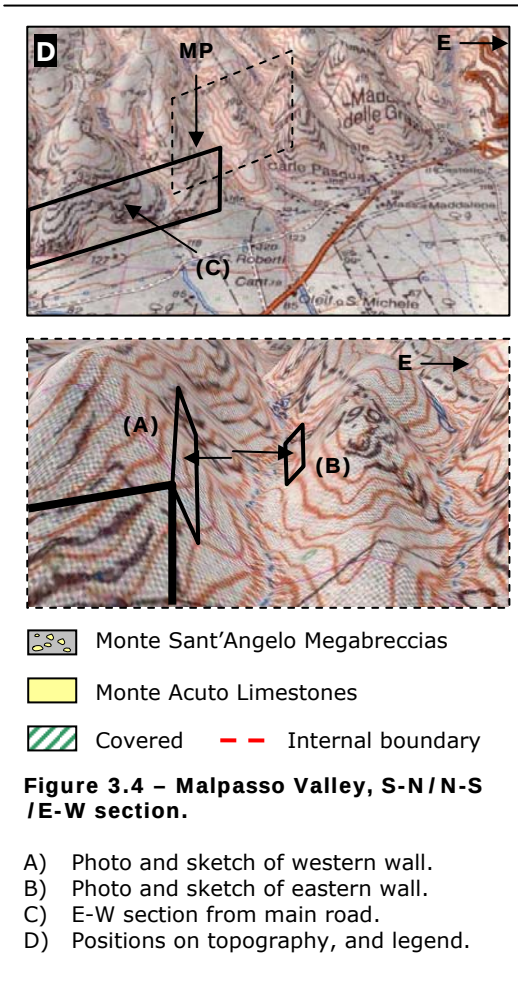

Figure 3.4 – Malpasso Valley, S-N/N-S /E-W section.

A) Photo and sketch of western wall.
B) Photo and sketch of eastern wall.
C) E-W section from main road.
D) Positions on topography, and legend.

<u>Interpretation</u>: Subfacies M1a originates from higher-energy areas on the platform margin. Extraclasts of this subfacies were eroded and re-deposited into lower-energy areas on the foreslope by erosion where

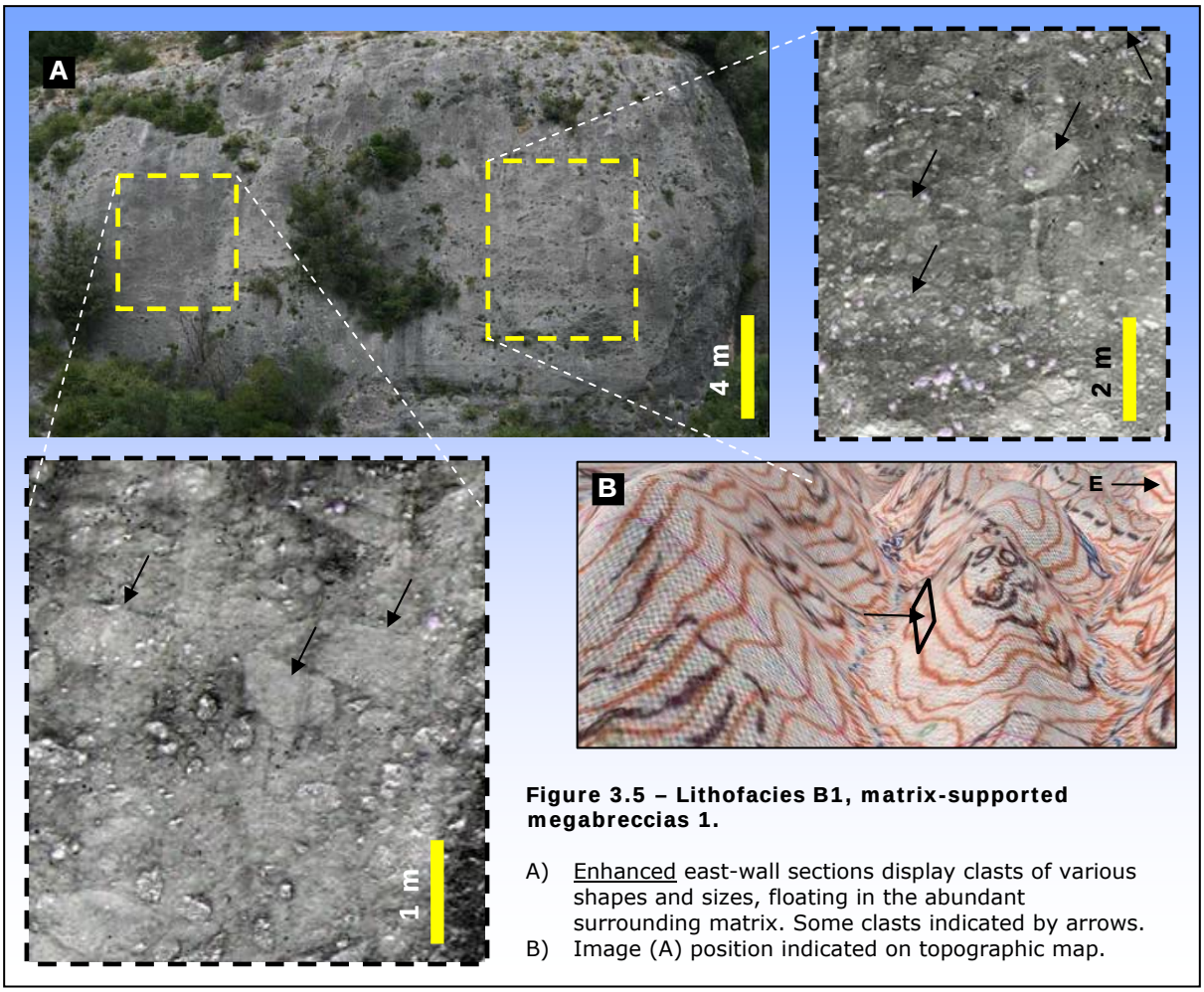

Figure 3.5 – Lithofacies B1, matrix-supported megabreccias 1.

A) Enhanced east-wall sections display clasts of various shapes and sizes, floating in the abundant surrounding matrix. Some clasts indicated by arrows.
B) Image (A) position indicated on topographic map.

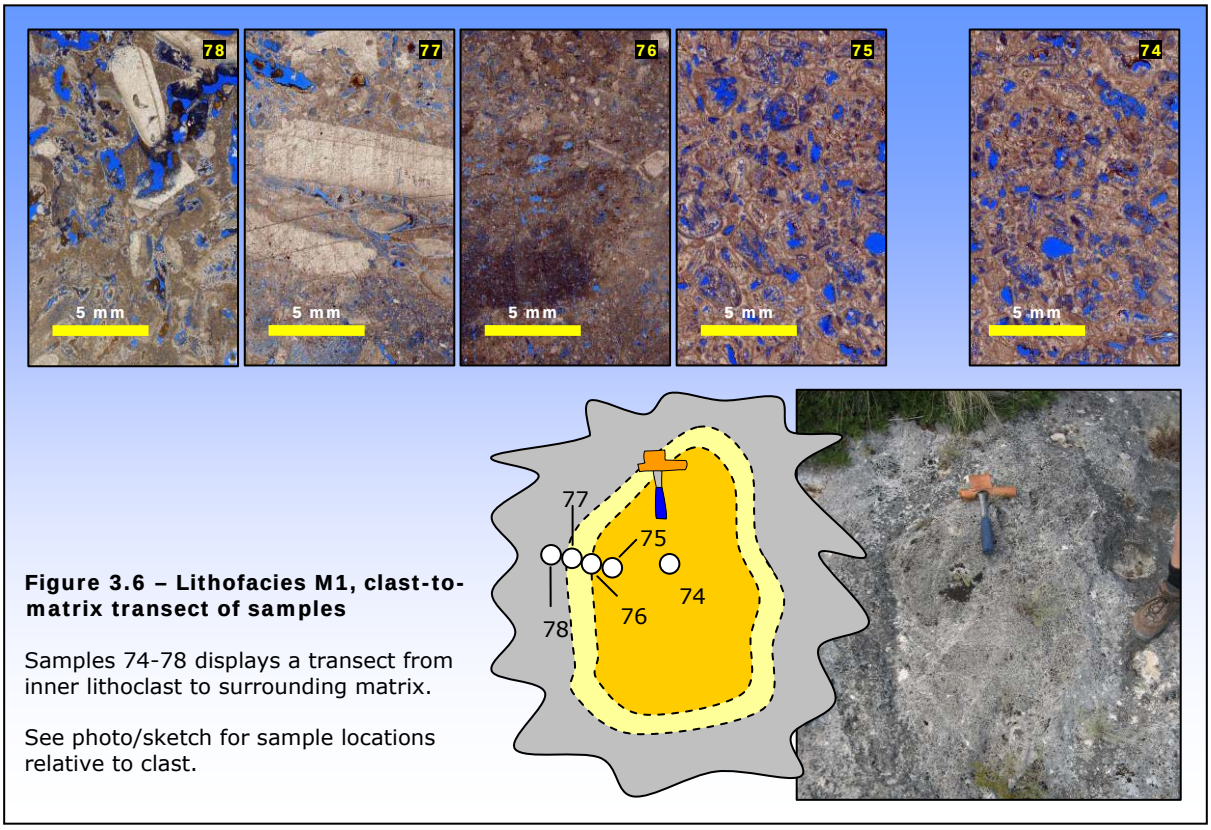

Figure 3.6 – Lithofacies M1, clast-to-matrix transect of samples

Samples 74-78 displays a transect from inner lithoclast to surrounding matrix.

See photo/sketch for sample locations relative to clast.

they were mixed with mud-rich fractions and lithified prior to re-sedimentation as lower-slope megabreccia components. This subfacies mainly contribute to lithoclasts of the megabreccias, but possibly also to the matrix as smaller fraction extraclasts. This subfacies may also have been produced through the disintegration of lithoclasts during transport.

Subfacies M1b displays grain-dominated packstones, cemented by micrite mud. Grains are unsorted and moderately rounded and consist mostly of skeletal grains. Remnants of rudist, bivalves and echinoderms are recognized. Micrite envelopes are present but not common, and locally observed surrounding grainstone and packstone extraclasts. Micrite mud is locally abundant, but confined to certain areas of the samples (*e.g.* sample 1-9, figure 3.7). Nonfabric-selective dissolution porosity is observed along with rare intraparticle pores within preserved skeletal fragments, but the subfacies is dominated by interparticle porosity. A fringe of isopachus cement surrounds most grains, which shape and size is generally defined through micrite envelopes. They are in turn coated with equant calcite cement that is the volumetrically dominant cement fraction (figure 3.7). *Orbitolina sp*. and *Echinoid* fragments are recognized.

Interpretation: Subfacies M1b is interpreted as deposits of semi-protected areas of the foreslope to the carbonate platform. Skeletal grains were derived from adjacent rudist colonies related to higher-energy parts of the platform. This subfacies lithified on the foreslope prior to re-deposition, and occurs within lithoclasts as well as the matrix to the lower-slope megabreccias. This suggests that disintegration of lithoclasts during transport may have contributed to the matrix.

Subfacies M1c displays mud-dominated packstones. Most grains are rudist-, bivalve- or echinoid fragments. Nonfabric-selective porosity is observed but the subfacies is dominated by interparticle and moldic porosity. The packstones locally grade into wackestones. Compaction-features are observed. Micro-porosity occurs within the mud-fraction of this subfacies, visible through weak epoxy staining of the fabrics. Rhombohedra-shaped pores that show no cementation occur, confined to micrite-dominated fabrics (figure 3.7).

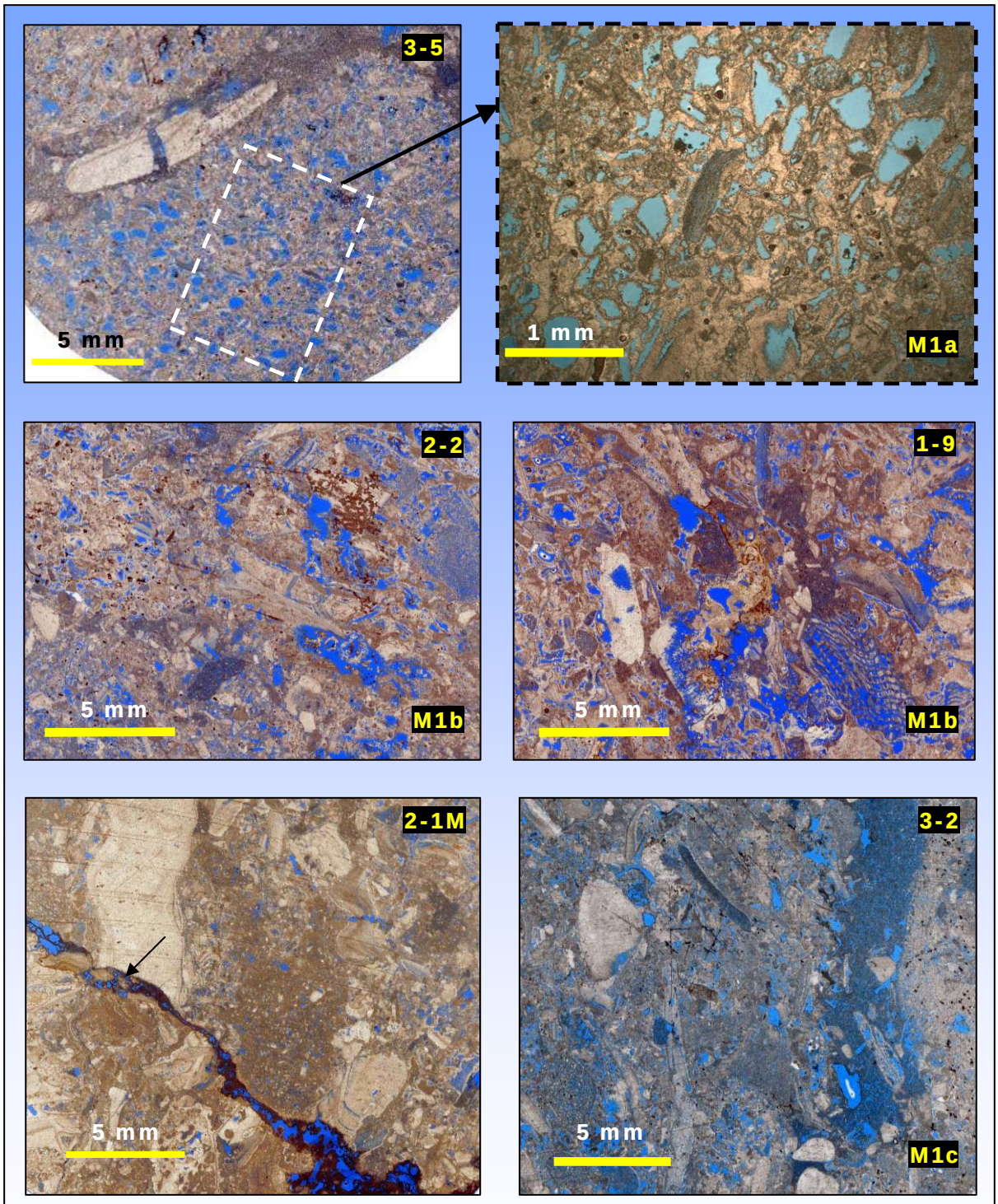

Figure 3.7 – Subfacies M1a, M1b and M1c

A) Subfacies M1a as displayed in sample 3-5.
B) Subfacies M1b as displayed in samples 2-2 and 1-9.
C) Subfacies M1c displayed in samples 2-1M and 3-2. Sample 2-1M originated from megabreccia matrix. This sample is cut by nonfabric-selective vug filled with recent silts (arrow).

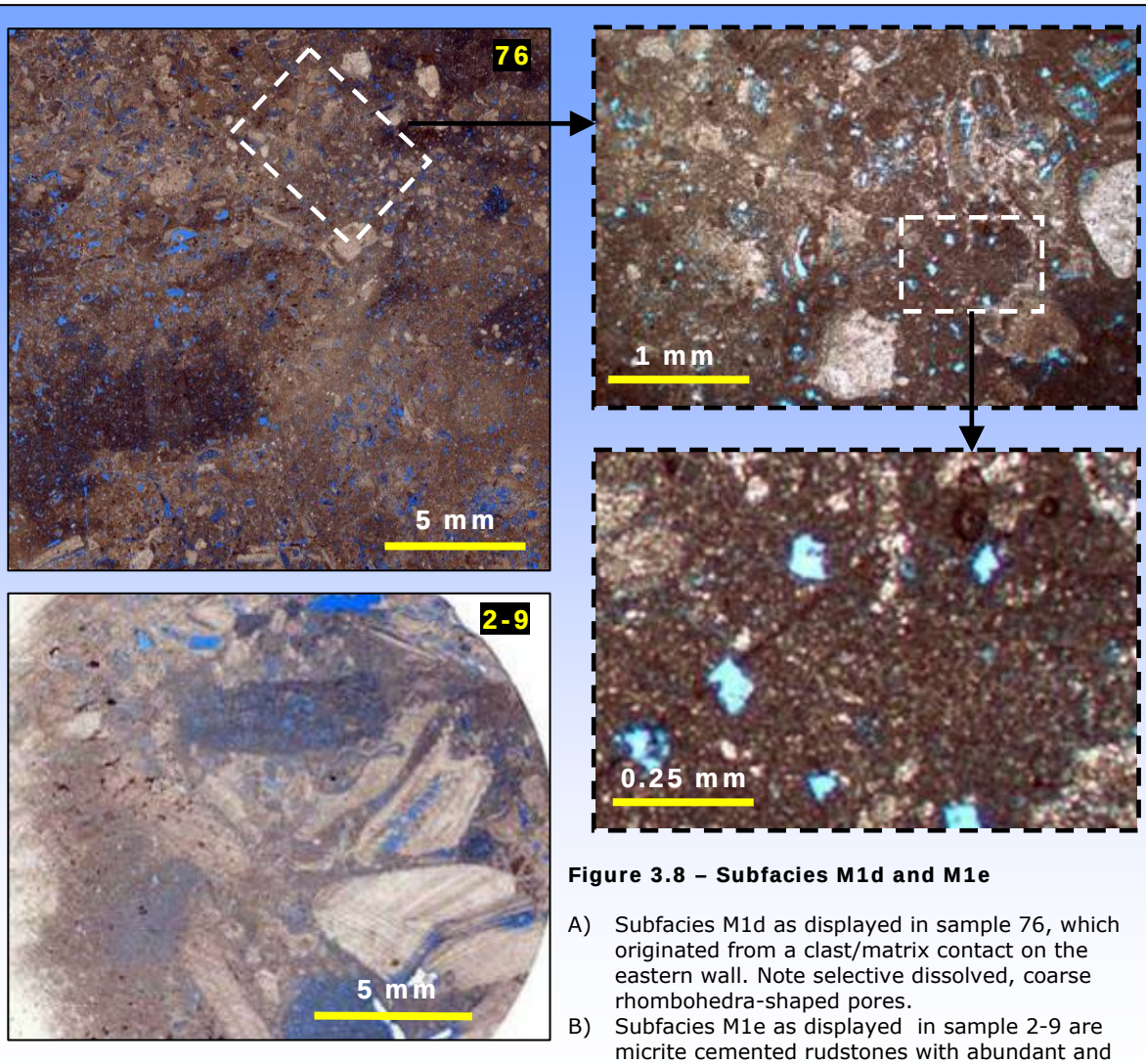

Figure 3.8 – Subfacies M1d and M1e

A) Subfacies M1d as displayed in sample 76, which originated from a clast/matrix contact on the eastern wall. Note selective dissolved, coarse rhombohedra-shaped pores.
B) Subfacies M1e as displayed in sample 2-9 are micrite cemented rudstones with abundant and rudist fragments.

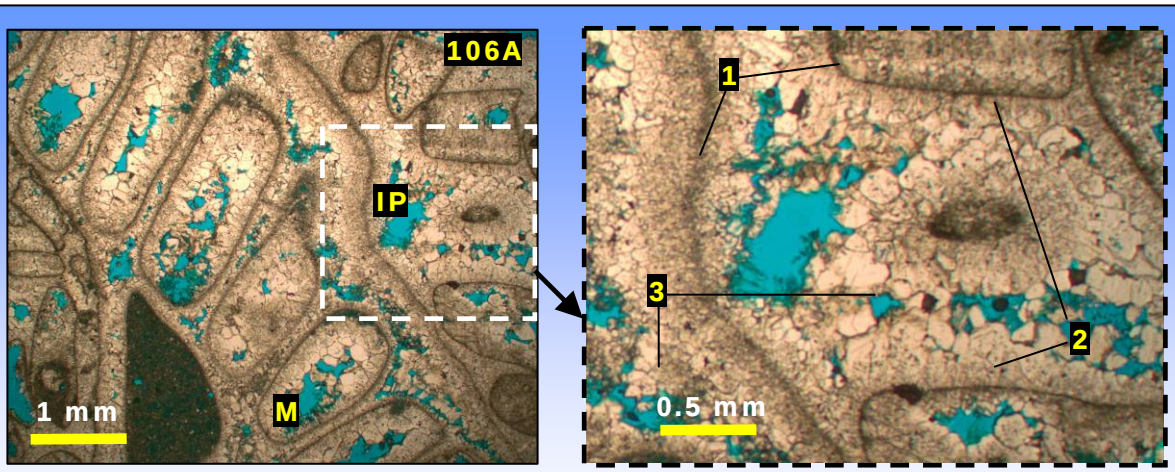

Figure 3.9 – Diagenetic observations

Sample 106 displays subfacies M1a – Grainstone. An isopachous, bladed calcite cement coats (2) individual grains that are defined by micrite envelopes (1). Equant calcite cement (3) precipitated onto the isopachous cement and within in interparticle (IP) and moldic (M) pores.

Interpretation: Subfacies M1c is interpreted as originating from lower-energy parts of the platform foreslope. They were lithified prior to re-deposition into lower-slope megabreccias. Grains were derived from adjacent populations of rudists, echinoderms and bivalves on the platform upper slope and margin.

Subfacies M1d consists of mud-dominated rudist rudstones with skeletal fragments in a micrite wackestone matrix. The subfacies is dominated by interparticle porosity but intraparticle porosity occurs rarely. Skeletal fragments within this lithofacies display little or no early marine calcite cementation (figure 3.8).

Interpretation: Subfacies M1d is interpreted as megabreccia matrix. They are sediments produced on the marginal areas, and transported to the lower-slope domain along with the matrix-supported debris-flows.

Subfacies M1e consists of micrite wackestones, with scattered rhombohedra-shaped pores which are confined to the micrite matrix. The subfacies only rarely show calcite cementation. Grains are skeletal fragments and pellets. No internal organization is observed (figure 3.8).

Interpretation: Subfacies M1e constitutes the matrix to the megabreccias along with other components. These sediments were derived from the marginal areas of the platform, and deposited onto the slope. Rhombohedra-shaped pores suggest the selective dissolution of dolomite or pyrite crystals. The lack of cement within these pores indicate that dedolomitization were late in the diagenetic history of these sediments.

INTERPRETATION OF UNIT M AND CORRESPONDING LITHOFACIES

Unit M/Lithofacies M1 are debris-flows that originated from the upper-slope and marginal environments where sediments lithified prior to re-deposition to the lower-slope domain. Matrix constitutes mostly similar subfacies as the lithoclasts, indicating similar source and disintegration of lithoclasts during transport. The internal segmentation of the megabreccia levels indicates multi-event deposition.

VICO DEL GARGANO

The Vico del Gargano Quarry is situated in the northern part of the Gargano, 2 km west of the village of Vico del Gargano and approximately 20 km north of the village of Monte Sant'Angelo, (figure 3.10). The quarry exposes a 360 m long N-S trending outcrop. A total of 36 plug samples were drilled from this locality during 4 days of May 2007.

4 units where mapped in the quarry; A through D. Each unit contains one or more lithofacies and subfacies which are described and interpreted below.

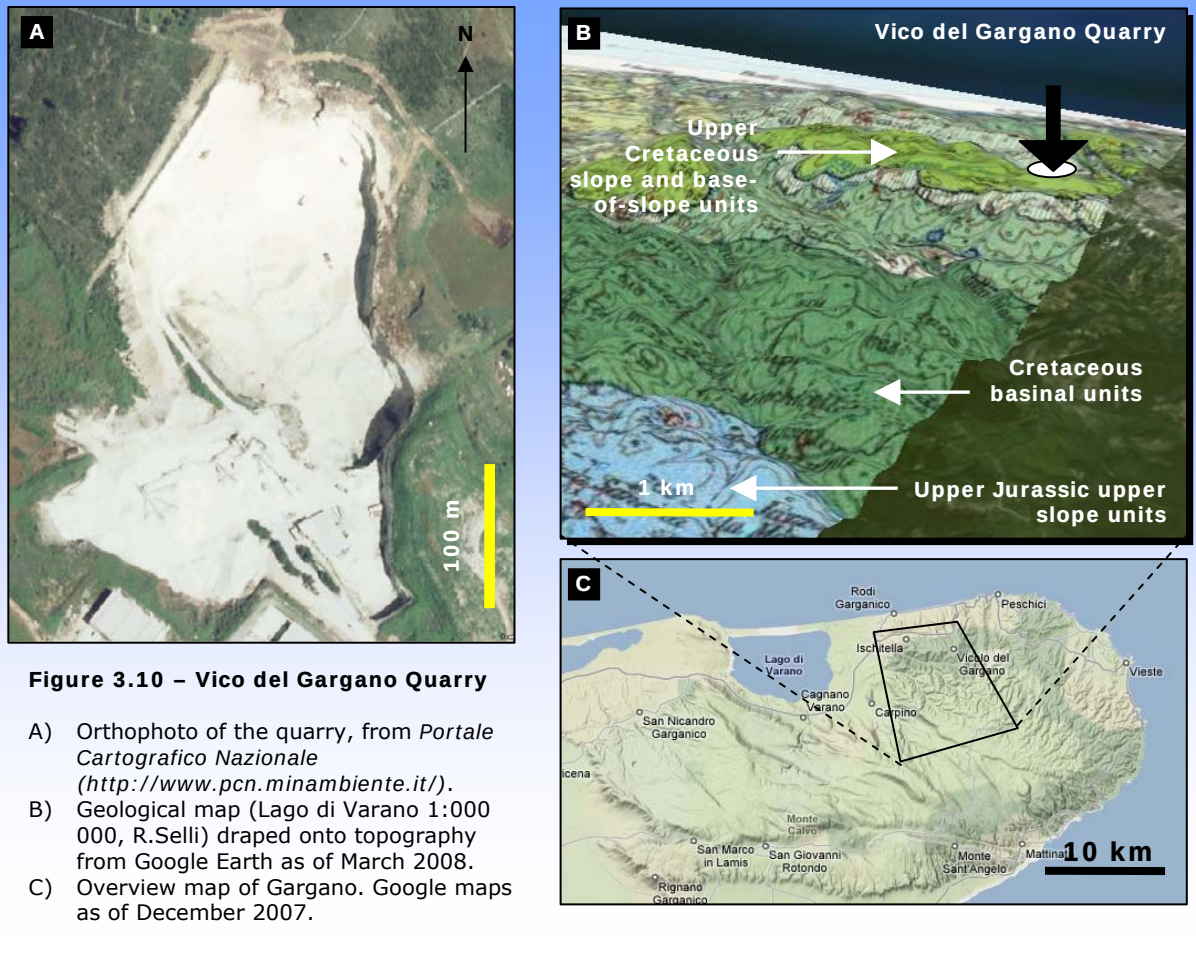

Figure 3.10 – Vico del Gargano Quarry

A) Orthophoto of the quarry, from *Portale Cartografico Nazionale (http://www.pcn.minambiente.it/)*.
B) Geological map (Lago di Varano 1:000 000, R.Selli) draped onto topography from Google Earth as of March 2008.
C) Overview map of Gargano. Google maps as of December 2007.

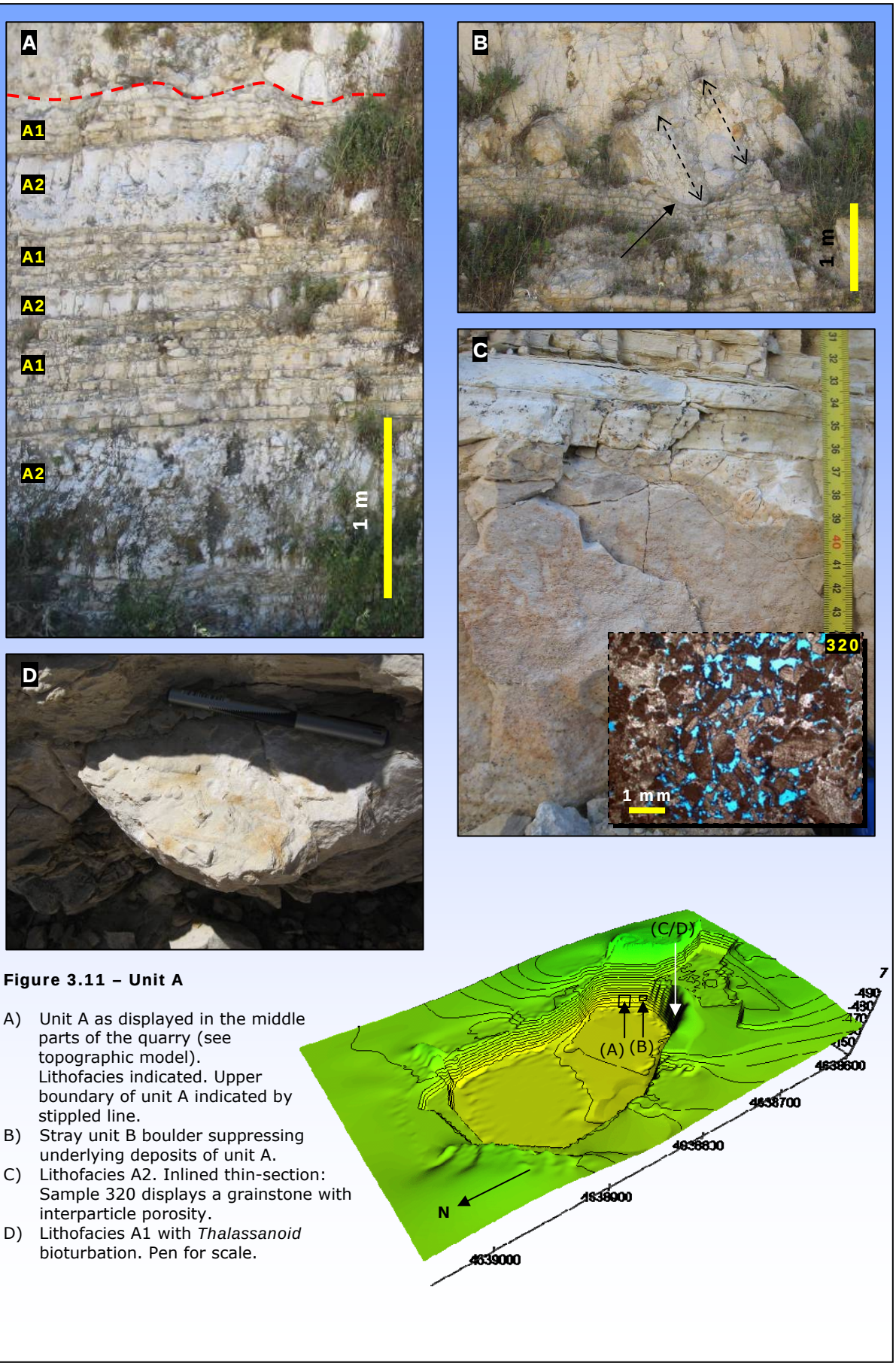

Figure 3.11 – Unit A

A) Unit A as displayed in the middle parts of the quarry (see topographic model). Lithofacies indicated. Upper boundary of unit A indicated by stippled line.
B) Stray unit B boulder suppressing underlying deposits of unit A.
C) Lithofacies A2. Inlined thin-section: Sample 320 displays a grainstone with interparticle porosity.
D) Lithofacies A1 with *Thalassanoid* bioturbation. Pen for scale.

DESCRIPTION OF UNIT A AND CORRESPONDING LITHOFACIES

Unit A is the lowermost unit mapped in the Vico del Gargano Quarry. The unit consists of two facies; Homogenous lime wackestone layers of facies A1 interbedded with graded grainstone/packstone beds of facies A2 (medium-to-coarse calcarenite). Sharp boundaries separate these interbedded facies, no erosive features are observed. No paleo-current indicators were observed. The unit displays a thickness of 5 meters in the mapped succession. Soft-sedimentation features are observed within the upper parts of this unit where it is locally suppressed by the overlying unit B (figure 3.11). No frequency or thickness trends of the internal layers of this unit are observed. Unit A is separated from the overlying unit B by a sharp boundary.

Lithofacies A1 consists of lime wackestones, confined to parallel laminae and thin (1-15 cm) beds. It is interbedded with lithofacies A2. *Thallasanoid* bioturbation is observed (figure 3.11). The database contains no samples from this facies.

Lithofacies A2 consists of graded calcarenite grainstones which are sharp-based, but show upper boundaries that locally appear more gradual. One thin-section (#320) is available from this facies, displaying a dominance of interparticle porosity between poorly sorted grains (figure 3.11). Some moldic porosity occur. Grains consist of rudist- and bivalve fragments and *Orbitolina sp.* as well as pellets of different origins. Grains are cemented by equant calcite sparite. No micrite mud is observed. Three beds of this facies are observed in the exposed succession (5 m). No vertical trends in terms of bed thickness, frequency or other features were derived from the exposed section.

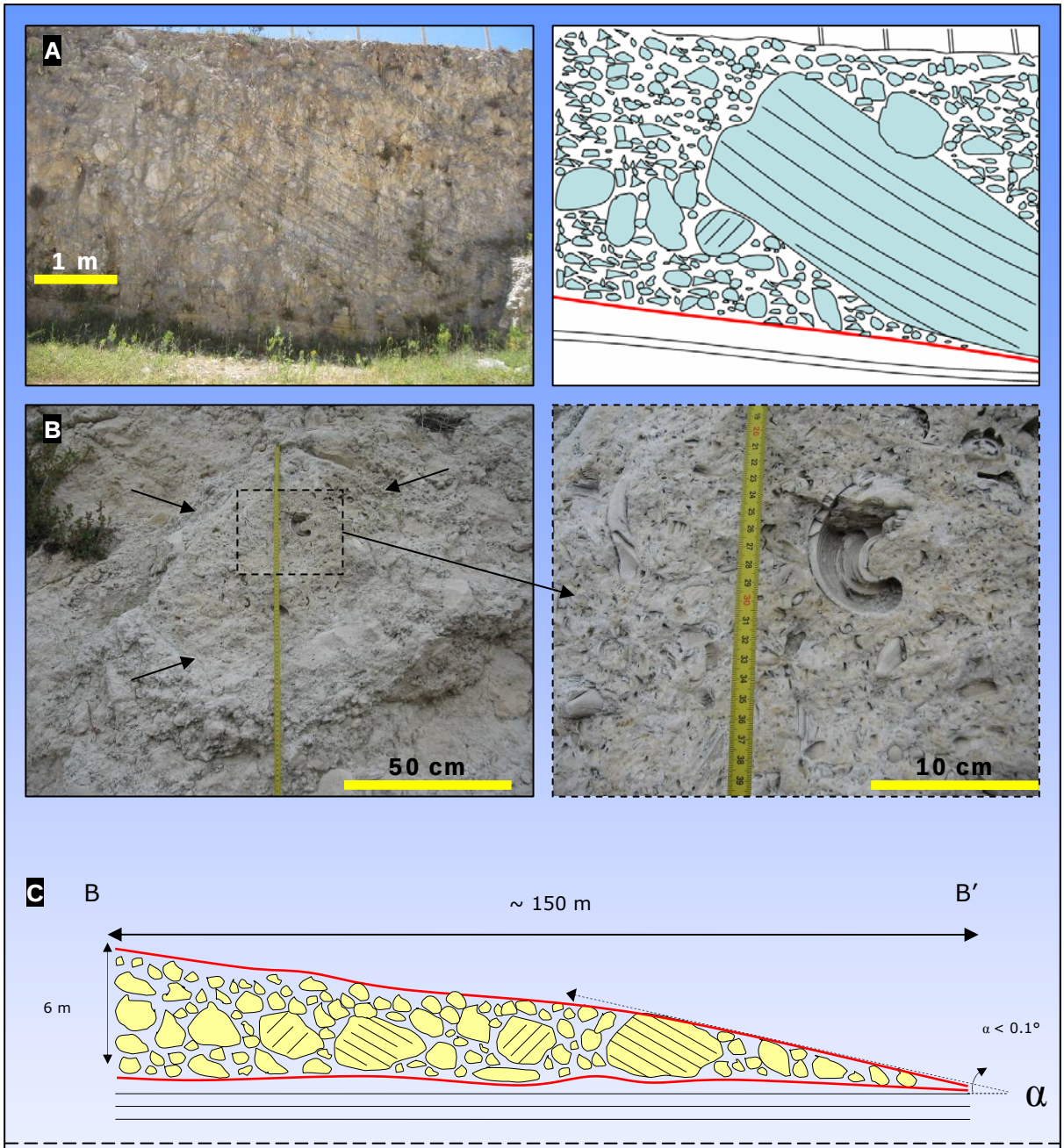

Figure 3.12 – Unit B / Lithofacies B1

A) Photo and sketch of lithofacies B1 as displayed in the southern most parts of the quarry.
B) Lithoclast displayed in the southern parts of the quarry with selection: Preserved rudist shell and abundant shell fragments. Arrows point to clast.
C) Unit B displays a pinch-out geometry between the underlying unit A and the overlying unit C. Mapped angle of deposit is less than 0.1° relative to top unit A datum.
D) Position of profile (C) and position of images (A) and (B) (arrow) on topographic quarry model.

INTERPRETATION OF UNIT A

Interpretation: Lithofacies A1 is interpreted as distal slope to proximal basin hemipelagic deposits, with fine grained materials deposited mainly from suspension probably related to high sediment production on the adjacent carbonate platform. These deposits mark periods of local non-deposition of coarser materials from the platform. Thalassanoid trace fossils suggest episodic halts in sediment supply or sufficient low sedimentation rates to accommodate biota on the sea-floor.

Interpretation: Lithofacies A2 is interpreted as low-density calciturbidites (T_{DE}) deposited in the distal slope to proximal basin environment. The absence of amalgamated turbidite beds indicates that deposition from turbiditic flows in this area were not very frequent during this time period, which in turn underpins the distal position of this succession relative to the carbonate factory.

Interpretation: Unit A is interpreted as turbidites interbedded with marine hemipelagic mudstones (background sedimentation) on the distal shelf/basin. This unit was not dated, but previously established stratigraphy (figure 2.4) indicate that this unit may be interpreted as the transition between Monte Sant'Angelo Limestones and Scaglia Fm/the transition between the upper Mattinata Limestones/Fucoid Marls.

DESCRIPTION OF UNIT B AND CORRESPONDING LITHOFACIES

Unit B and lithofacies B1 are the same entity and are here subsequently not described separately.

Lithofacies B1 is a poorly sorted, polygenic matrix-supported rudist rudstone megabreccia. The base and top of the unit are sharp and non-erosive. Individual lithoclasts range from cm to meter scale. Some larger lithoclasts show preserved internal sedimentary structures. Other lithoclasts show an abundance of rudist shell fragments as well as whole preserved rudist shells. No matrix is observed within this lithofacies. No segmentation or organization is observed. Mapped thickness is 7 meters in the southernmost parts of the quarry, thinning towards the north and pinching out between units A and C in the middle parts of the quarry (figure 3.12). Unit B/Lithofacies B1 is here represented only by some stray outlying boulders (figure 3.12).

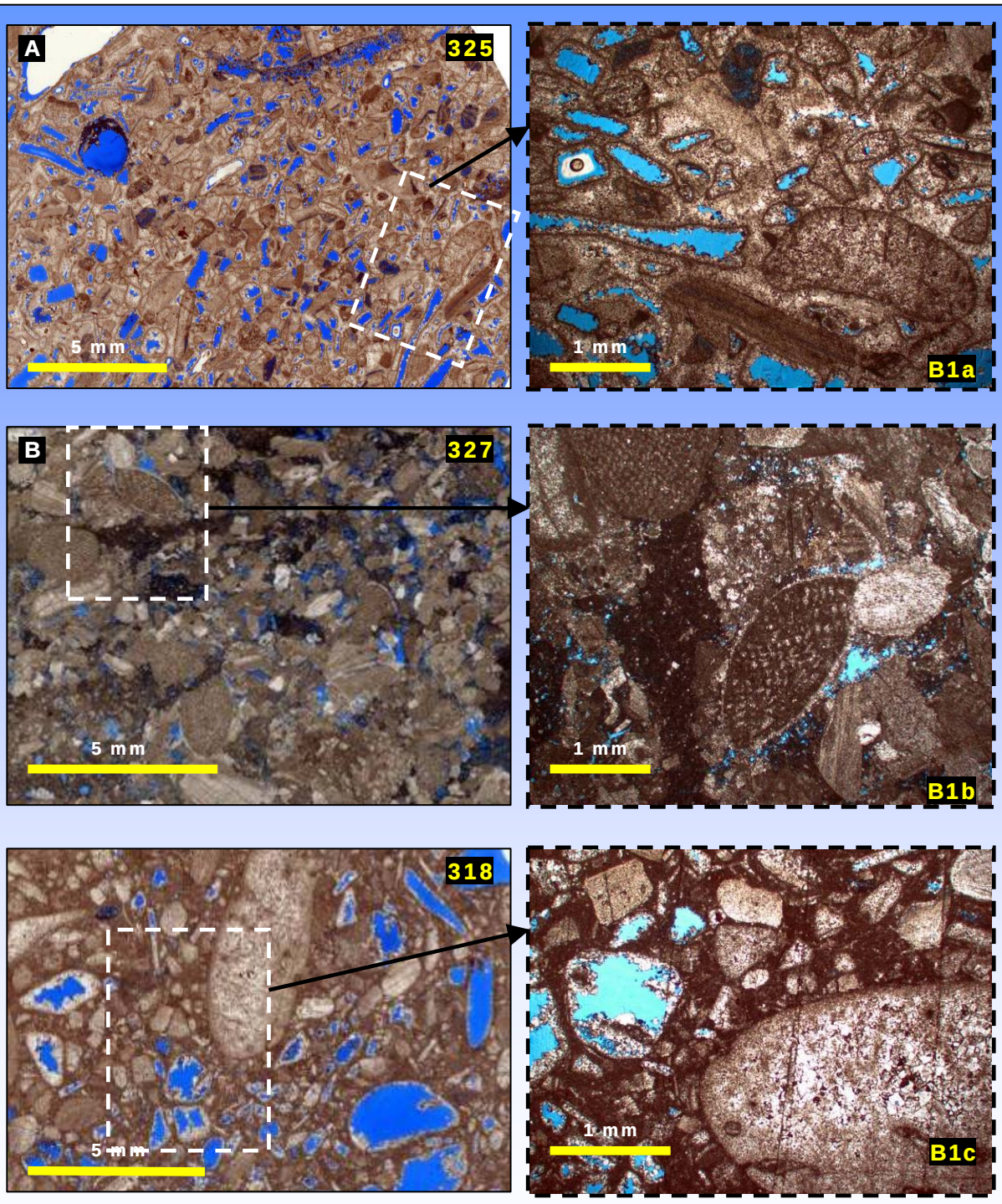

Figure 3.13 – Subfacies B1a, B1b and B1c

A) Subfacies B1a – Grainstone. Sample 325 originates from a lithofacies B1 clast.
B) Subfacies B1b – Grain-dominated packstones. Sample 327 displaying *Orbitolina sp.*
C) Subfacies B1c – Mud-dominated packstones. Sample 318 displays subfacies B1c and originates from a B1 megabreccia clast.

DESCRIPTION AND INTERPRETATION OF SUBFACIES TO LITHOFACIES B1

Subfacies B1a is a grainstone dominated by moldic porosity (figure 3.13). Grains display a bimodal distribution of well-rounded, well-sorted lime sands and poorly sorted, less rounded skeletal fragments. Individual grains show borings and have well developed micrite envelopes. Isopachous cement precipitated onto the commonly dissolved grains. Equant cement grows onto the early isopachous rim.

Interpretation: Subfacies B1a sands originate from high-energy areas of the platform margin, where reworking by tides and/or waves produced this relatively mature sediment. Rudist probably colonized the sand-banks from which this subfacies was derived, and produced the described skeletal fragments. These were also subject to reworking in this higher-energy environment, but to a lesser extent, prior to lithification. This subfacies lithified and underwent diagenetic alterations prior to erosion and re-sedimentation.

Subfacies B1b displays a grain-dominated packstone, cemented by lime mud (figure 3.13). Rudist fragments are abundant and constitute the bulk of the poorly sorted, moderately rounded grains of this packstone (rudstone). *Orbitolina sp.* is common but not abundant throughout the available samples. Grains are coated by thin rims of isopachous, bladed cement. Interparticle porosity is dominant, but samples also display selective-dissolution moldic pores.

Interpretation: Subfacies B1b is interpreted to originate from low-energy areas of the platform margin-to-upper slope. Grains were derived from the adjacent higher-energy marginal. They were lithified prior to their re-deposition.

Subfacies B1c show is a mud-dominated packstone with cemented skeletal grains and well rounded pebbles. Grains are poorly sorted and variably rounded (figure 3.13). Moldic porosity is dominant, but interparticle porosity occurs. Some molds are lined with calcite cement.

Interpretation: Subfacies B1c originates from the protected low-energy environments in the marginal platform area. Grains originate from higher-energy areas on the adjacent platform margin.

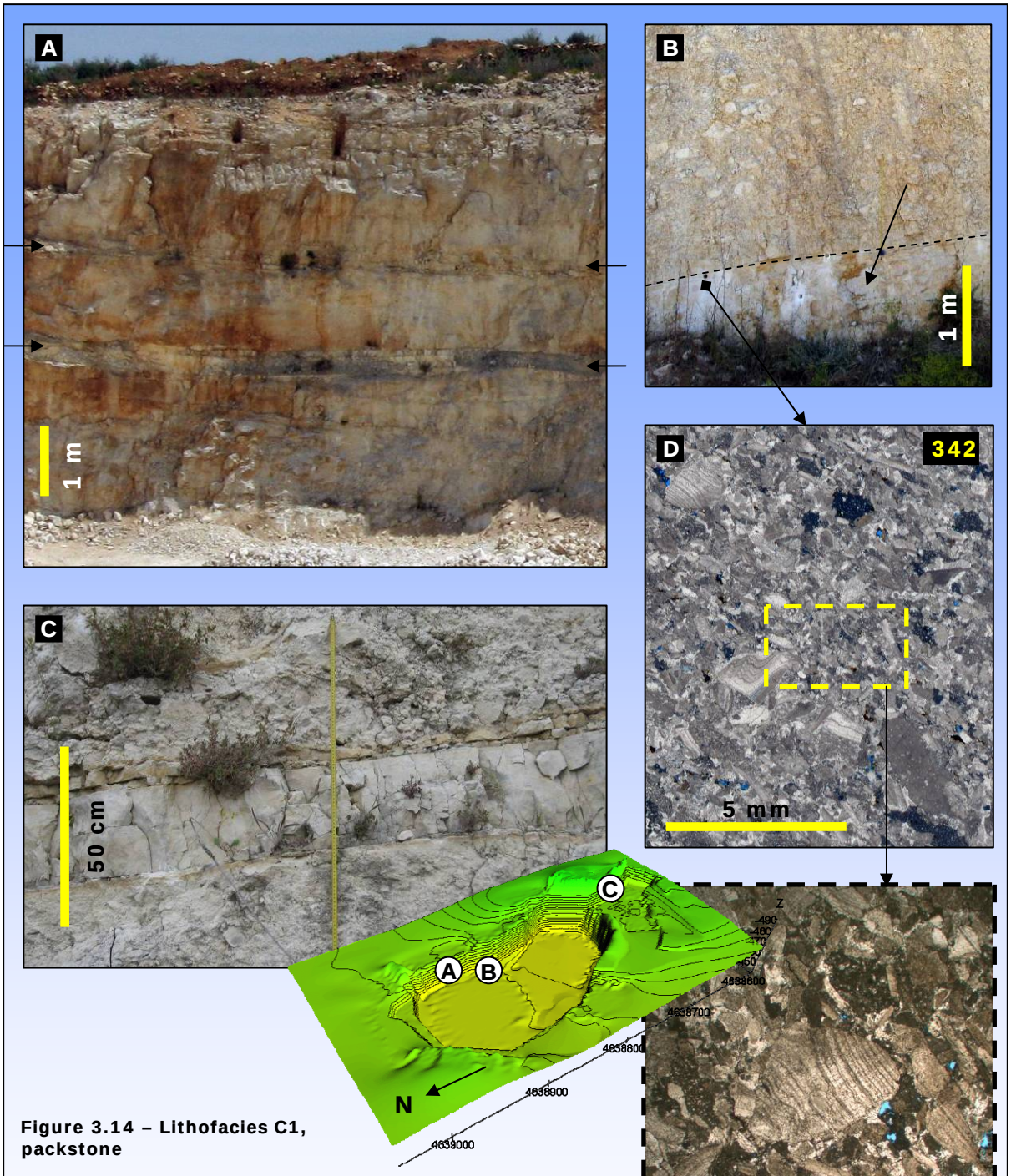

Figure 3.14 – Lithofacies C1, packstone

A) Southern parts of Vico del Gargano quarry east wall display facies C1 (indicated by arrows) separating segments of upper unit C. Due to faulting in this area, these clinoforms of unit C in this particular area appear horizontal, while as in the rest of the quarry, they dip toward the north.
B) Facies C1 displayed further north with respect to (A). See topographic model with positions indicated. Holes are sample-sites. Stapled line indicates the boundary towards overlying segment of facies C2 – matrix-supported megabreccia.
C) Facies C1 separating units B and C, in the southern parts of the quarry.
D) Sample 342 displays a dense packstone with rounded skeletal grains and little porosity.

INTERPRETATION OF UNIT B

Interpretation: Unit B/lithofacies B1 is interpreted as a single-event, grain-flow deposit which originated on the upper-slope/marginal areas of the platform, deposited on the lower-slope. The lack of matrix indicates that lithoclasts were densely lithified prior to re-sedimentation, and also indicates that transport distance was short. This is underpinned by the occurrence of large, irregular clasts with preserved internal bedding of the platform interior environment.

DESCRIPTION OF UNIT C AND CORRESPONDING LITHOFACIES

Unit C constitutes the bulk of the mapped Vico del Gargano succession. It consists of two lithofacies; C1 (packstone) and C2 (matrix-supported rudist megabreccias 2). The latter is the dominant facies, whereas the first only appear in thin (~ 30 cm) intervals within the succession, defining clinoforms (Rich, 1951) separating the megabreccia bodies.

Unit C caps unit B but where unit B is pinched out (middle and northern parts of the quarry), unit C rests directly onto unit A. Total mapped thickness of unit C is 46 meters with internal megabreccia bodies showing thicknesses of approximately 5-10 meters. Some clinoforms consists of 10-30 cm packstone layers that locally show evidences of soft-sediment deformation.

Lithofacies C1 consists of dense packstones. Its grains are of bimodal distribution with fairly sorted and rounded sands and scattered larger skeletal fragments (*Orbitolina sp.*, bivalves and rudists) (figure 3.14). Grains are moderately rounded and skeletal fragments are less than 2 mm in size.

Lithofacies C2 is a matrix-supported rudist megabreccia. It is segmented into multiple stacked 5-10 beds, separated by clinoforms (figure 3.15). Compared to lithofacies B1, these megabreccias are better sorted and appear more organized. The present dataset does not support mapping of subfacies within these megabreccias. Boundaries are well defined, and apparently non-erosive.

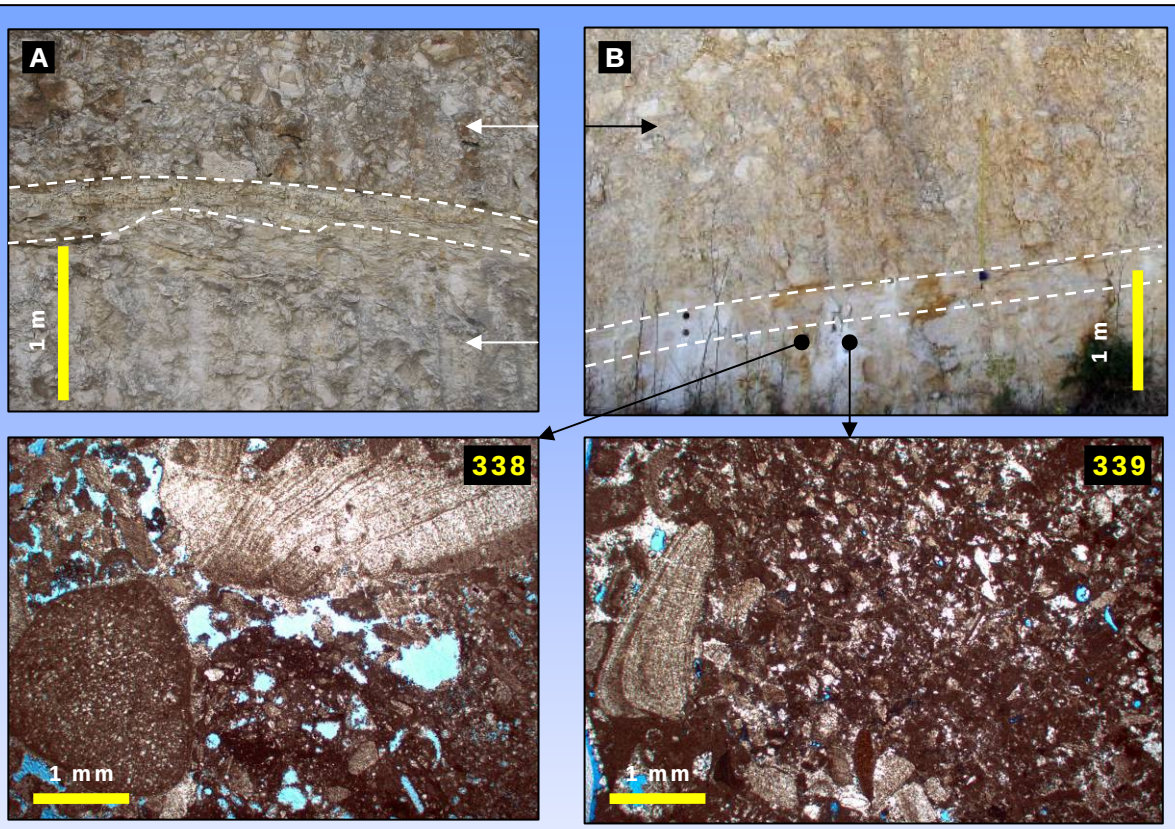

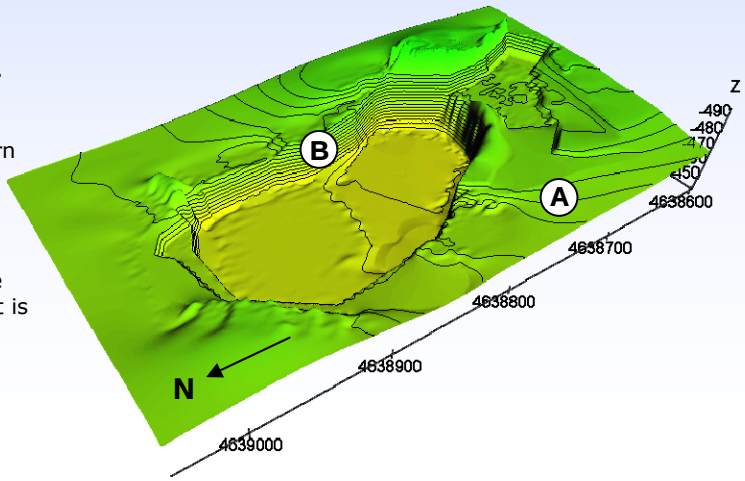

Figure 3.15 – Lithofacies C2, matrix-supported megabreccias 2

A) Facies C2 as displayed in the western parts of the outcrop (old quarry), separated by a soft-sediment deformed intralayer of facies C1. White arrows indicate facies C2.
B) Facies C1 as displayed in the middle parts of the main quarry. Lower unit is facies C1. Facies C2 is indicated by black arrow.

Samples 338 and 339 display mud-dominated *Orbitolina* packstones.

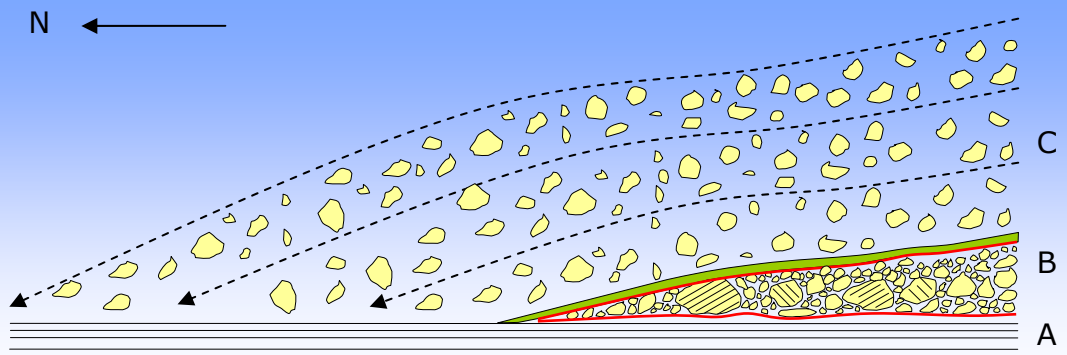

Figure 3.16A – Unit C downlaps onto unit A.

INTERPRETATION OF UNIT C

Interpretation: Lithofacies C1 is interpreted as the result of highstand shedding (Eberli & Ginsburg, 1989; James & Kendall, 1992; Schlager et.al.*, 1994; Maurer, 2000; Rendle & Reijmer, 2002) of sediments derived from the adjacent carbonate platform. These sediments were deposited as low-density turbidites or grain-flows. It constitutes the clinoforms that separate the megabreccias of lithofacies C2.*

Interpretation: Lithofacies C2 consists of matrix-supported megabreccias which are interpreted as debris-flow deposits on the lower-slope. Lithoclasts were derived from the upper slope and marginal areas of the adjacent carbonate platform. Matrix composition resembles that of litholasts, reflecting the disintegration of lithoclasts and incorporation of additional facies during transport.

Interpretation: Unit C is interpreted as debris flow deposits laid down on the lower slope. Main source of sediments was the marginal- and upper-slope environments. Unit C downlap onto unit A (figure 3.16A/B), and is segmented by clinoforms.

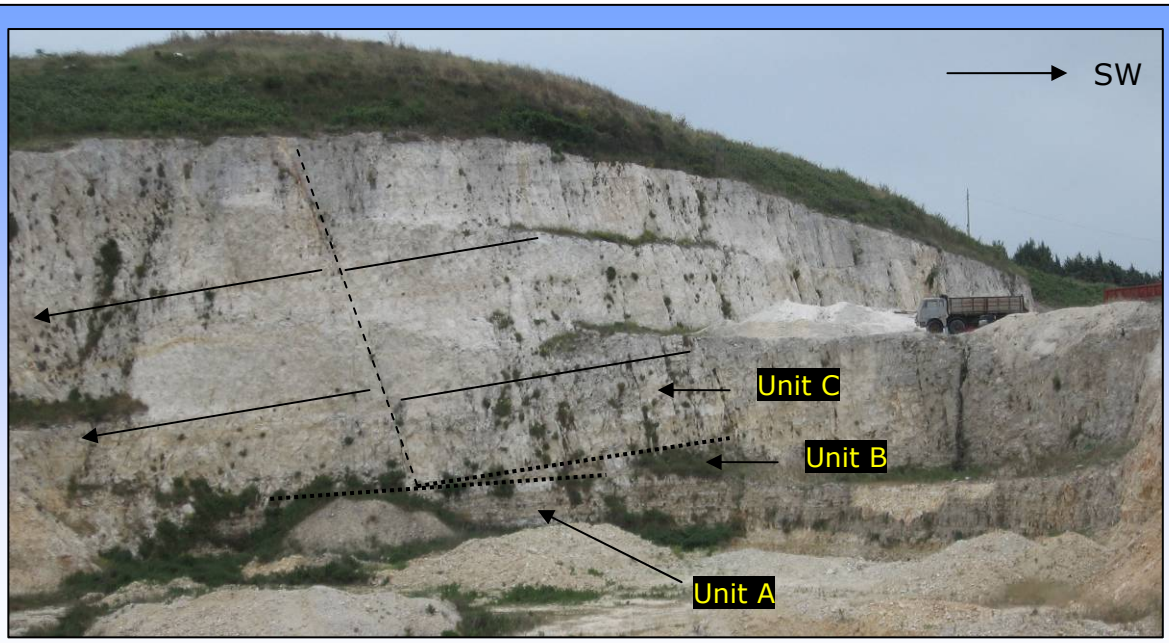

Figure 3.16B – Unit C downlaps onto unit A

Middle quarry, looking south-east.

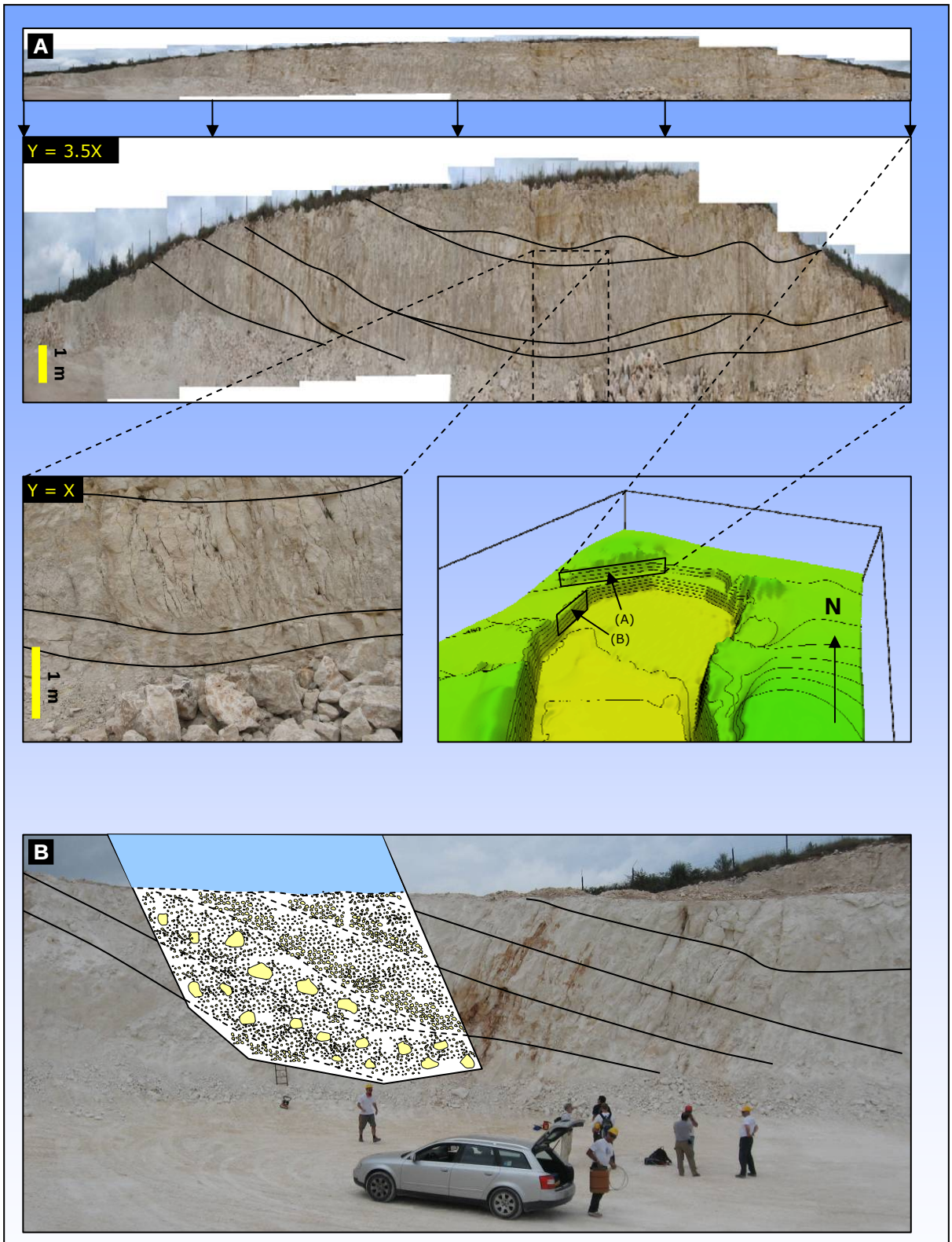

Figure 3.17 – Unit D

A) Overview photo-stitch displaying the upper north quarry wall, non-distorted photo and 3X vertical distance photo with some internal boundaries indicated.
B) Lower, westernmost parts of northern quarry wall. Internal boundaries indicated. Sketch slices photo and displays changes in fabric.

DESCRIPTION OF UNIT D AND CORRESPONDING LITHOFACIES

Unit D is, in stratigraphic terms, the uppermost mapped unit of the Vico del Gargano quarry succession. It displays multiple internal boundaries, separating two mapped facies; matrix-supported megabreccias (D1) and coarse graded grainstones (D2) and the overall package display the shape of an anticline (figure 3.17).

The internal unit D bodies thin towards E and W and generally thicken towards the intra-body centers. Some internal boundaries show erosive lower bases. This unit is mapped on the same level as the uppermost parts of unit C. The transition between the mapped upper parts of unit C and unit D is not exposed.

Lithofacies D1 consists of matrix-supported megabreccias confined to lense-shaped bodies of around 1 meter that thin towards the west and the east in the exposed section. No evidence of erosion was observed in relations to these confined megabreccia bodies. Subfacies of this lithofacies are described below.

Lithofacies D2 is interbedded with the megabreccias of lithofacies D1. It displays graded grainstones, confined to bodies showing thicknesses of up to 1 meter. Lateral termination is not observed, but the erosive beds generally thin toward the edges of the exposed section, towards east and west. The lower parts of these deposits are coarse calcarenites to fine calcirudites and may locally classify as floatstones. They grade up trough calcarenites that show planar laminations. Rare layers display massive sands above the planar laminated subdivision. The grainstones are dominated by interparticle porosity between calcarenite skeletal fragments that are well sorted but not particularly rounded (fig 3.18). Benthic foraminifers are common, but not abundant. Rudist- and bivalve fragments are observed. Nonfabric-selective porosity occurs along with rare intraparticle porosity, but the general dominance is of interparticle porosity.

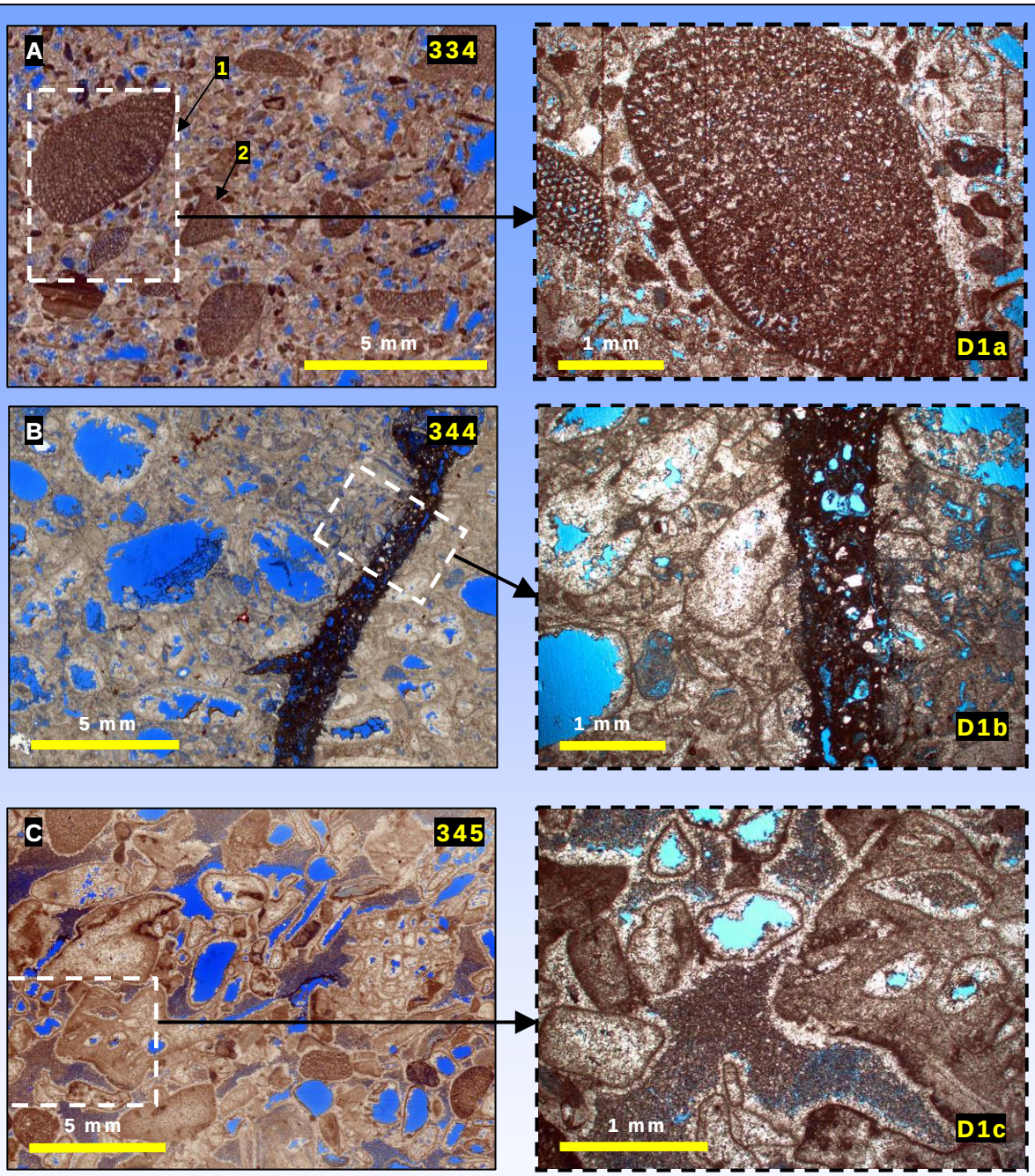

Figure 3.18 – Subfacies D1a, D1b and D1c

A) Subfacies D1a – Grainstones. Sample 334 displays abundant benthic foraminifers. 1: *Orbitolina (Conicorbotilina) Concava*, 2: *Orbitolina (Conicorbitolina) conica (D'Archiac,* 1837).
B) Subfacies D1b – Grain-dominated packstones. Sample 344 display dominance of moldic porosity, cut by late nonfabric-selective pore with recent silts.
C) Subfacies D1c – Mud-dominated packstones. Sample 345 displays rounded grainstone extraclasts, rounded pebbles with bladed calcite cement coating and skeletal fragments.

DESCRIPTION AND INTERPRETATION OF SUBFACIES TO LITHOFACIES D1

Subfacies D1a consists of grainstones with an abundance of well preserved benthic forams of different sizes, but they are generally significantly larger than the grainstone grains. The grainstones display well-sorted, poorly rounded skeletal fragments.

Interpretation: Subfacies D1a is interpreted as extraclasts derived from the foreslope where it originally was deposited through gravity-driven processes and highstand-shedding. Benthic foraminifers accumulated on top of this sandy deposit. It was re-deposited through debris-flows and now occurs within lithoclasts and matrix to the megabreccia beds of lithofacies D1. Benthic foraminifers are interpreted as Orbitolina (Conicorbitolina) conica sp. and Orbitolina (Conicorbitolina) concava sp. (D'Archiac, 1837) (figure 3.18A).

Subfacies D1b consists of grain-dominated packstones cemented by micrite mud. Grains are pellets and rudist fragments. Non-fabric selective porosity and intraparticle porosity is observed, but the subfacies is dominated by interparticle porosity. Moldic pores are defined by micrite envelopes, and lined with calcite cement. However, the grains show very little calcite cement coating.

Interpretation: Subfacies D1b consists of extraclasts derived from the upper slope and margin. It was re-sedimented through debris-flows and occurs in both matrix and clasts of the D1 megabreccias. The lack of cement on the outside (coatings) of grains and the abundant calcite cement on the inside (linings) of moldic pores, suggest that cementation occurred post-depositional of these megabreccias.

Subfacies D1c displays mud-dominated packstones with micrite-cemented extraclasts of grainstones (figure 3.18B) and packstones (figure 3.18C), as well as bivalve fragments. Moldic pores are abundant and most grain shapes are preserved only by micrite envelopes. Molds are lined, and most extraclasts are coated with, isopachous bladed calcite cement.

Interpretation: Subfacies D1c packstones are interpreted as elements originating from the platform margin and/or foreslope environments. These sediments were lithified prior to re-deposition.

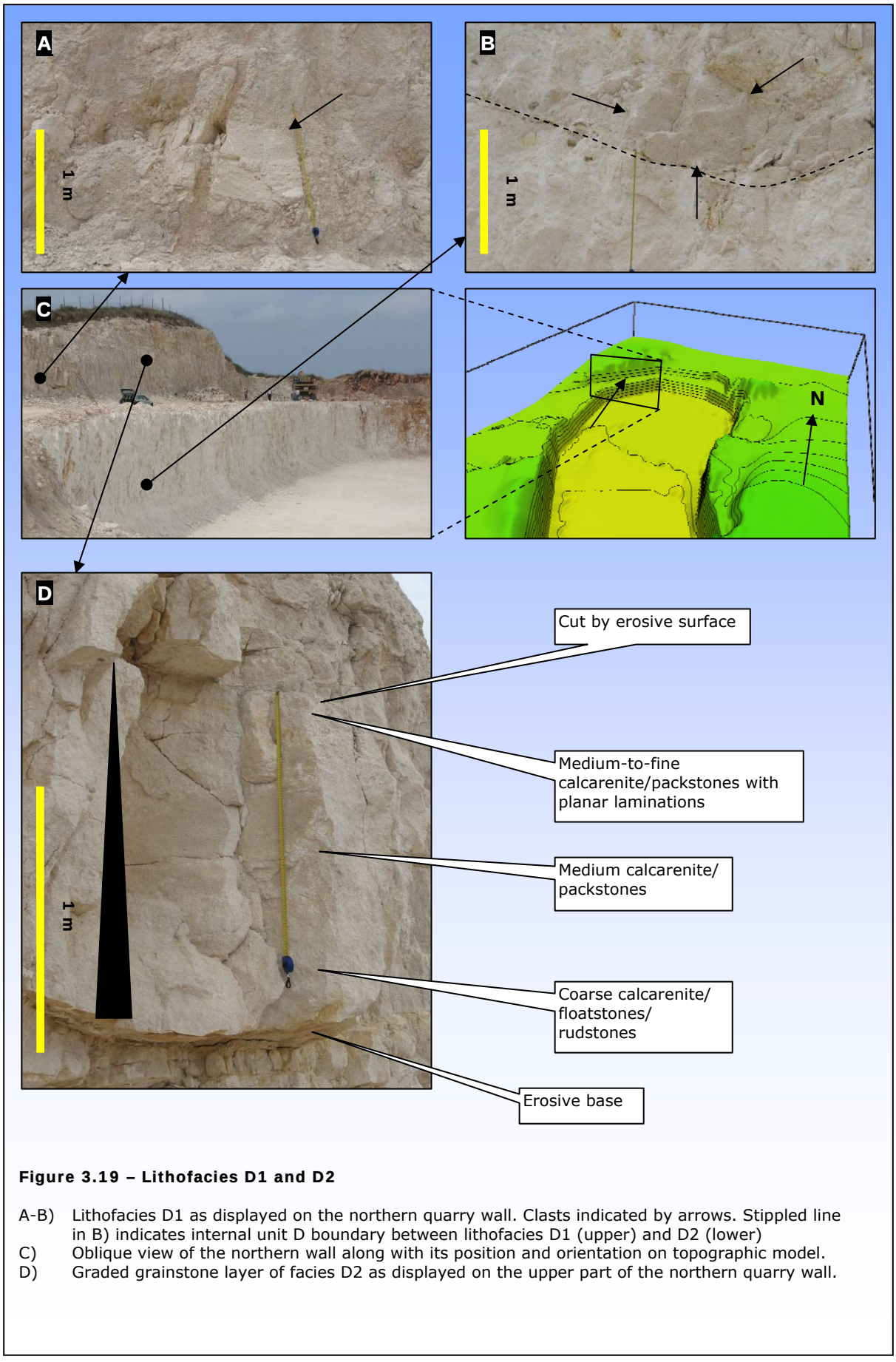

Figure 3.19 – Lithofacies D1 and D2

A-B) Lithofacies D1 as displayed on the northern quarry wall. Clasts indicated by arrows. Stippled line in B) indicates internal unit D boundary between lithofacies D1 (upper) and D2 (lower)
C) Oblique view of the northern wall along with its position and orientation on topographic model.
D) Graded grainstone layer of facies D2 as displayed on the upper part of the northern quarry wall.

INTERPRETATION OF UNIT D

Interpretation: Lithofacies D1 is interpreted as debris flows on the middle-to-lower slope. Lithoclasts were derived from the marginal areas of the platform, where they were lithified or semi-lithified prior to re-sedimentation. Subfacies D1a (grainstones) are recognized within both lithoclasts and matrix to these megabreccias, indicating that matrix and lithoclasts predominantly was produced by sediments from the same source. The disintegration of lithoclasts, and possibly the incorporation of additional facies during transport contributed to the matrix.

Interpretation: Lithofacies D2 consists of grainstones which are interpreted as proximal turbidite flow deposits commonly displaying Bouma-divisions A and B and rarely C (Bouma, 1962) (figure 3.19). Their paths were largely controlled by submarine topography, and an overall channeled pattern is recognized.

Interpretation: Unit D displays an alternating succession of debris-flow deposits (D1) and proximal turbidites (D2). Depositional pattern suggests that the deposits are channeled, by the control of submarine topography. Sediments were derived from the marginal areas of the platform, where high-energy environments produced mature sediments, but mud-dominated facies also occur within this unit indicating that lower-energy environments also contributed to the components of this unit.

PETROPHYSICAL DATA

This section presents the petrophysical database, according to locality (tables 3.2A/B). Samples that lack permeability and/or porosity measurements are omitted from all further presentations of data related to poroperm transforms and relationships. Each sample is assigned a numerical sample ID. Samples # 0-200 refer to Malpasso Valley samples, while samples #300-400 refer to Vico del Gargano samples. Samples originating from the Malpasso west-wall grid (figure 3.20) also have individual grid-ID's referring to the samples position within the grid (*Column#-Row#*). *Measured permeability* and *measured porosity* refer to numbers derived from laboratory measurements. *Estimated porosity* and *estimated permeability* refer to numbers derived from estimation methods.

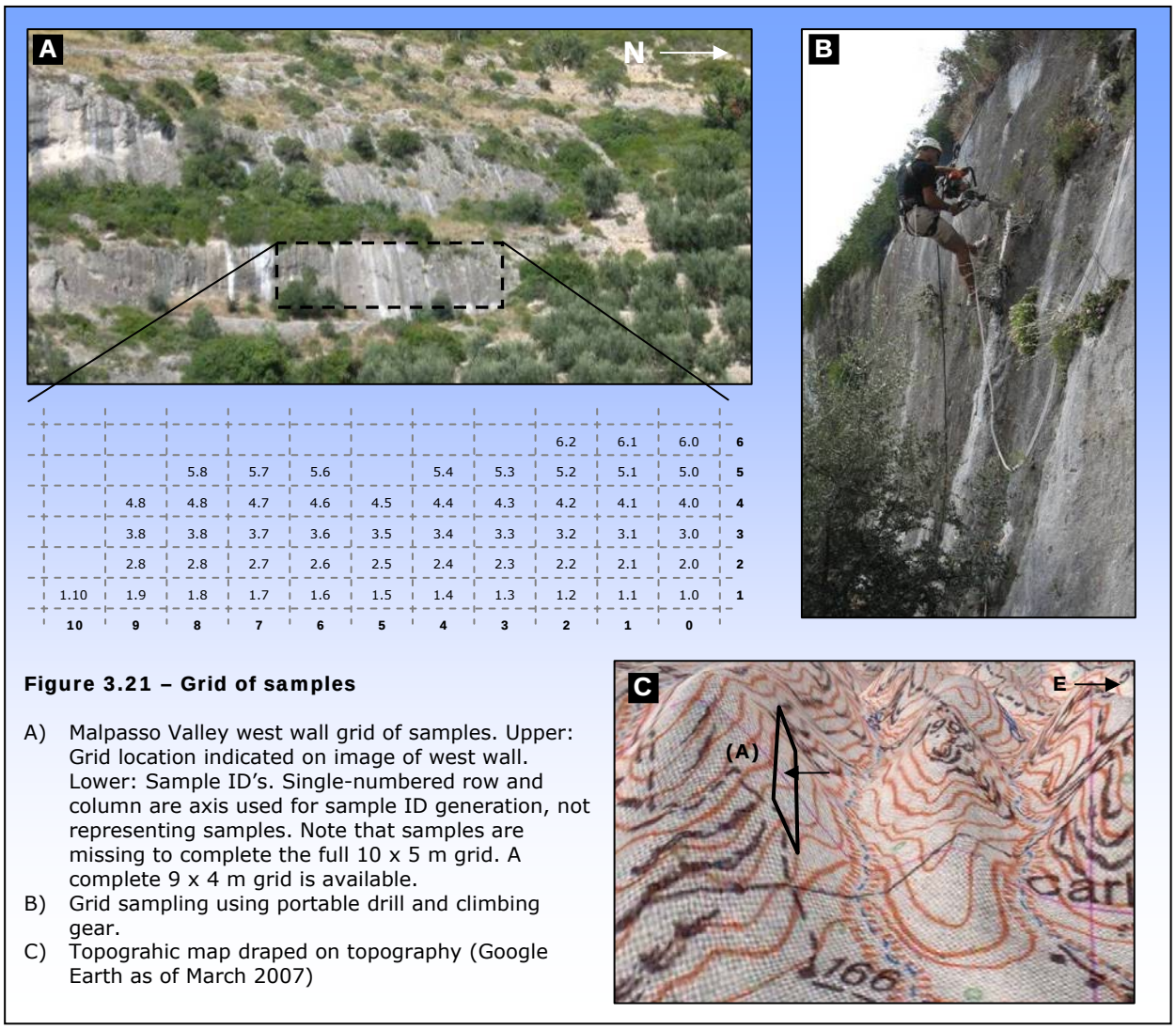

Figure 3.21 – Grid of samples

A) Malpasso Valley west wall grid of samples. Upper: Grid location indicated on image of west wall. Lower: Sample ID's. Single-numbered row and column are axis used for sample ID generation, not representing samples. Note that samples are missing to complete the full 10 x 5 m grid. A complete 9 x 4 m grid is available.
B) Grid sampling using portable drill and climbing gear.
C) Topograhic map draped on topography (Google Earth as of March 2007)

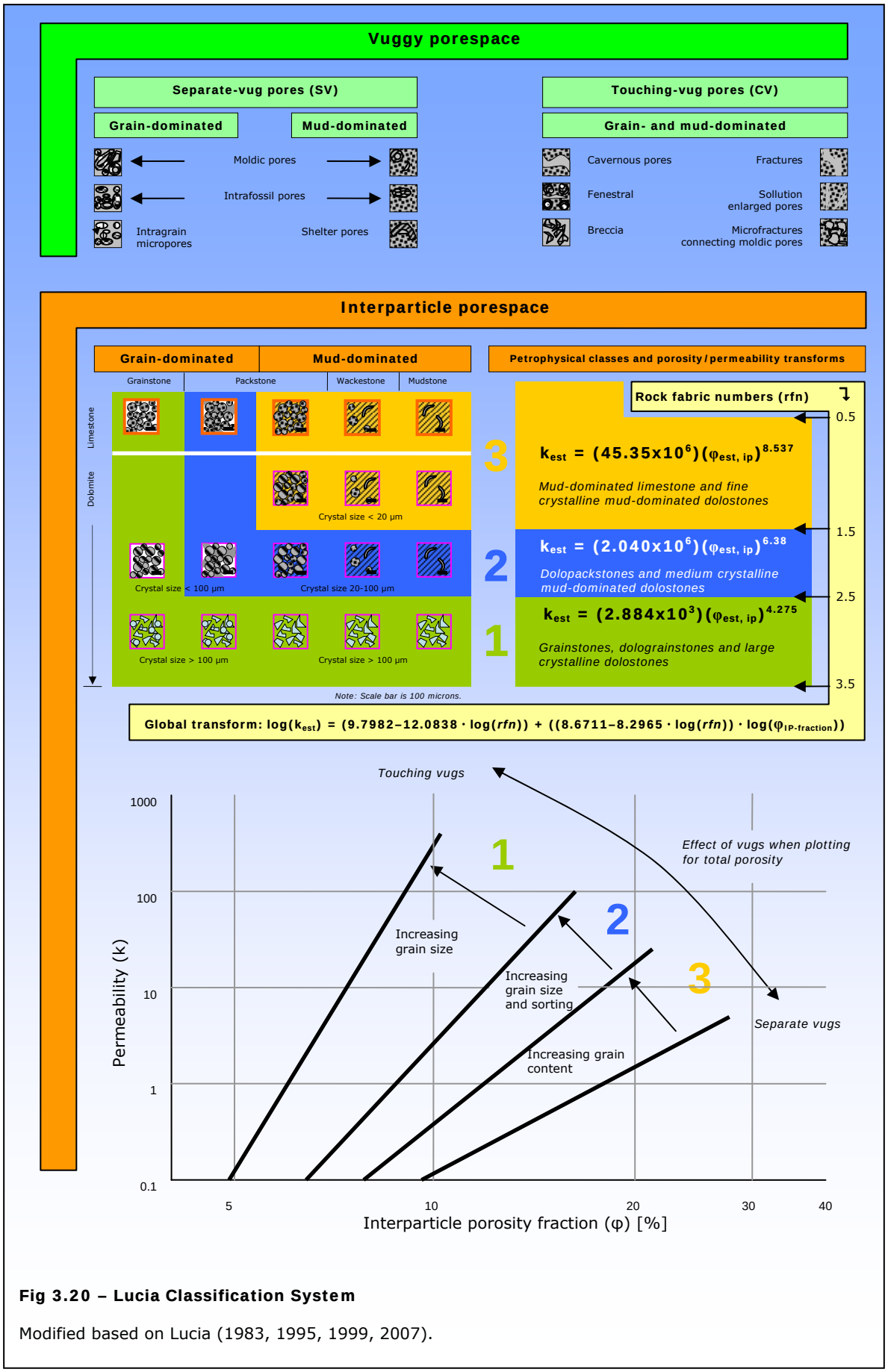

Fig 3.20 – Lucia Classification System

Modified based on Lucia (1983, 1995, 1999, 2007).

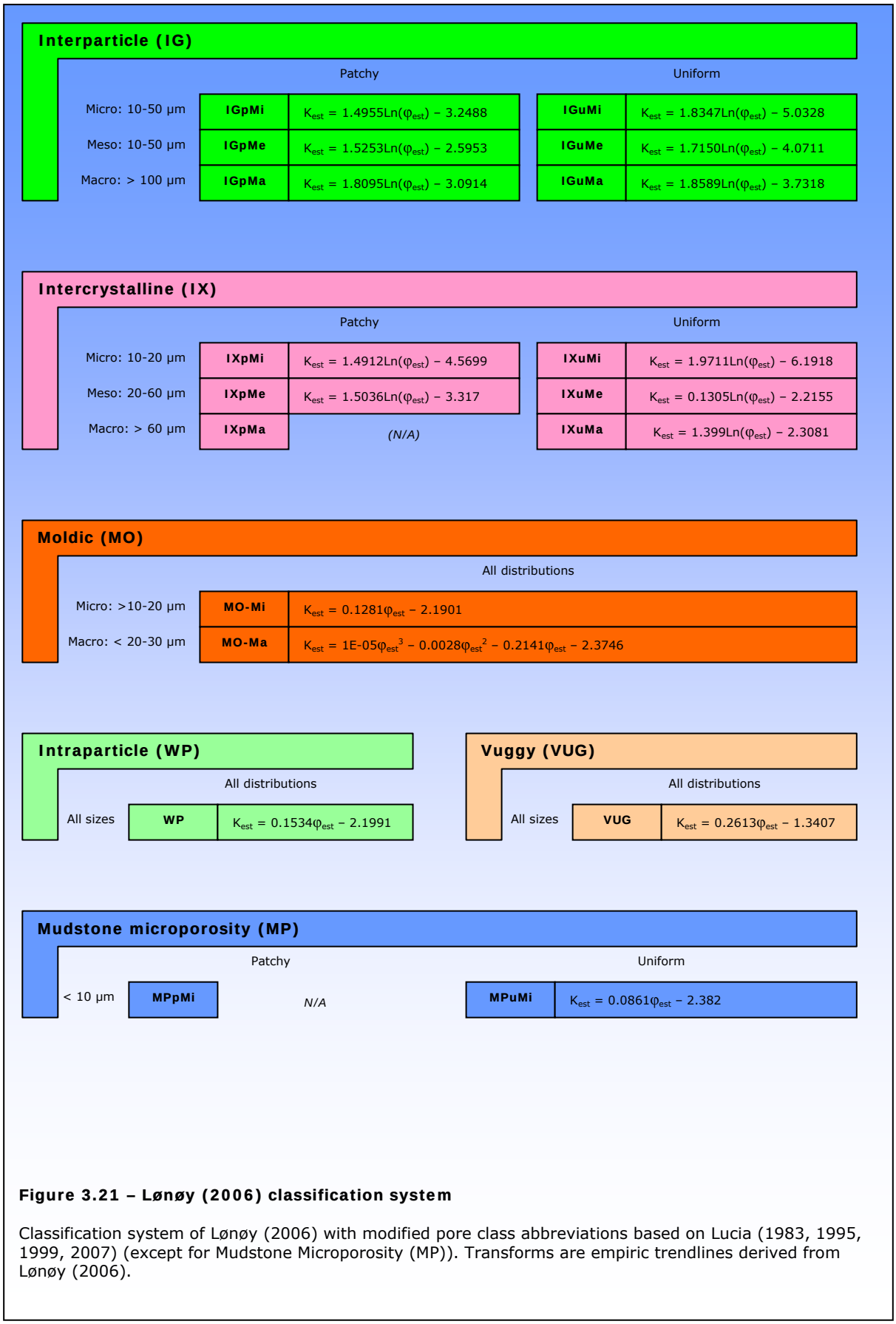

Figure 3.21 – Lønøy (2006) classification system

Classification system of Lønøy (2006) with modified pore class abbreviations based on Lucia (1983, 1995, 1999, 2007) (except for Mudstone Microporosity (MP)). Transforms are empiric trendlines derived from Lønøy (2006).

Table 3.2A – Petrophysical data, Malpasso Valley

						Lucia (1983, 1995, 1999, 2007)			Lønøy (2006)		
Grid ID	ID	Lithofacies/ subfacies	$\varphi_{meas, eff}$	$k_{meas, abs}$ [mD]	$\varphi_{est, eff}$	Dominant poretype	IP fraction	$k_{est, abs}$ [mD]	Dominant poretype	$k_{est, abs}$ [mD]	Remarks
1.0	32	M1a	**18.8 %**	**25.2**	**17.1 %**	IP	15.3 %	**528.6**	IGuMe	**9.1**	
1.1	22	M1a	**21.8 %**	**6.83**	**19.6 %**	SV	7.5 %	**0.2**	MO-Ma	**11.6**	
1.2	23	M1a	**22.5 %**	**305**	**17.2 %**	IP	1.9 %	**0.0**	IGuMe	**18.5**	
1.3	24	M1c	**23.8 %**	**132**	**14.6 %**	TV	4.1 %	**0.0**	VUG	**201.1**	
1.4C	25	M1d	**19.9 %**	**2.02**	**10.4 %**	SV	6.0 %	**0.0**	MO-Ma	**7.2**	
1.4M	25	M1c	**18.0 %**	**4.19**	**3.9 %**	TV	2.7 %	**0.0**	VUG	**26.4**	
1.5	26	M1c	**15.6 %**	**1.05**	**7.1 %**	SV	1.1 %	**0.0**	MO-Ma	**2.1**	
1.6	27	M1b	**15.0 %**	**0.49**	**6.5 %**	IP	5.6 %	**0.1**	IGuMe	**3.8**	
1.7	28	M1a	**12.0 %**	**45.8**	**5.8 %**	IP	12.0 %	**67.1**	IGuMe	**1.6**	
1.8	29	M1b	**20.4 %**	**31.9**	**7.3 %**	IP	8.4 %	**0.3**	IGuMe	**12.6**	
1.9	30	M1b	**21.6 %**	**158**	**15.0 %**	IP	7.8 %	**1.6**	IGuMe	**15.9**	
1.10	31	M1a	**20.9 %**	**104**	**19.2 %**	IP	7.0 %	**0.6**	IGuMe	**13.8**	
2.0	33	M1b	**17.9 %**	**29**	**4.7 %**	IP	5.4 %	**0.0**	IGuMe	**7.5**	
2.1C	38	M1d	**24.4 %**	**268**	**20.2 %**	TV	10.0 %	**1.0**	VUG	**250.4**	
2.1M	38	M1c	**15.9 %**	**2.64**	**8.1 %**	TV	1.4 %	**0.0**	VUG	**12.7**	
2.2	43	M1b	**21.5 %**	**13.6**	**10.0 %**	SV	6.9 %	**0.1**	IGuMe	**15.5**	
2.3	48	M1a	**20.5 %**	**9.89**	**13.5 %**	SV	4.8 %	**0.0**	IGuMe	**12.9**	
2.4	52	M1a	**24.9 %**	**158**	**11.1 %**	SV	4.6 %	**0.0**	MO-Ma	**23.8**	
2.5	56	M1b	**16.5 %**	**5.04**	**4.5 %**	IP	7.0 %	**0.1**	IGuMe	**5.5**	
2.6	70	M1b	**22.0 %**	**248**	**14.5 %**	SV	10.8 %	**1.6**	VUG	**108.6**	
2.7	59	M1b	**23.2 %**	**209**	**15.8 %**	IP	2.6 %	**0.0**	IGuMe	**21.1**	
2.8	63	M1c	**25.2 %**	**23.9**	**7.0 %**	IP	3.1 %	**0.0**	IGuMe	**29.1**	
2.9	67	M1d	**24.4 %**	**7.48**	**4.5 %**	IP	6.0 %	**0.0**	MO-Ma	**21.2**	
3.0	34	M1b	**22.1 %**		**5.5 %**	SV	8.0 %	**0.2**	IGuMe	**17.3**	No measured k
3.1	39	M1d	**18.5 %**	**2.42**	**5.6 %**	SV	4.0 %	**0.0**	MO-Ma	**4.9**	
3.2	44	M1c	**21.4 %**	**36**	**8.8 %**	IP	12.8 %	**4.5**	IGuMe	**15.2**	
3.3	49	M1d	**23.1 %**		**10.9 %**	IP	16.2 %	**18.9**	IGuMe	**20.6**	No measured k
3.4C	53	M1a	**20.8 %**	**0.67**	**18.9 %**	IP	14.5 %	**342.8**	MO-Ma	**9.0**	
3.4M	53	M1b			**7.3 %**	IP			IGuMe		Bad quality thin-section
3.5	57	M1b	**20.0 %**	**2.67**	**9.0 %**	IP	8.0 %	**0.2**	IGuMe	**11.7**	
3.7	60		**21.4 %**	**23.9**	**0.0 %**						No thin-section
3.8	64	M1a	**15.2 %**	**2.02**	**7.3 %**	IP	9.1 %	**6.1**	IGuMe	**4.0**	
3.9	68	M1b	**27.6 %**	**200**	**10.6 %**	SV	22.1 %	**8.7**	MO-Ma	**40.9**	
4.0	35	M1c	**23.7 %**	**38**	**7.3 %**	SV	10.1 %	**1.0**	MO-Ma	**18.2**	
4.1	40	M1a	**24.2 %**	**54**	**8.6 %**	SV	2.4 %	**0.0**	MO-Ma	**20.4**	
4.2	45		**20.4 %**	**12.9**	**0.0 %**						No thin-section
4.3	50	M1c	**16.0 %**	**52.3**	**9.2 %**	IP	14.4 %	**1.1**	IGuMe	**4.8**	
4.4	54	M1b	**14.1 %**	**2.66**	**3.2 %**	IP	12.7 %	**4.2**	IGuMe	**2.9**	
4.5	58	M1c			**7.9 %**	TV			VUG	**0.0**	No measurements
4.6	72	M1d	**20.3 %**	**19.7**	**10.0 %**	IP	12.2 %	**3.3**	IGuMe	**12.3**	
4.7	61	M1a	**23.7 %**	**46.2**	**17.4 %**	IP	9.5 %	**8.5**	IGuMe	**22.9**	
4.8	65	M1d			**10.6 %**	SV			MO-Ma		No measurements
4.9	69	M1c	**15.6 %**	**7.12**	**2.3 %**	SV	1.6 %	**0.0**	MO-Ma	**2.1**	
5.0	36	M1c	**16.9 %**	**6.8**	**2.8 %**	IP	8.5 %	**0.3**	IGuMe	**6.0**	
5.1	41	M1c	**21.9 %**	**39.3**	**16.0 %**	SV	4.4 %	**0.0**	MO-Ma	**12.0**	
5.2	46	M1b	**12.1 %**	**3.01**	**6.4 %**	IP	4.8 %	**0.0**	MO-Ma	**0.7**	
5.3	51	M1b	**18.7 %**	**7.76**	**12.7 %**	IP	11.2 %	**2.0**	IGuMe	**9.0**	
5.4	55	M1b	**17.6 %**	**26.4**	**8.9 %**	IP	12.3 %	**3.5**	IGuMe	**7.0**	
5.5	??	M1b	**14.7 %**	**0.32**	**7.4 %**	TV	4.4 %	**0.0**	VUG	**8.2**	
5.6	73	M1b	**17.4 %**	**4.72**	**7.5 %**	IP	12.2 %	**3.3**	IGuMe	**6.8**	
5.7	62	M1a	**18.3 %**	**0.648**	**10.4 %**	SV	7.3 %	**0.9**	MO-Ma	**4.7**	
5.8	66	M1a	**13.7 %**	**5.75**	**11.0 %**	SV	2.7 %	**0.0**	MO-Ma	**1.1**	
6.0	37	M1a	**27.6 %**	**142**	**9.0 %**	IP	13.8 %	**220.2**	IGuMe	**41.7**	
6.1	42	M1a	**23.7 %**	**15.5**	**10.1 %**	IP	16.6 %	**1076.8**	IGuMe	**22.8**	
6.2	47	M1b	**10.1 %**	**0.17**	**4.5 %**	SV	6.1 %	**0.0**	MO-Ma	**0.3**	
	74	M1a	**19.0 %**	**3.515**	**10.3 %**	SV	1.5 %	**0.0**	MO-Ma	**5.7**	
	75	M1a	**22.6 %**	**11.165**	**26.5 %**	SV	4.3 %	**0.0**	MO-Ma	**14.0**	
	76	M1e	**19.0 %**	**9.431**	**6.9 %**	IP	6.9 %	**0.0**	IGuMe	**9.4**	
	77	M1d	**20.2 %**	**586.842**	**10.0 %**	IP	11.1 %	**1.9**	IGuMe	**12.1**	
	78	M1c	**20.7 %**	**1.129**	**9.2 %**	TV	10.0 %	**1.0**	VUG	**67.6**	
	80	M1b	**29.0 %**		**16.7 %**	SV	8.7 %	**4.0**	MO-Ma	**52.5**	No measured k
	82A	M1b	**21.5 %**	**40.5**	**16.1 %**	SV	2.2 %	**0.0**	MO-Ma	**10.8**	
	82B	M1b	**21.4 %**		**16.6 %**	SV	6.4 %	**0.3**	MO-Ma	**10.4**	No measured k
	83A	M1c	**29.1 %**	**134**	**13.1 %**	IP	17.5 %	**30.3**	IGuMe	**51.3**	
	83B	M1c	**21.2 %**	**12.1**	**3.5 %**	SV	6.4 %	**0.1**	MO-Ma	**10.0**	
	84A	M1c	**20.4 %**	**30.5**	**14.2 %**	TV	8.2 %	**0.3**	VUG	**61.5**	
	84B	M1c	**13.2 %**	**0.921**	**4.1 %**	SV	5.3 %	**0.1**	MO-Ma	**1.0**	
	85A	M1a	**22.5 %**	**203**	**10.3 %**	SV	4.5 %	**0.0**	MO-Ma	**13.8**	
	85B	M1c	**12.1 %**	**2.07**	**2.7 %**	SV	3.6 %	**0.0**	MO-Ma	**0.7**	
	100A	M1a	**22.4 %**	**3.81**	**15.8 %**	SV	2.2 %	**0.0**	Mo-Ma	**13.4**	
	100B	M1c	**22.2 %**	**12.8**	**13.3 %**	IP	15.5 %	**14.8**	IGuMe	**17.6**	
	101A	M1d	**18.5 %**		**7.0 %**	SV	7.4 %	**0.1**	MO-Ma	**4.9**	No measured k
	101B	M1c	**17.6 %**	**7.97**	**3.8 %**	IP	12.3 %	**3.6**	IGuMe	**7.1**	
	102	M1a	**21.4 %**	**12.9**	**16.3 %**	IP	12.8 %	**117.1**	IGuMe	**15.2**	
	103	M1d	**21.1 %**	**10.9**	**2.1 %**	IP	12.7 %	**4.2**	IGuMe	**14.4**	
	105A	M1b	**23.6 %**	**22.24**	**29.0 %**	TV	3.5 %	**0.0**	VUG	**187.9**	
	105B	M1c	**17.6 %**	**2.75**	**4.1 %**	IP	12.3 %	**3.5**	IGuMe	**7.0**	
	106A	M1a	**15.4 %**	**0.33**	**13.0 %**	IP	4.6 %	**0.0**	IGuMe	**4.1**	
	106B	M1b	**14.4 %**	**0.108**	**10.2 %**	SV	2.2 %	**0.0**	MO-Ma	**1.4**	
	107	M1b	**17.0 %**	**3.751**	**5.8 %**	SV	1.7 %	**0.0**	MO-Ma	**3.2**	
	108A	M1b	**22.7 %**		**34.4 %**	TV	7.9 %	**1.8**	VUG	**138.1**	No measured k
	108B	M1b	**27.5 %**	**37.26**	**19.7 %**	SV	11.0 %	**31.1**	MO-Ma	**40.5**	
	109	M1c	**19.3 %**	**7.167**	**4.1 %**	SV	7.7 %	**0.1**	MO-Ma	**6.2**	
	110	M1c	**20.1 %**	**2.86**	**15.4 %**	SV	8.0 %	**0.3**	MO-Ma	**7.6**	
	111	M1c	**22.7 %**	**17.73**	**8.3 %**	SV	6.8 %	**0.1**	MO-Ma	**14.4**	
	112A	M1d	**16.9 %**	**1.56**	**8.6 %**	SV	6.8 %	**0.1**	MO-Ma	**3.1**	
	112B	M1c	**16.6 %**	**8.389**	**15.4 %**	IP	13.3 %	**5.6**	IGuMe	**5.6**	
	113	M1d	**16.0 %**	**2.44**	**5.8 %**	SV	6.4 %	**0.1**	MO-Ma	**2.4**	

Table 3.2B – Petrophysical data, Vico del Gargano

					Lucia (1983, 1995, 1999, 2007)			Lønøy (2006)		
ID	Lithofacies/ subfacies	$\varphi_{meas,\ eff}$	$k_{meas.\ abs}$ [mD]	$\varphi_{est,\ eff}$	Dominant poretype	IP fraction	$k_{est.\ abs}$ [mD]	Dominant poretype	$k_{est.\ abs}$ [mD]	Remarks
313	B1b	22.1 %	0.537	17.4 %	SV	4.4 %	0.0	Mo-Ma	12.6	
314	B1b	25.0 %		13.3 %	SV	7.5 %	1.0	Mo-Ma	24.2	No measured k
318	B1c	19.8 %	0.311	15.6 %	SV	2.0 %	0.0	Mo-Ma	7.1	
319	C1	7.7 %	1.87	0.6 %	IP	7.7 %	2.0	IGuMe	0.3	
320	A1	8.4 %	1.71	5.7 %	IP	6.3 %	0.2	IGuMe	0.4	
325	B1a	14.2 %	0.021	13.3 %	SV	5.7 %	0.1	MO-Ma	1.3	
326	B1b	8.2 %	0.336	4.4 %	SV	0.8 %	0.0	MO-Ma	0.2	
327	B1b	10.3 %	2.41	3.2 %	IP	9.3 %	2.0	IGuMe	0.8	
328	B1b	6.1 %	0.120	3.5 %	IP	5.5 %	0.0	IGuMe	0.1	
332	C2	6.6 %	0.008	2.7 %	SV	2.0 %	3.0	MO-Ma	0.1	
333	C2	12.9 %	8.69	9.4 %	SV	3.9 %	0.0	MO-Ma	0.9	
334	C2	12.0 %		6.3 %	IP	9.6 %	9.4	IGuMe	1.6	No measured k
335	C2	13.5 %	0.62	3.9 %	SV	5.4 %	0.0	MO-Ma	1.1	
337	C1	20.2 %	2.76	4.2 %	IP	0.0 %	3.0	IGuMe	12.1	
338	C2	12.6 %		2.9 %	IP	11.3 %	0.4	IGuMe	1.9	No measured k
339	C2	10.8 %	0.189	1.0 %	IP	6.5 %	4.0	IGuMe	1.0	
340	C1	6.6 %		1.8 %	IP	6.6 %	0.4	IGuMe	0.1	No measured k
341	C1	2.8 %	0.012	0.0 %	IP	2.8 %	0.0	IGuMe	0.0	
342	C1	3.5 %	0.017	0.2 %	IP	3.5 %	0.0	IGuMe	0.0	
343	D1c	17.7 %	5.58	5.2 %	SV	8.8 %	2.0	MO-Ma	3.9	
344	D1b	31.6 %	58.4	15.8 %	SV	9.5 %	8.4	MO-Ma	81.4	
345	D1c	13.9 %	6.26	6.7 %	SV	4.2 %	3.0	MO-Ma	1.2	
346	D1a	17.4 %	735	11.2 %	IP	9.0 %	5.4	IGuMe	6.7	
351	D2	24.1 %	8453	17.9 %	IP	15.6 %	621.2	IGuMe	24.3	
352	D2	22.9 %	878	12.8 %	IP	22.9 %	161.6	IGuMe	19.9	
353A	D1a	15.0 %	0.659	10.1 %	IP	9.0 %	3.0	IGuMe	3.8	
353B	D1a	17.8 %	1.3	11.5 %	IP	14.2 %	283.5	IGuMe	7.3	
354	D1	21.6 %	838	12.1 %	IP	0.0 %	4.0	IGuMe	15.7	

4 STRATIGRAPHIC ANALYSIS

Data include four megabreccia units; Unit M (Malpasso Valley) in the south, Units B, C and D (Vico del Gargano) in the northern parts of Gargano. They show important differences in terms of depositional pattern, fabric and diagenetic succession. Logged sections are presented in chapter 3.

IMPORTANT DIFFERENCES AND SIMILARITIES

On outcrop scale, the southern and northern successions differ in terms of depositional pattern. The southern megabreccias (unit M) display an aggrading pattern of deposition, while the most prominent megabreccia unit of the northern succession (unit C) displays a prograding pattern of deposition that downlaps onto underlying distal slope facies of unit A. See figure 4.1 for geographic position of the individual units.

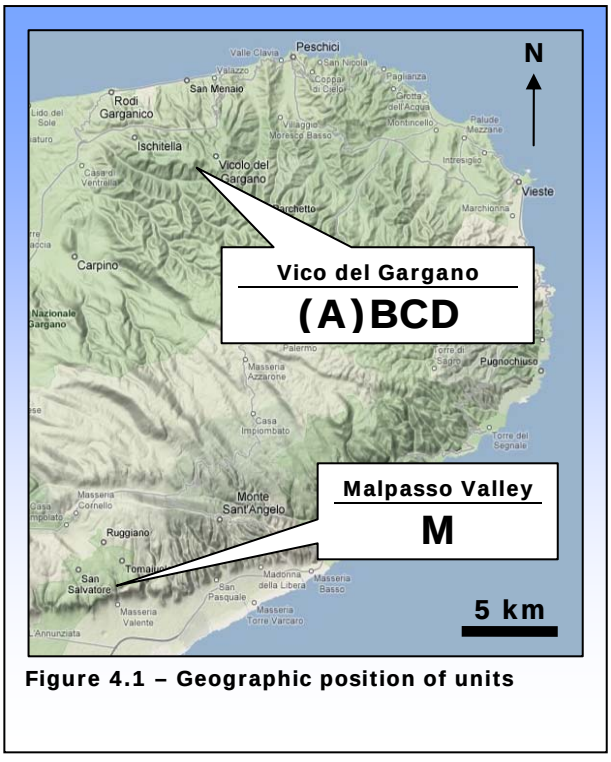

Figure 4.1 – Geographic position of units

The individual megabreccias differ in terms of fabric. Unit B displays clast-supported, poorly sorted and chaotic megabreccias with irregular lithoclasts that span from some few cm to several meters across. Units M and C display more organized, better sorted matrix-supported megabreccias. Unit C is segmented and display individual beds of 5-10 m that are separated by dense packstone clinoforms, while unit M display amalgamated beds of 10-15 m. Unit D exhibit megabreccias that are confined to thinner (1-2 m) beds, and interbed with proximal turbidites. Matrix is locally abundant and lithoclasts are scattered to a greater extent than the previously discussed units. Unit D appears to be controlled to some extent by submarine topography, and display a channeled geometry.

The three megabreccia units (M, C and D) that display matrix-supported fabrics were deposited as multiple-event debris-flows. These were matrix-supported also

during transport, and the breccias show indications of lithoclast disintegration during transport. The clast-supported unit B is interpreted as a grain-flow deposit in relations to a single-event submarine landslide, and displays no matrix.

Among the features that these breccias share, is the apparent similarities in textures and composition of lithoclast and matrix for the individual units. This indicates that matrix and lithoclasts of each unit were derived mostly from the same sources, which for all megabreccias was interpreted to be the corresponding marginal areas and related sub-environments. Differences in margin environments are, however, interpreted. It is suggested that lithoclast fragmentation occurred during transport and as such contributed to the matrix component. Diagenetic alterations of the sediments also appear to display a common succession of dissolution and cements for lithoclasts/matrix which will be further presented towards the end of this chapter.

PATTERNS AND MECHANISMS

Unit B is the stratigraphic lowermost megabreccia of the Vico del Gargano succession. The underlying unit A was deposited on the distal slope to proximal basinal areas, and it is assumed that it records more or less the paleo-horizontal level. Using this unit as a datum, the angle of unit B is less than 1 degree and no changes in this angle are mapped within the Vico del Gargano quarry. This suggests that unit B was deposited as a sheet-like accumulation, and the interpretation of this unit as a talus-like deposit caused by rock-fall is not very likely. Such a depositional model would probably entail to a larger extent the disintegration of larger lithoclasts and a higher angle that might be expected to close in on the angle of repose. Instead, a low-angled slope is suggested. Schlager *et.al.* (1991) published a similar interpretation of the depositional mechanism of such deposits (see also Schlager, 2005, fig 7.19). As pointed out by Spence & Tucker (1997); limestone megabreccias may form on a wide range of slope angles, including on very low-angled and low-relief slopes. The catastrophic appearance of unit B/lithofacies B1 indicates that its deposition was sudden and not preceded by other similar margin-derived sediments. This suggests that the trigger-mechanism that released this landslide was probably not related to platform growth in response to changes in relative sea-level.

The progradational pattern that is displayed by the northern megabreccias (i.e. unit C) is interpreted as the record of high sediment production rates that exceeded vacant accommodation space, promoting the progradation of the platform.

Unit C downlaps onto unit A and by such it defines an important surface which corresponds to the top of unit A. In a sequence stratigraphic setting, this surface may be interpreted as the maximum flooding zone (Posamentier & Allen, 1999) which marks the onset of the highstand systems tract. Graziano (2001) stated that the Monte Sant'Angelo Megabreccias was associated with the highstand systems tract. This surface may possibly be related to a higher-frequency cycle that impacted on the Apulian platform margin. However, the present dataset does not allow for any confirmation of this, nor does it support any further discussion on the sequence stratigraphic meaning of these deposits. The relation between this surface and unit B is not exposed. Unit B is, however, interpreted to be positioned below the downlap surface and it is expected that unit C downlaps also onto unit B (figure 4.2B).

TRIGGERS

It is suggested that unit B is the result of a major seismic event that destabilized the platform margin and upper slope by the sudden increase in pore-pressure which was induced by the prograding seismic shock-wave (*e.g.* Spence & Tucker, 1997). Seismic shocks probably constitutes the most common exogenic trigger causing seafloor instability (*e.g.* Cook *et.al.*, 1972; Naylor, 1978, 1981; Field *et.al.*, 1982; Mutti *et.al.*, 1984; Marjanac, 1985; Mullins *et.al.*; 1986, Hine *et.al.*, 1992; Spence & Tucker, 1997) and most megabreccias have commonly been interpreted as the results of synsedimentary tectonics (*e.g.* Castellarin, 1972, Bernouilli *et.al.*, 1990).

Unit C is interpreted as the deposits of debris-flows that displayed some degree of cyclic occurrence. This coincides with the interpretation of unit M (Malpasso Valley). These flows originated from the upper-slope and fore-slope, and were probably also matrix-supported during transport. Seismic triggers are suggested also for these deposits, but it is likely that oversteeping of the upper-slope during highstands of the relative sea-level (*e.g.* Graziano, 2001) destabilized the slope and laid the foundations for failures.

Graziano (2001) states that synsedimentary tectonics to a large extent controlled the deposition of the Monte Sant'Angelo Megabreccias and he further notes that such seismic activity during the Cenomanian were recorded by the coeval shallow-water deposits of the Apulian Platform (Iannone, 1996). The observations of this study agree with Graziano (2001) in terms of dominant trigger mechanisms for these gravitational events being seismic events caused by synsedimentary tectonics. Tectonic activity during the Cenomanian has also been recorded for the Adriatic Carbonate Platform (Vhlacovic *et.al.*, 2005; Husinec & Jelaska, 2006).

A SUGGESTED PRINCIPAL MECHANISM

The aggrading pattern of the Malpasso Valley succession suggests that accommodation space exceeded sediment supply, which prevented the south-eastward progradation of the platform during this highstand of the relative sea-level. While the succession mapped on the northern parts of the Gargano (Vico del Gargano) suggest a 'keep-up' type platform response, the southern (Malpasso Valley) suggests more that of a 'catch-up' type response, on outcrop scale. This differentiated response is here seen in relations to differentiated rates of subsidence for this area during the Cenomanian, coinciding with, and largely controlling, the deposition of the Monte Sant'Angelo Megabreccias.

Such differential subsidence implies that the area was either tilted or segmented by faults. Graziano (2001) describes the activity of normal faults that dissected the Apulian margin during late Aptian – early Albian *p.p.* times, related to the deposition of the Posta Manganaro Megabreccias (see fig 2.3), which are confined to the southern Gargano area. Such margin-parallel fault-systems may have been active, or re-activated during Cenomanian times. This agrees with Borgomano (2000), who described activity of normal faults during Cenomanian times. Amphitheatre-like scallops on the margin of the Apulian Platform that formed during Cenomanian times was described by Bosellini *et.al.* (1999), suggesting large-scale failures. This study agrees with the speculations of previously published studies, and normal faults that dissected the margin is interpreted (figure 4.1A) for the Malpasso Valley depositional model. However, no margin-cutting faults are interpreted in the proposed depositional model for the northern succession (Vico del Gargano) (figure 4.1B). Posta Manganaro

Megabreccias, as described by Graziano (2001), are confined to the southern Gargano only. This may imply that active segments belonging to the same fault system were only directly affecting the southern succession. However, synsedimentary tectonics that was related to the displacement in these faults may also have affected the northern succession.

The proposition of normal faults transecting the margin only for the southern succession match the indications of high subsidence rates in the south and subsequent elevated accommodation space generation that promoted an aggrading pattern. The northern succession, however, did not record elevated accommodation space but is still influenced by synsedimentary tectonics.

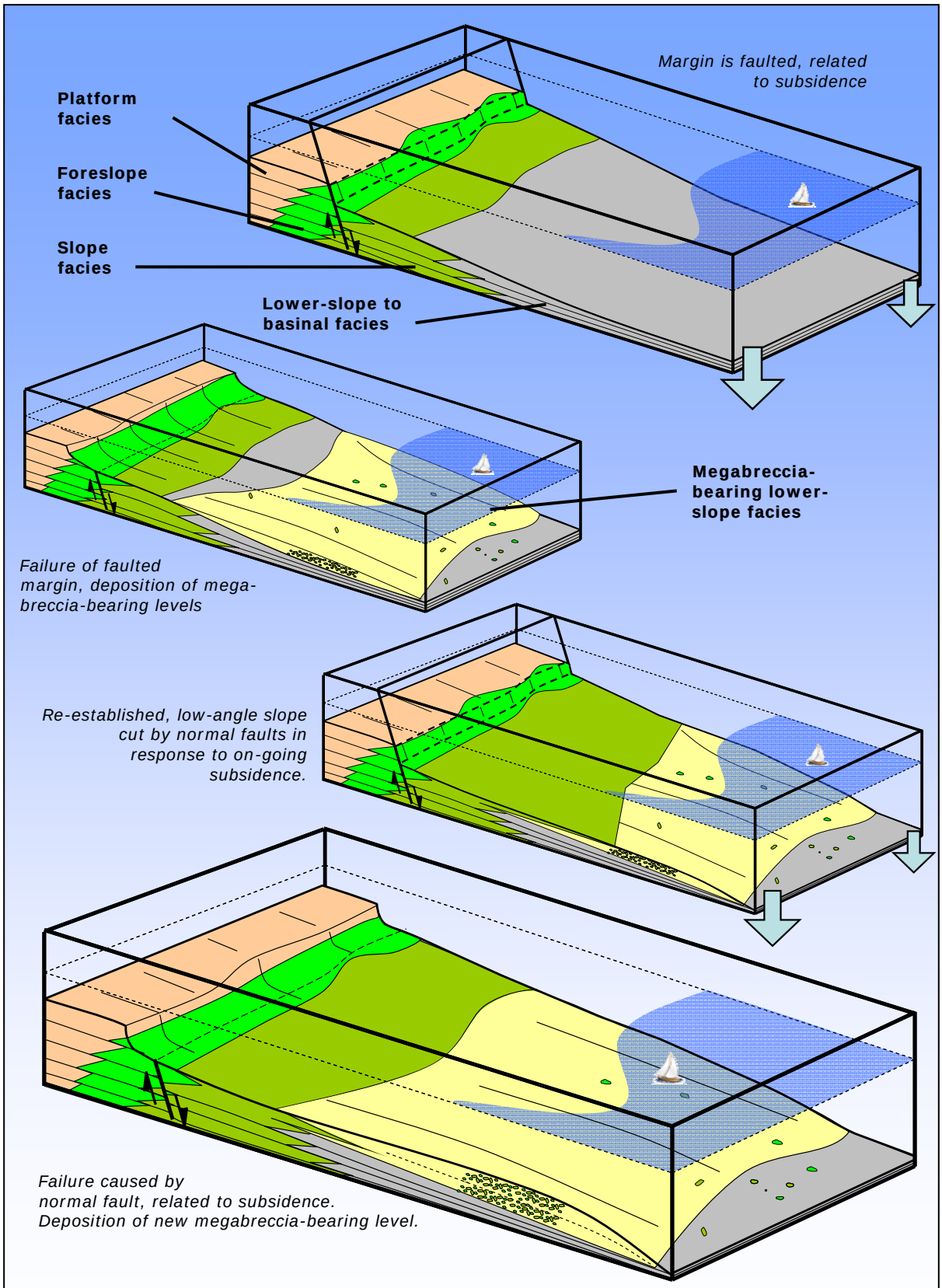

Figure 4.2A – Proposed depositional model for the Malpasso Valley succession

Fault is interpreted and its position, orientation and displacement are hypothetical. Not to scale. Facies distributions and volumes are hypothetical. Sea-levels are hypothetical.

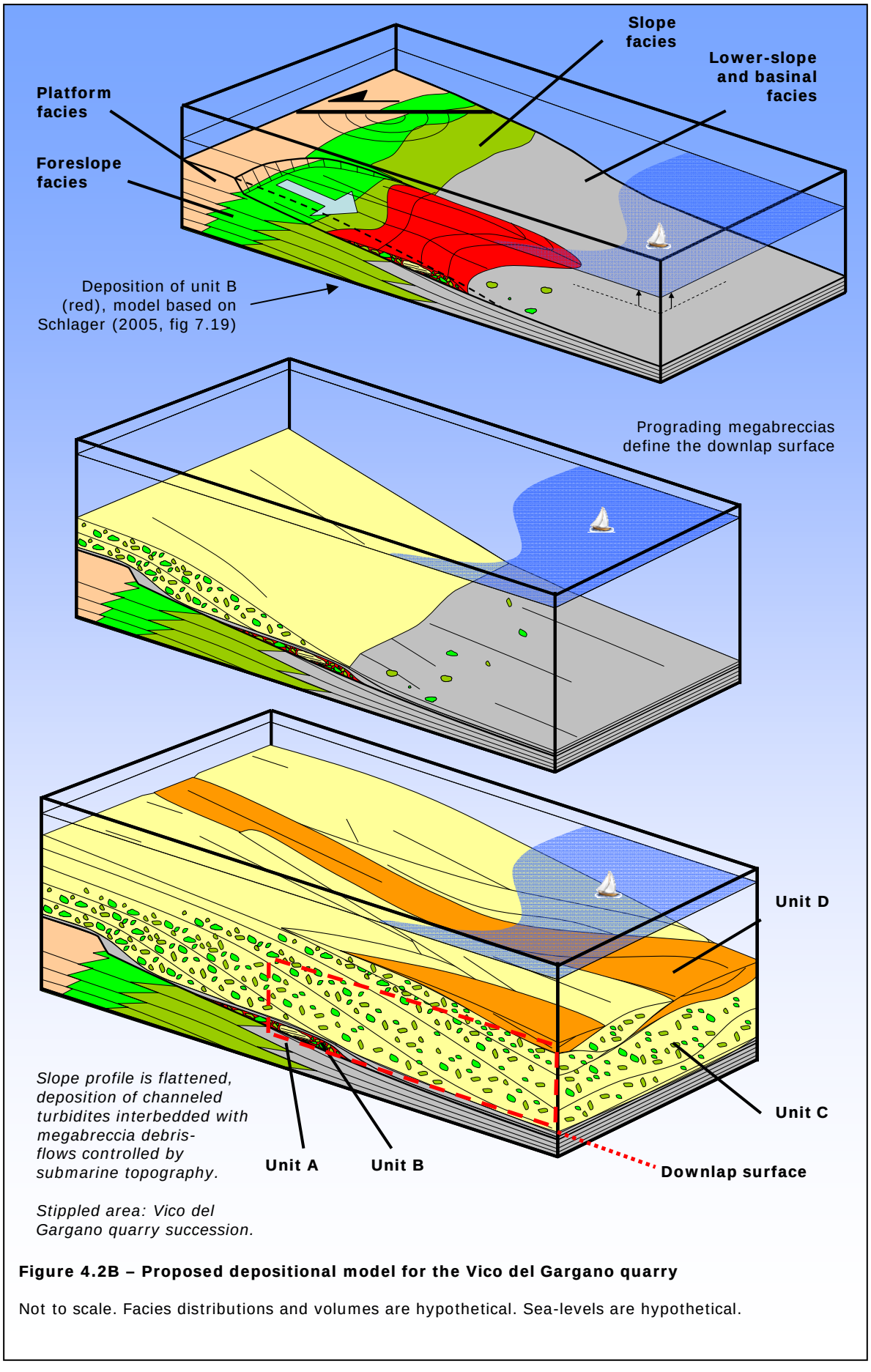

Figure 4.2B – Proposed depositional model for the Vico del Gargano quarry

Not to scale. Facies distributions and volumes are hypothetical. Sea-levels are hypothetical.

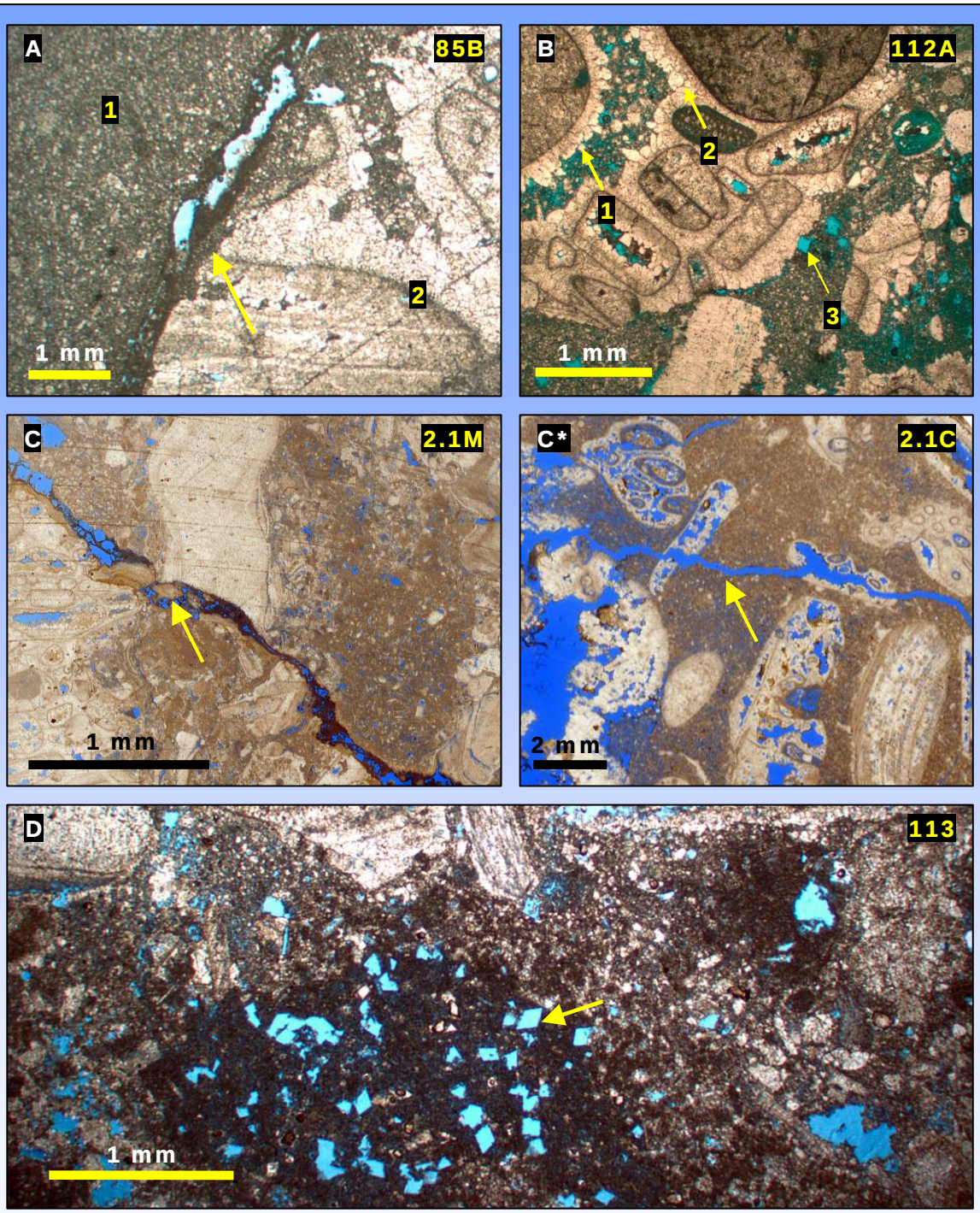

Figure 4.3 – Diagenesis

A) Sample 85B displays an extraclast confined by an erosion surface that cut grains, micrite envelopes and cements. Sample originates from a clast-matrix contact on the eastern wall of the Malpasso Valley outcrop.
B) Sample 112A display an extraclastic packstone (floatstone) with two distinct cement generations. An isopachous rim of "dog-tooth" marine phreatic calcite cement (1) is subsequently coated by drusy equant calcite (2). Selective dissolution of rhombohedra shaped grains are confined to micrite matrix only in the present dataset, and is here shown (3) to affect calcite cement growth on adjacent grains. This sample originates from a lithoclast on the eastern wall of the Malpasso Valley.
C) Samples 2.1C and 2.1M displays nonfabric-selective late dissolution pores indicated by arrows. These samples originate from a lithoclast and the surrounding matrix, respectively.
D) Sample 113 from a matrix sample on the Malpasso eastern wall. It displays rhombohedra-shaped fabric-selective pores that suggest dissolution of pyrite or dolomite crystals.

DIAGENETIC HISTORY

The diagenesis of the Monte Sant'Angelo Megabreccias displays a succession of cementation and dissolution that can be grouped into three major stages and domains;

1) Marine-phreatic diagenesis is characterized by the development of micrite envelopes (Bathurst, 1966, early grain dissolution and an isopachous rim of bladed calcite cements (figure 4.3B). The isopachous cement coats the micrite envelopes that preserve grain shape, and line the moldic pores that resulted from grain dissolution. This indicates that precipitation of this cement coincided with the dissolution of grains.

2) Meteoric-phreatic diagenesis is characterized by extensive, equant calcite ('doog-tooth') cement that obstructs both initial and secondary porosity of these sediments. This cement generation coats the isopachous cement. Observations of compaction structures that affect this cement generation places it prior to the burial diagenesis in the diagenetic history.

3) Burial diagenesis is characterized by compaction features. The occurrence of stylolites in unit A (Vico del Gargano) indicates burial depths of at least 800 m (*e.g.* Shinn & Robbin, 1983; Railsback, 1993; Tucker, 1993). Compaction affected the matrix to the megabreccias more than the equivalent lithoclasts which it surrounds. While compaction structures were observed within representative matrix-samples, no such structures were observed within lithoclast samples. This reflects that the lithoclasts were previously lithified prior to re-deposition and that the majority of overburden was consequently absorbed mostly by the non-lithified matrix.

4) Late diagenesis occurred during Tertiary uplift and subsequent sub-aerial exposure (*e.g.* Borgomano, 2000) and is characterized by the development of nonfabric-selective vuggy porosity that affects both matrix and lithoclasts (fig 4.3C). Fresh-water leaching is also suggested by Graziano (1994, 2001) to have developed during Turonian uplift and exposure of the Apulian Platform. Rare meteoric blocky calcite also characterize this domain, which locally add a cement generation to the two previously described (figure 4.3B)

The selective dissolution of rhombohedra pores (figure 4.3D) confined to the micrite matrix indicates the fabric-selective dolomitization and subsequent

dedolomitization (von Morlot, 1847), probably by the effect of fresh-water leaching related to recent uplift and sub-aerial exposure. The absence of calcite within these pores suggests that the meteoric-phreatic precipitation of equant cements preceded the dedolomitization.

Cathodoluminescence was performed on samples of the present database, but the samples did not illuminate presumably due to low presence of magnesium (Mn) and iron (Fe), possibly suggesting that the carbonate succession is very clean and unpolluted by siliciclastic sources. Samples were stained using Alizarinrot S and Kaliumhexacyanoferrat (III) (Dickons, 1966) to display a red staining of cement and grains. Some areas were not stained, presumably by the effect of LMC. No bluish colours were observed, indicating that iron-rich calcite or iron-rich dolomites are not present (Dickons, 1966; Lindholm & Finkleman, 1972; James & Choquette, 1990). Preliminary examination of samples using electron microscope (SEM/BSE) did not display any occurrence of dolomite in zones that apparently did not stain.

5 PETROPHYSICAL ANALYSIS

The foundation for the petrophysical analysis is the data presented in chapter 3. The classification system for porosity in carbonates developed by Lucia (1983, 1995, 1999, 2007) is commonly used by reservoir engineers, mainly because it links pore classification to flow properties and numerical modeling of properties. The system developed by Choquette & Pray (1970) is preferred by petroleum geologists as it links the classification of pore-types to depositional setting and diagenetic history. The system developed by Lønøy (2006) is based on an empiric approach, and was aimed at obtaining higher coefficient of correlations in the classification a large carbonate database.

Different definitions of 'vuggy porosity' exist. In this discussion, the term refers to all pores that are not interparticle, as applied by Lucia (1983, 1995, 1999, 2007). In contexts where vuggy porosity (sensu Lønøy, 2006) is discussed, the term 'VUG' is used.

Poroperm classes are introduced (figure 5.1) and results are discussed within the framework of these. The purpose of poroperm classes is to enable the discussion the combined signature of porosity and permeability without implementing reservoir properties, which also rely on additional parameters. 1 mD is generally considered an absolute low for hydrocarbon production, and a corresponding boundary of 5% porosity was chosen to denote poroperm class 1. The boundaries between classes 2 and 3 were set at 15% porosity and 10 mD.

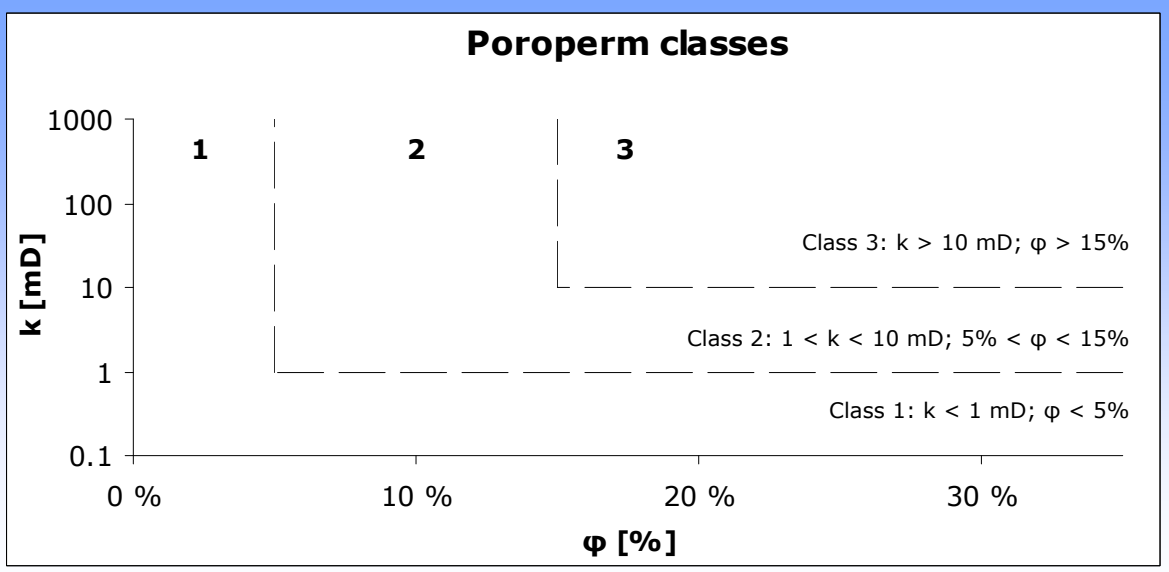

Figure 5.1 – Poroperm classes

BIAS IN POROSITY ESTIMATIONS

Porosity was estimated for all samples where thin-sections were available, and the results were compared to measurements derived from standard laboratory methods (figure 5.2A). Two conclusions may be drawn from this plot; 1) Estimated values are as a trend lower than their measured counterparts, and 2) a significant scatter indicates that the offset from the neutral line (where measured equals estimated values) is not constant.

It was suggested that quality of thin-sections may be partly responsible for this bias. Thin-sections were classified according to this, on a scale of 1 (porosity not visible, very poor quality) to 4 (porosity well defined, thin-section is of good quality) but no trends were observed (figure 5.2B). It was further investigated whether pore-types could be linked to this bias, but as displayed in figure 5.3C, no apparent trend was observed when plotting according to petrophysical classes (Lucia, 1983, 1995, 1999, 2007) that is founded on a modified Dunham classification based on fabric.

The scatter in the differences between estimated and measured values is probably caused by scale-issues, as thin-sections represent poorly the fabric and porosity of the plug sample.

It is further suggested that the general elevation of measured values is caused by estimation from image analysis failing to include pores with diameter below the point of visual distinction. This includes microporosity (*e.g.* Lønøy, 2006) but may also include smaller fractions of all poretypes. Hence, lower porosity is estimated.

The present database does not support empiric corrections to these measurements.

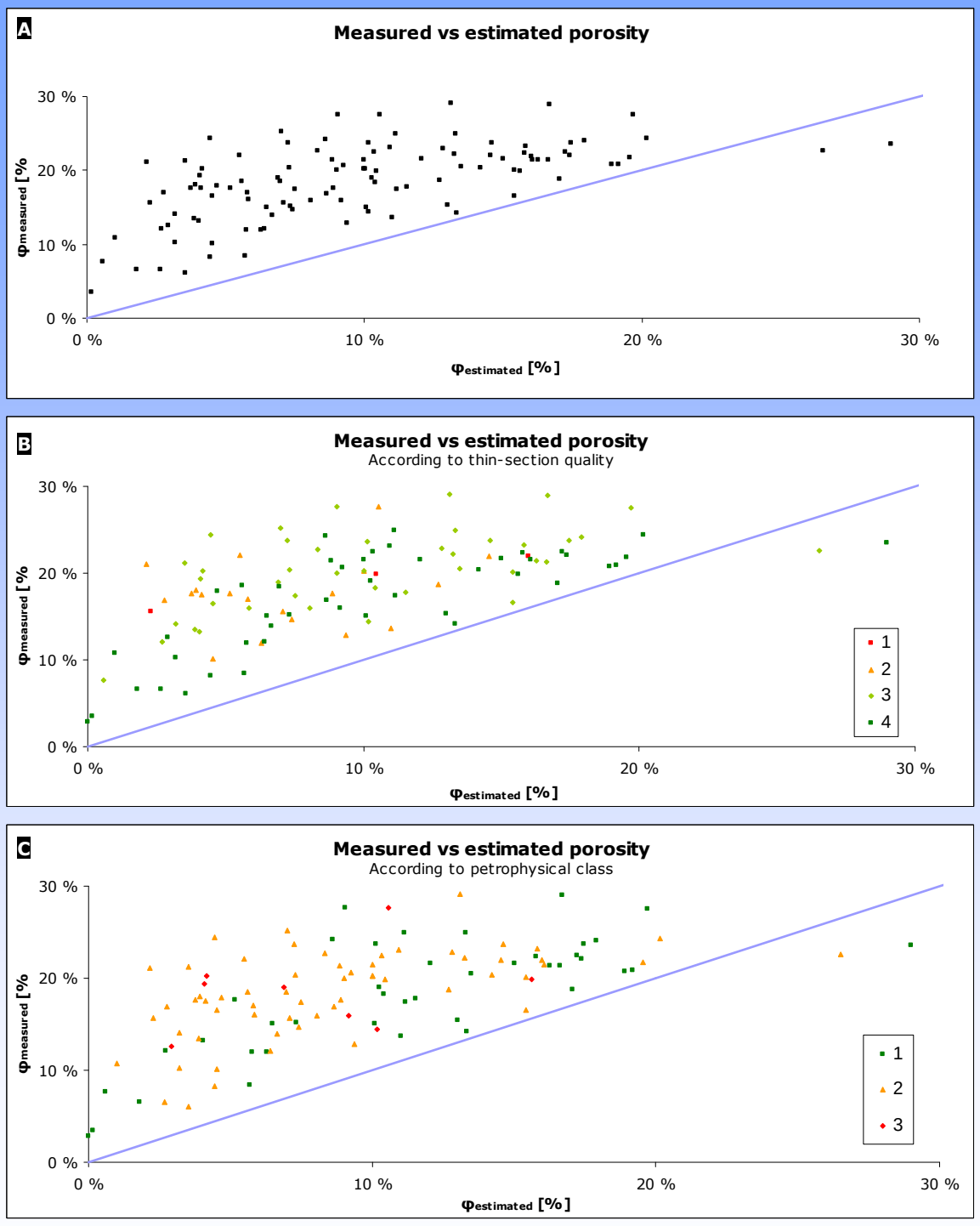

Figure 5.2 – Measured vs. estimated porosity

A) Measured vs. estimated porosity (no classification)
B) Classified according to descriptive thin-section quality (1-4)
C) Classified according to petrophysical class (fabric) (1-3) (Lucia, 1983, 1995, 1999, 2007).

LØNØY CLASSIFICATION SYSTEM

Figure 5.3 displays datapoints representing samples classified according to the system developed by Lønøy (2006). Present dataset trendlines and the original trendlines provided by Lønøy are included in the plots, for comparison.

Classifying the present database using this system evidently does not produce reliable coefficients of correlations. This must, however, be seen in relations to the relative low number of samples of this database, which limits the reliability of these results. These plugs have been measured predominantly using gas-permeability corrected for Klinkenberg effect (Klinkenberg, 1941) (*see also appendix 1 for extended introduction to these methods*), which is the same method as used by in the development of this system (Lønøy, 2006). However, Lønøy (2006) reports that most plugs had a diameter of 2.5 cm (~ 1 in.) (some VUG-dominated plugs were larger). The present database consists of plugs which diameters are 3.8 cm (1.5 in.) and 5 cm (2 in.). The use of larger plugs may reflect in the lowered coefficient of correlations. This illustrates the heterogeneity of carbonates, and depicts the difficulties in obtaining reliable porosity-permeability transforms. Another noticeable effect was that the use of slightly larger plugs apparently increases the correlation coefficient for VUG-dominated samples. However, Lønøy (2006) states that larger samples were utilized in the classification of VUG-dominated samples.

Important is also the fact that very few samples show dominance of only one poretype, which is a decisive factor for this system (Lønøy, 2006). In relations to this, Lønøy (2006) note that samples of mixed pore-types plot between end-members, but show a bias towards the pore-type which has the highest permeability. This database further contains only three poretypes included in this system and as such, any discussion regarding the Lønøy-system based on these results is at best fragmental.

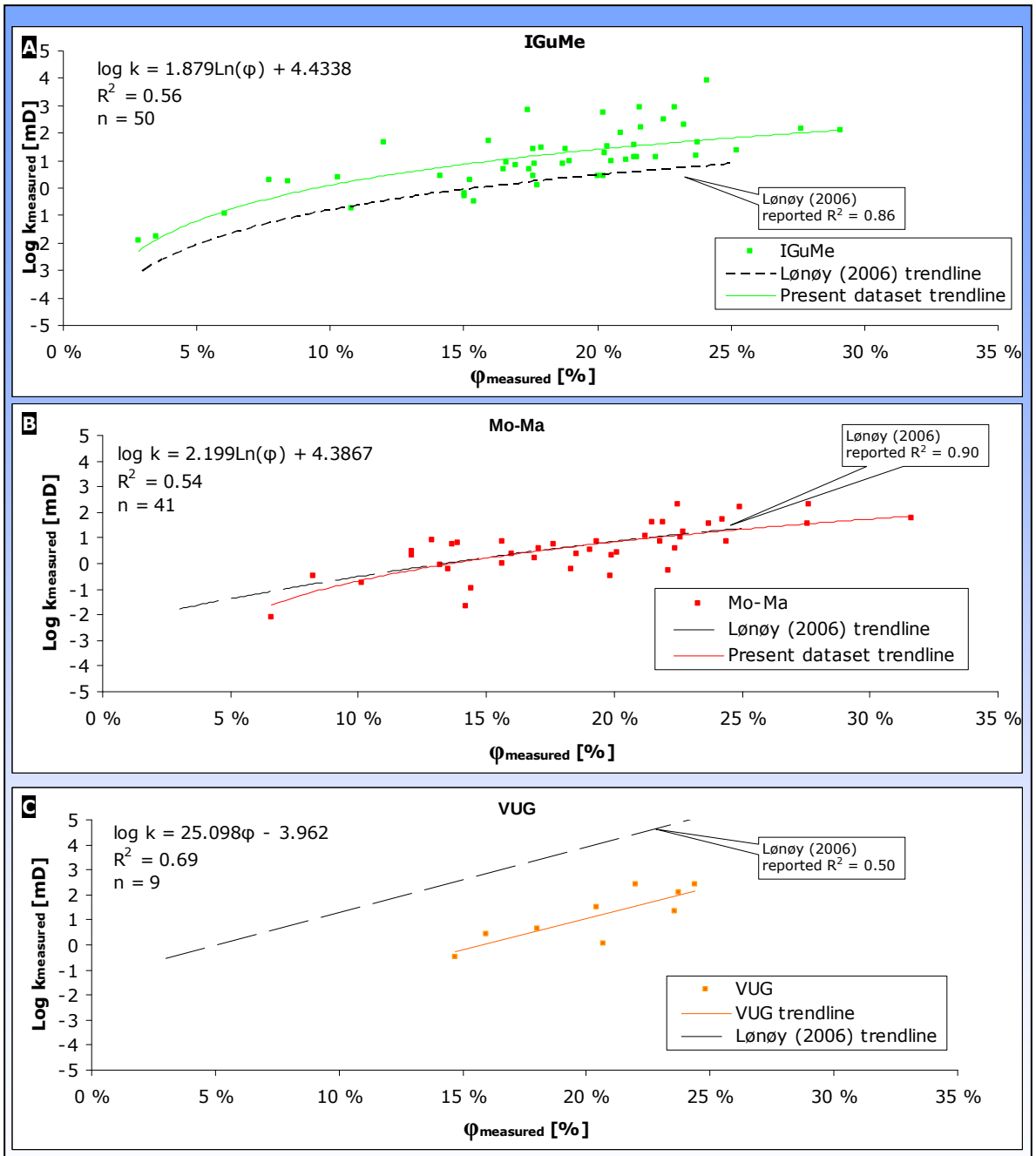

Figure 5.3 – Lønøy (2006) pore-types

Poroperm for poretypes according to Lønøy (2006).

A) Samples dominated by interparticle mesopores (IGuMe)
B) Samples dominated by moldic macropores (Mo-Ma)
C) Samples dominated by vuggy pores (VUG)

CHOQUETTE & PRAY CLASSIFICATION SYSTEM

The database was classified according to the system developed by Choquette & Pray (1970). However, this provided no unique poretype groups. Figure 5.3 displays pore-types according to the system of Lønøy (2006), but these classes also correspond to the pore-classes Interparticle (A), Moldic (B) and Channel (C) as defined by Choquette & Pray (1970) for the present database. As such, no further petrophysical investigations have been undertaken based on this classification system.

LUCIA CLASSIFICATION SYSTEM

The classification system developed by Lucia (1983, 1995, 1999, 2007) is based on the premise that permeability is mainly controlled by interparticle porosity and touching vugs, but may be predicted for interparticle porosity only. The presence of separate vugs (SV) (*i.e.* moldic pores) will elevate porosity but the pores are only connected through the surrounding interparticle porosity. Presence of touching vugs (TV) (*i.e.* fractures, dissolution enhanced fractures, channels (*sensu* Choquette & Pray, 1970) and other nonfabric-selective pores) may cause dramatic increase in permeability without the equivalent increase in porosity (*e.g.* Lucia, 2007; Lucia & Ruppel, 1996). The fact that the Lucia-system is based on the premise that permeability may be predicted from the interparticle porosity fraction only causes the Lucia-system to suffer from the bias related to porosity estimation from thin-section images (figure 5.2).

The present database was classified according to the Lucia-system, and corresponding poroperm plots are presented in figure 5.4. Figure 5.4A-C display petrophysical classes 1, 2 and 3, respectively, according to dominant pore-types. Trendlines are provided for the datasets. No trendlines are provided for class 3 samples, and for touching-vug dominant class 1 samples, due to low number of samples. Trendlines show that this grouping does not support good correlations of porosity and permeability for the present dataset.

Figure 5.4D display all samples according to petrophysical class along with trendlines obtained without concern for the dominant type of porosity. The coefficient of correlation was significantly lower for these trendlines, compared to those presented in figures 5.4ABC.

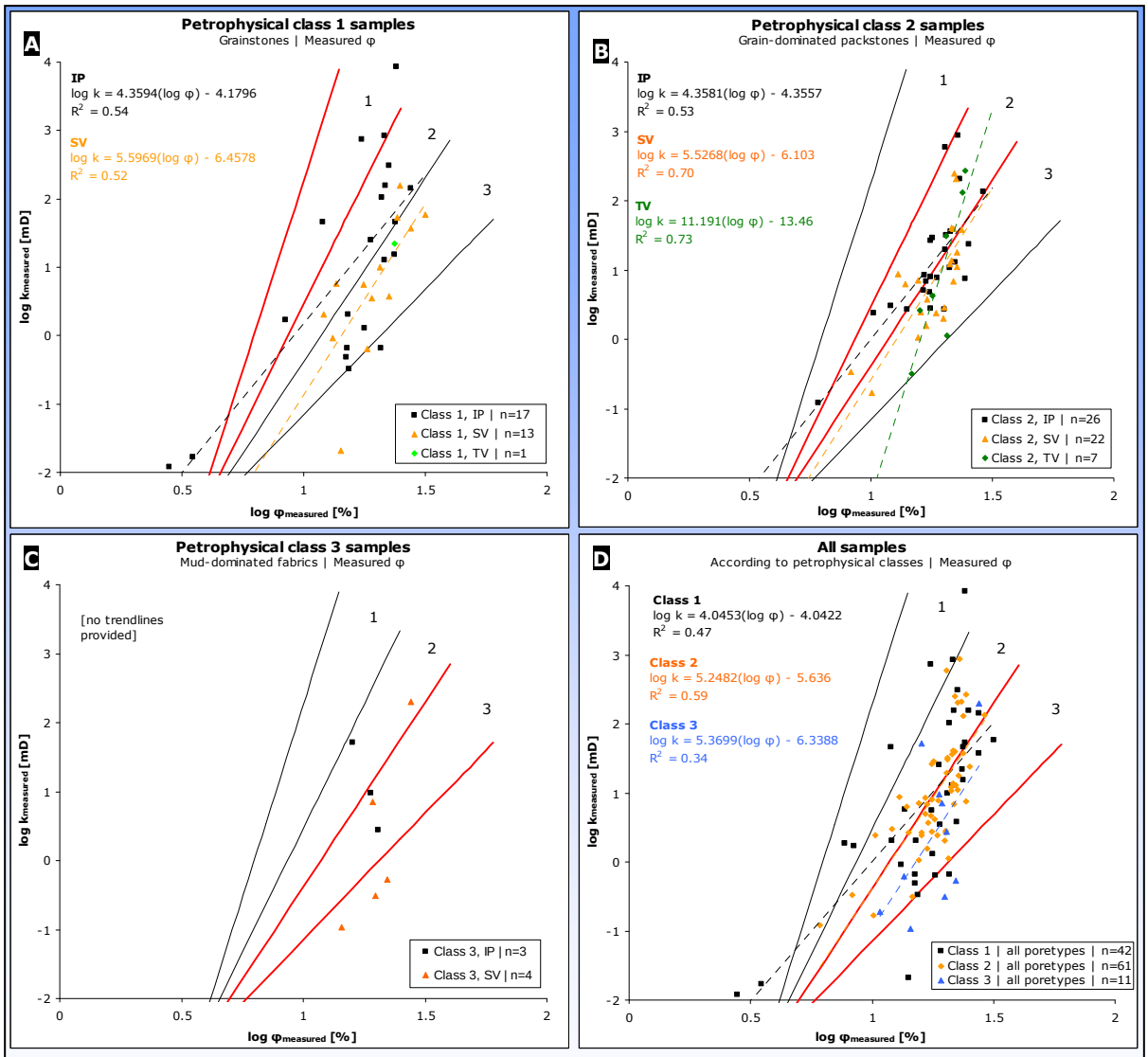

Figure 5.4 – Lucia (1983, 1995, 1999, 2007) classification system

A) Petrophysical class 1 datapoints (grainstones) according to dominant poretypes. TV-dominant provides no trendline (n=1)
B) Petrophysical class 2 datapoints (grain-dominated packstones) according to dominant poretypes.
C) Petrophysical class 3 datapoints (mud-dominated fabrics) according to dominant poretypes. No trendlines provided due to the low number of samples.
D) All samples according to petrophysical class.

PERMEABILITY PREDICTION AND COMPARISON OF SYSTEMS

Figure 5.5 display predicted permeability based on porosity using the systems of Lønøy (2006) and Lucia (1983, 1985, 1999, 2007). The datapoints derived using the Lønøy-system apparently conforms better to the neutral line than do the values derived using the Lucia-system. The amount of scatter for the Lucia-system estimates compared to those of the Lønøy-system is likely to be related to previously discussed uncertainties related to the estimation method. These are significantly larger than the uncertainties attached to the laboratory measurements. The Lucia-system suffers from this, and results display higher degree of scatter.

Figure 5.5 also displays that, for the Lønøy-system, the VUG-group apparently trend higher than estimated values, while IGuMe and Mo-Ma groups scatter equally on both sides of the neutral line. This may suggest that a bias is related to the former poretype group that acts on these results in addition to the general scatter. For the Lucia-system, an apparent bias is recognized for class 3 datapoints (correspond to samples of mud-dominated fabrics).

An important effect that is not covered by the Lucia-system is cement. This was also noted by Lønøy (2006). The petrophysical classes of the Lucia-system are, for limestones, founded on the Dunham classification with modifications, along with grain size and sorting. This is unaffected by cement that may reduce porosity and obstruct permeability through narrowing of the pore-throats and subsequently increase the spread of datapoints. The Lønøy-system is based on pore size and distribution. The latter is a new contribution to pore classification, and is not covered by the Lucia-system or the Choquette & Pray (1970) system. It may, however, be argued as to what impact the porosity distribution have on porosity/permeability transforms and relations.

The prediction of permeability based on porosity that was performed for this database suggests that the system developed by Lønøy (2006) yields better correlations to measured values compared to the Lucia-system. It also indicates that increased plug sizes capture better the heterogeneous fabric of these samples, resulting in poorer correlations between porosity and permeability. Subsequently, the prediction of permeability is less reliable when increasing sample sizes.

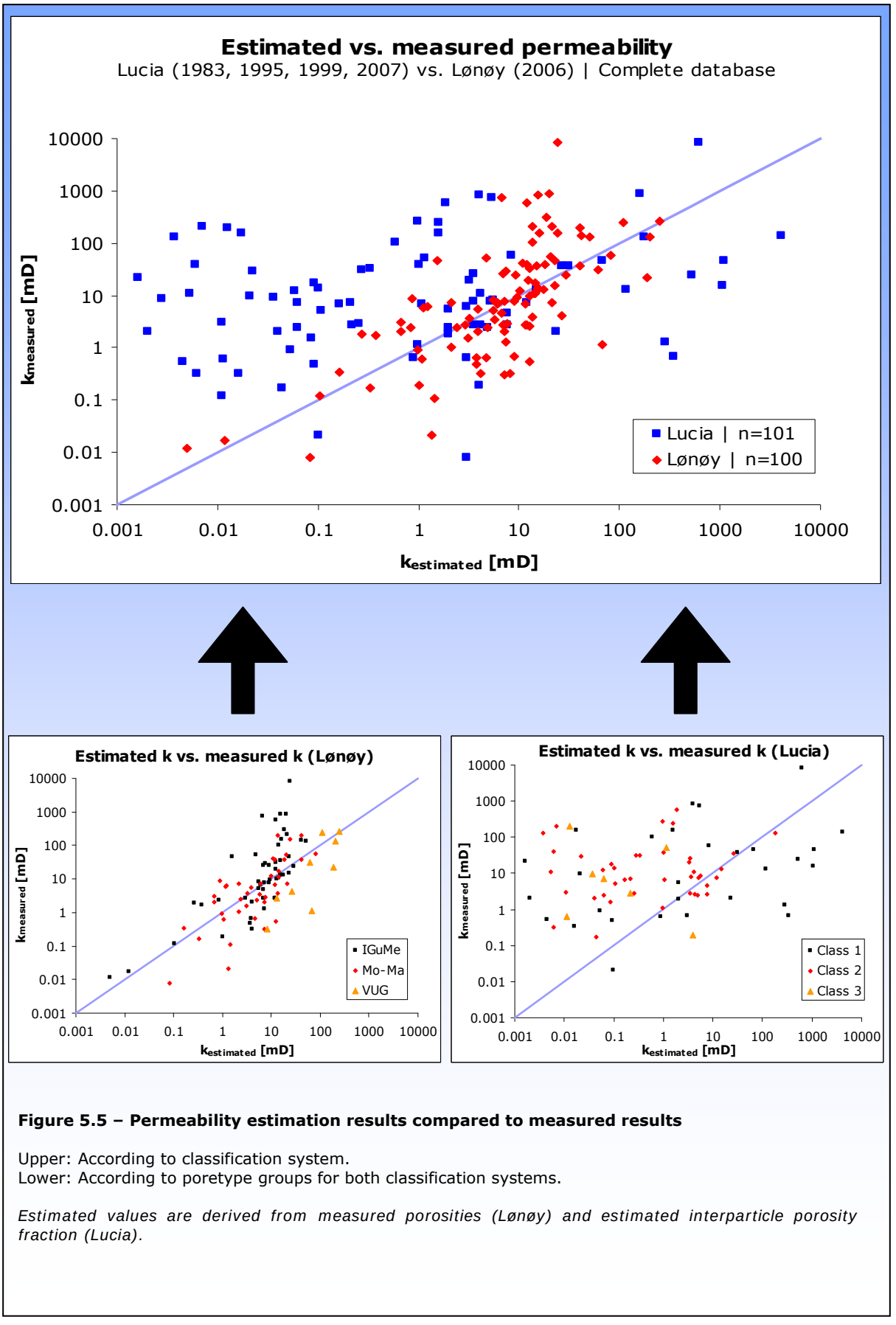

Figure 5.5 – Permeability estimation results compared to measured results

Upper: According to classification system.
Lower: According to poretype groups for both classification systems.

Estimated values are derived from measured porosities (Lønøy) and estimated interparticle porosity fraction (Lucia).

MALPASSO VALLEY

Figure 5.7 display poroperm values for the Malpasso Valley samples, subdivided according to origin (lithoclast/matrix/unknown). All datapoints in this plot correspond to samples of lithofacies B1, which is the only mapped lithofacies within the studied succession of this outcrop. Representative lithoclast- and matrix datapoints are plotted in figure 5.7A. While lithoclast samples apparently show no trends, the matrix datapoints apparently conform to a linear trendline (R^2 = 0.82, n=7).

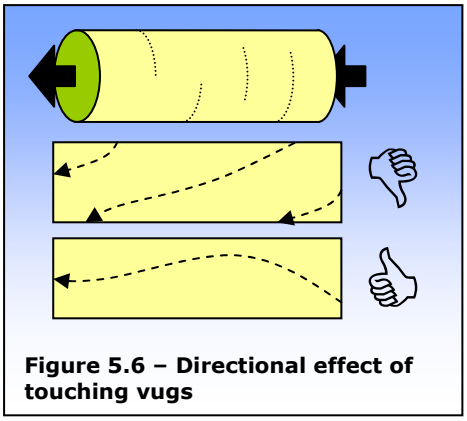

Figure 5.6 – Directional effect of touching vugs

Figure 5.7B, C and D combined displays datapoints corresponding to the complete population of samples derived from the Malpasso Valley outcrop (unit B, lithofacies B1). Samples pertaining to petrophysical class 1 plot predominantly within classes 2 and 3. This effect is expected based on observation of separate vugs (moldic pores) dominance in this dataset. Data points representing samples that were assigned to petrophysical class 2 predominantly plot in classes 2 and 3. The offset towards class 3 indicates presence of separate vugs, which is confirmed through sedimentological analysis of these samples. Apparently, no datapoints reflect the presence of touching vugs, which were observed within the 7 samples that are classified as TV-dominant. This may reflect that thin-sections fail to capture the dominant fabric of the sample. Although touching vugs are present (as confirmed from thin-sections) they may also be oriented in directions that fail to increase measured permeability using standard laboratory methods. In order to promote permeability through a plug sample, a network of vugs must transect both short-ends of the plug sample (figure 5.6). This reflects that measuring of increased permeability due to touching-vug networks is directional dependent.

An apparent similarity of all three petrophysical classes was that datapoints scatter irrespectively of dominant poretypes. A possible dependence is observed for class 3 samples, but the number of samples does not support statistically reliable conclusions. In terms of poroperm classes (figure 5.7E), unit M plots predominantly within classes 2 and 3.

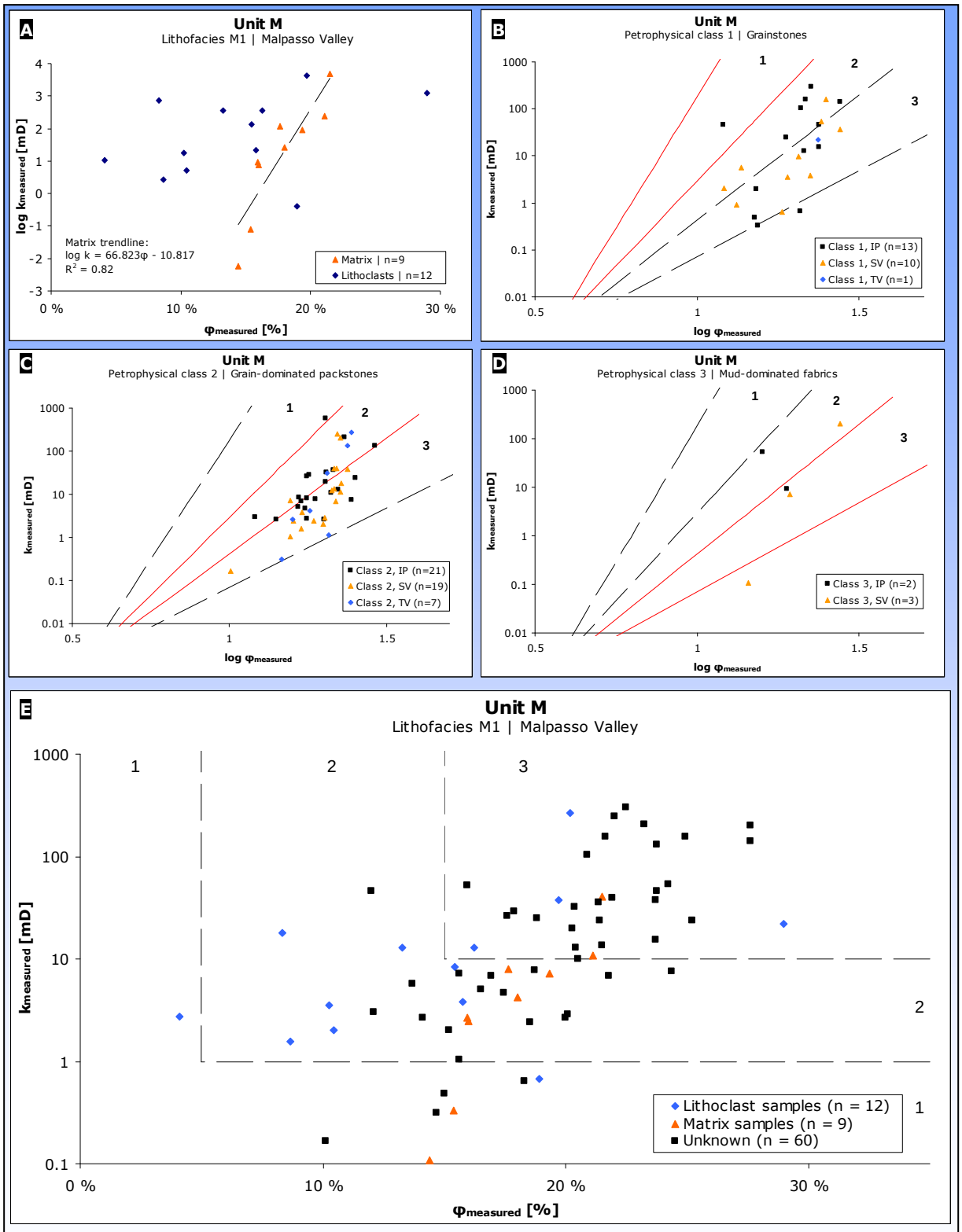

Figure 5.7 – Malpasso Valley samples

A) Representative lithoclast- and matrix samples. Matrix samples (log k) conform to a linear trendline.
B-D) According to petrophysical class and dominant poretypes.
E) Complete unit M dataset according to origin. Boundaries of poroperm classes indicated.

UNIT B

Results from samples originating from unit B (Vico del Gargano quarry) are displayed in figure 5.8. Lithofacies B1 (clast-supported rudist megabreccias) is the only lithofacies mapped within this unit. The samples were classified according to origin (lithoclast/ unknown). Very little matrix was observed within this unit, and no matrix samples were recovered.

Plotting the poroperm values of lithoclasts vs. unkown samples suggests that the lithoclasts plot at higher porosities than the samples of no confirmed origin. It may be speculated as to whether the unknown samples pertain to the megabreccia matrix, which consists of the same fabric as lithoclasts. It is expected that the matrix will suffer for compaction effects more than the already lithified lithoclasts. Hence, it is expected that it displays lower porosity values compared to lithoclast interiors. Diagenetic effects may also cause this segmentation, as flow-properties through the megabreccia unit may be selective in terms of lithoclasts and matrix. These effects may explain the two trends displayed in this figure 5.8A.

The unit B sample population plotted according to subfacies (figure 5.8B) shows that samples belonging to the "unknown" group of figure 5.8A all pertain to subfacies B1b – grain-dominated packstones. These datapoints plot in petrophysical class 2, which is expected based on their fabric. The plot also reveals that lithoclast samples belong to subfacies B1a (grainstones) and B1c (mud-dominated fabrics). These samples are, in terms of petrophysical properties, expected to differ significantly. However, they both plot below petrophysical class 3. In relations to this, it is emphasized that the number of samples from this unit is very low and not statistically representative. Figure 5.8D displays poroperm data from unit B plotted according to assigned petrophysical class. It displays that datapoints belonging to class 2, based on fabric, plot in their expected class. Samples pertaining to class 3 plot below their expected class. However, this is expected as both datapoint represent samples that are dominated by separate vuggy porosity.

The dataset does not support the detailed discussion of these apparent trends. However, the offset in terms of petrophysical classes that are displayed by these datapoints seem to match the sedimentological observations performed on their corresponding samples.

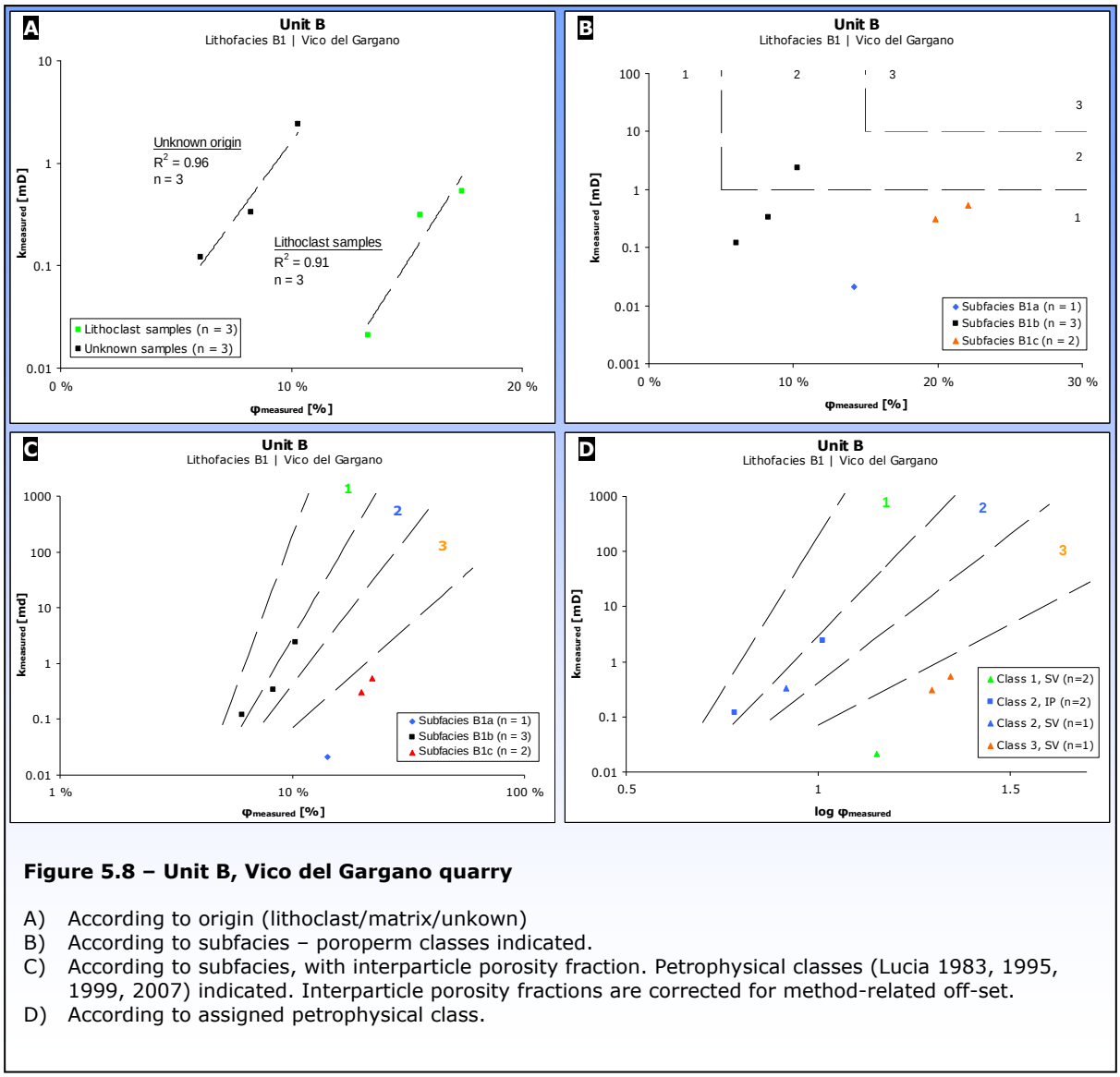

Figure 5.8 – Unit B, Vico del Gargano quarry

A) According to origin (lithoclast/matrix/unkown)
B) According to subfacies – poroperm classes indicated.
C) According to subfacies, with interparticle porosity fraction. Petrophysical classes (Lucia 1983, 1995, 1999, 2007) indicated. Interparticle porosity fractions are corrected for method-related off-set.
D) According to assigned petrophysical class.

UNIT C

Poroperm measurements were obtained for eight samples belonging to unit C. Two belong to facies C1 (packstone) and seven pertain to unit C2 (matrix-supported megabreccias 2). Among these, six originated from the matrix and one originated from a lithoclast. In terms of petrophysical classes (figure 5.9A), the datapoints that correspond to these samples plot within their expected petrophysical classes. The petrophysical effect of vugs in this dataset is not observed, nor is it confirmed through thin-sections.

When plotted for measured values (figure 5.9B), the single datapoint corresponding to a lithoclast sample plot within poroperm class 1. The datapoints of matrix samples plot within the domain of class 2. A low number of samples gathered from unit C produced petrophysical results. This is reflected in the number of datapoints in these plots and does not allow for extended elaboration on patterns.

Lithofacies C1 is a dense packstone that constitute clinoforms between the C2 megabreccia bodies. It is expected, based on stratigraphic analysis, that these have low poroperm values. They may act as seals or baffles to flow, segmenting this unit in terms of reservoir quality. Figure 5.9B displays towards a confirmation of this as the C1-datapoints are confined to the lower left low-perm/low-porosity corner of the plot. The apparent ability of this lithofacies to segment unit C into flow-units has implications for reservoir of this unit.

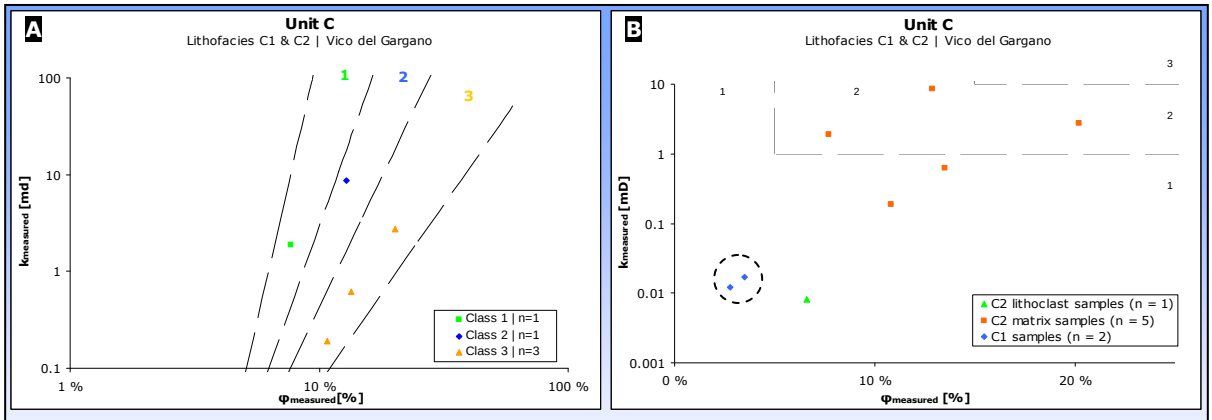

Figure 5.9 – Unit C, Vico del Gargano quarry

A) Unit C according to petrophysical classes (Lucia, 1983, 1995, 1999, 2007). Samples that plot below 0.1 mD is omitted from this plot.
B) Unit C according to lithofacies. C2 is divided according to origin. Poroperm classes indicated. Circled datapoints represent lithofacies C1 samples.

UNIT D

Poroperm measurements were available for a total of 9 samples belonging to unit D. Among these, 7 samples pertain to lithofacies D1 (matrix-supported rudist megabreccias 3) while the remaining two originated from lithofacies D2 (graded grainstones). When plotted according to the Lucia (1983, 1995, 1999, 2007) system (figure 5.10A), datapoints corresponding to subfacies D1a (*Orbitolina* grainstones) predominantly plot in the class 3 domain. This reflects the dominance of separate vugs in these samples. The same effect is noted for datapoints corresponding to subfacies D1b (grain-dominated packstones) but the offset is apparently less than similar offset of subfacies D1a. Subfacies D1c (mud-dominated packstones) produce datapoints that plot in the upper parts of class 3/lower class 2. This may reflect occurrence of separate vugs in the corresponding samples. However, the number of datapoints within this dataset does not support detailed discussion of their plotting patterns. The datapoints representing samples of lithofacies D2 show plot within poroperm class 3 (figure 5.10B), as do datapoints corresponding to the matrix to the D1 megabreccias. Lithoclast datapoints, however, predominantly plot within poroperm class 2.

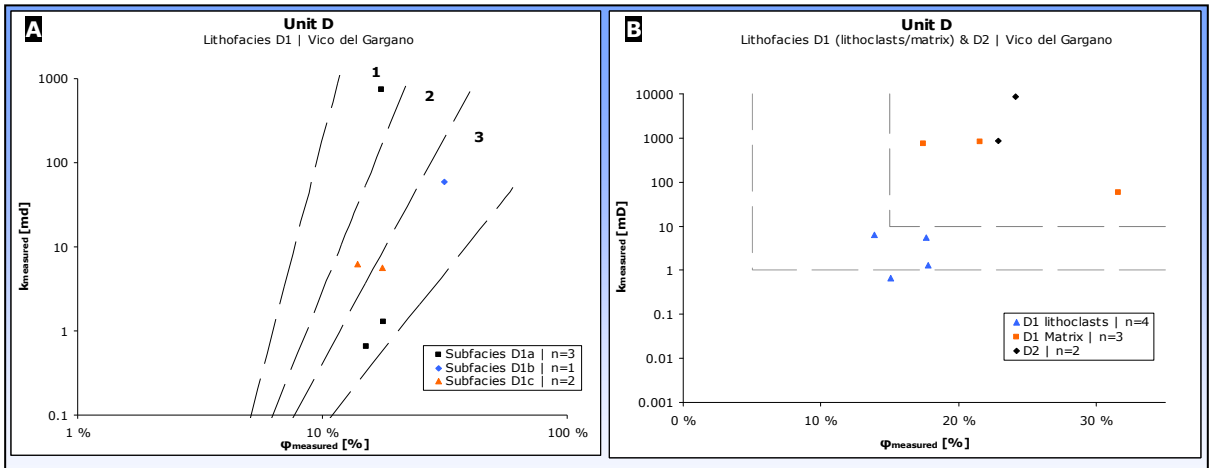

Figure 5.10 – Unit D, Vico del Gargano quarry

A) Unit D according to petrophysical classes.
B) Unit D according to lithofacies. D1 is divided according to origin. Poroperm classes indicated.

COMPARISON OF MEGABRECCIA UNITS

The datapoints responding to the population of megabreccia samples (unit M, lithofacies B1, C2 and D1) are displayed in figures 5.11 and 5.12. All samples pertaining to other facies are omitted (unit A, lithofacies C1 and D2). Figure 5.11 displays poroperm signatures of the Monte Sant'Angelo Megabreccias in terms of poroperm classes, according to lithofacies. While facies B1 is clast-supported (unit B, Vico del Gargano) the remaining samples are derived from matrix-supported breccias.

Facies M1 (Malpasso Valley) and D1 (Vico del Gargano) predominantly plot within poroperm classes 2 and 3, while facies B1 and C2 (Vico del Gargano) predominantly plot within classes 1 and 2.

A derivation from this plot is that the clast-supported breccias of facies B1 along with the lithoclasts of the matrix-supported facies C2 plot below 1 mD which may be considered a lower-end for hydrocarbon production. C2 matrix, on the other hand, plot in poroperm class 2.

Although facies B1 and C2 differ in terms of depositional mechanism and fabric, this indicates that the low reservoir quality of their lithoclasts is a similarity which they share. The lithoclasts are derived from the leeward platform margin (*e.g.* Borgomano, 2000), and it is suggested that this area locally displayed poor ability to produce sediments with high porosity/permeability. It may be speculated wether the margin that fed these deposits at this time was dominated by low-energy environments. The undulating platform margin may include protected areas or embayements that accumulate finer grain fractions and locally contribute to low-reservoir properties in their lithified form. Scallops that were created by platform margin collapses may created such protected parts of the margin. The matrix of unit C2, however, probably consists of dissintegrated lithoclasts and other materials derived from adjacent areas and possibly from the lower slope, where it was swept along and mixed with the megabreccia debris-flows. This re-sedimentation of small sized fragmented materials may promote reservoir conditions more than the lithified lithoclasts that maintained their internal fabric during transport. The matrix-supported debris-flows of facies M1 plot above 1 md and locally show permeability and porosity values meeting the requirments for poroperm class 3. In terms of reservoir properties, this poroperm class must be considered favourable.

Figure 5.12 is the summary of previously presented plots according to petrophysical classes displaying, however, only datapoints derived from megabreccia samples. This plot reflects the effects of vuggy porosity that shifts the clouds of datapoints towards the left (touching vugs) or right (separate vugs). Samples pertaining to class 1 display an offset towards classes 2 and 3, indicating that the poroperm signature of these grainstones were significantly affected by the moldic porosity which they contain. This result is expected based on sedimentological analysis of these samples. It may be speculated on whether the effect of touching vugs is also present. This may counter-effect the effect of separate vugs, but the former probably overprints the latter based on observations of the fabric of the corresponding samples.

Samples that were assigned to class 2 display the same trend, but the effect of separate vugs for this population is less than for those of class 1. This class displays the effect of touching vugs, which shift selected datapoints leftwards.

Datapoints reflecting samples that pertain to petrophysical class 3 displays a larger degree of scatter compared to the two former classes. They predominantly plot within their expected class. The effect of touching vugs in terms of porosity and permeability units is not as severe as potentially may be assumed from the appearance in this logarithmic plot but this class nevertheless displays a noticeable effect of both touching- and separate vugs.

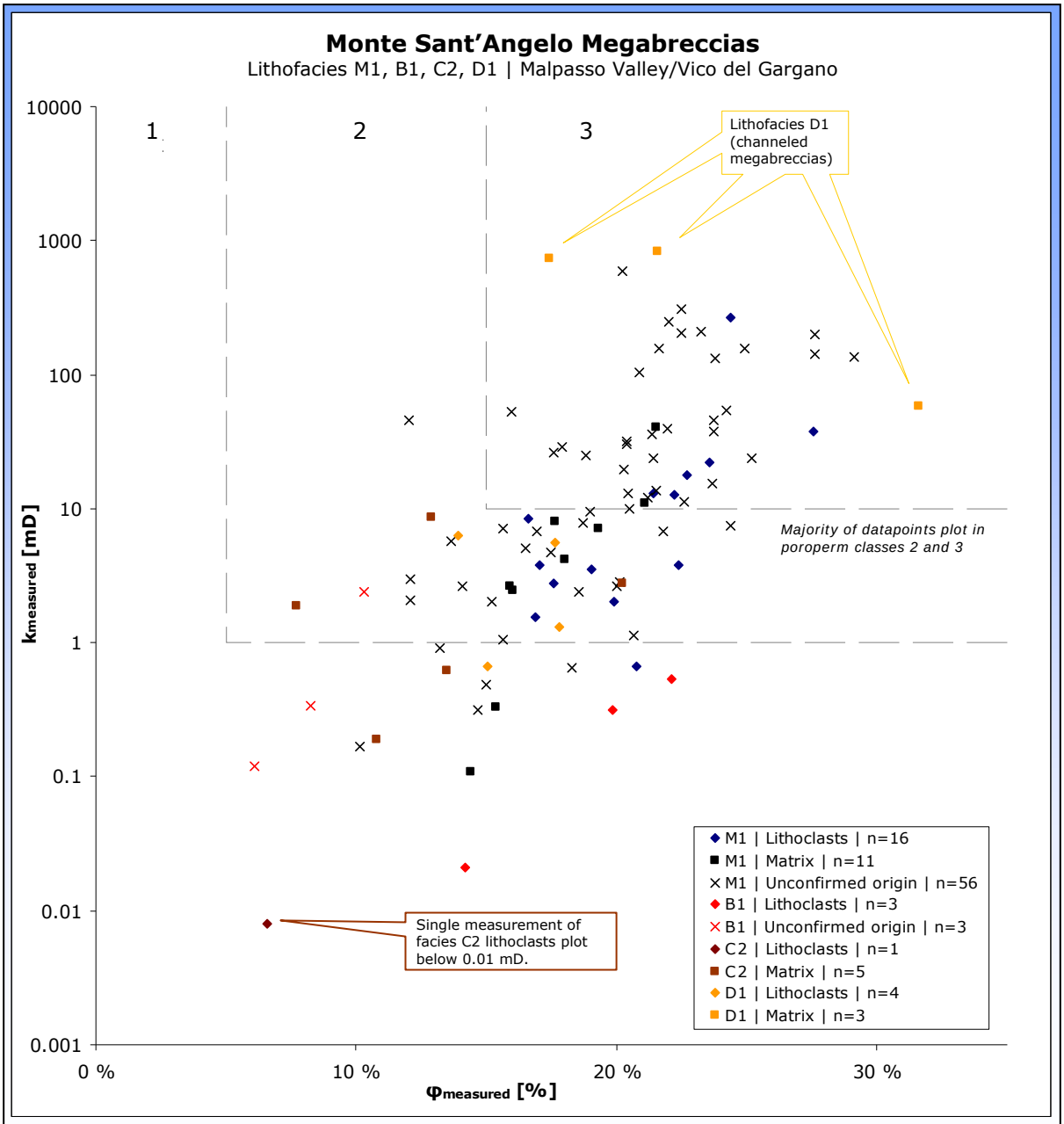

Figure 5.11 – All megabreccia samples by lithofacies and clast/matrix/unknown

Poroperm classes indicated. Lithofacies B1 is clast-supported.

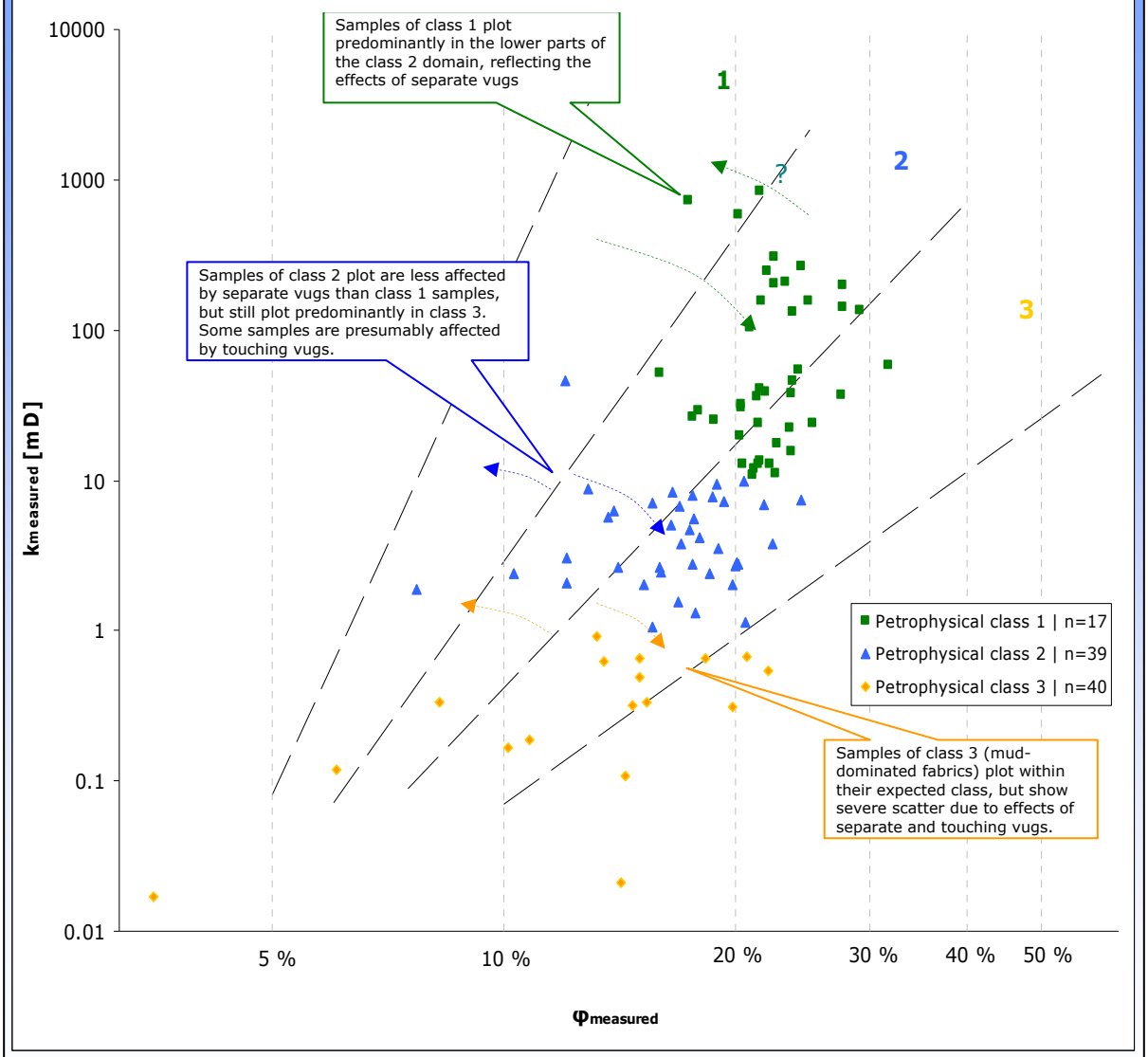

Figure 5.12 – All megabreccia according to assigned petrophysical class

Poroperm classes indicated. Lithofacies B1 is clast-supported.

MALPASSO GRID OF SAMPLES AND STATISTICAL ANALYSIS

The datapoints corresponding to 50 samples derived from the Malpasso Grid were plotted according to their height level in the grid (figure 5.12A&B). No vertical trends were recognized in these plots. The grid, however, represents one megabreccia-bearing bed of debris-flows. Although no intra-bed vertical trends were derived, vertical trends on reservoir scale are not investigated.

Figure 5.12C: 26 (52%) grid samples pertain to poroperm class 3, 18 (36%) samples belong to poroperm class 2 while the remaining 6 (12%) samples belong to poroperm class 1. Among the 100 samples derived from all megabreccias (both localities) (figure 5.11), 42 (42%) belong to poroperm class 3, 39 (39%) belong to class 2 while 19 (19%) belong to class 3. Of the 79 samples that were derived from the Malpasso Valley outcrop (lithofacies M1) only, 39 (50%) samples belong to class 3, 32 (40%) samples pertain to class 2 while the remaining 8 (10%) belong to poroperm class 1. A total of 94 samples were derived from matrix-supported megabreccias (lithofacies M1, C2 and D1). Among these, 42 (45%) samples meet the requirements for poroperm class 3, 38 (40%) belong to class 2 while 14 (15%) samples are placed within poroperm class 3.

Statistical analysis of values derived from the grid, compared to selected sample populations (table 5.1A & B) suggest that the arithmetic mean permeability values of the grid only differ from those of the clast-supported megabreccias (unit B) with statistical significance, for both permeability values. For porosity values, no significant differences were derived from the present dataset. The differences in variance between grid-derived values and other selected populations differed with statistical significance for all compared populations except the population consisting of all samples from the Malpasso Valley. In other words, the grid-derived poroperm values did show significantly different variances than all populations that included Vico del Gargano-samples.

These observations suggest that the clast-supported megabreccias cannot be represented by the Malpasso West Wall grid in terms of poroperm signatures but that the grid is sufficiently representative of the megabreccias exposed in the Malpasso Valley. This underpins the use of flow-units within which representative poroperm values are obtained.

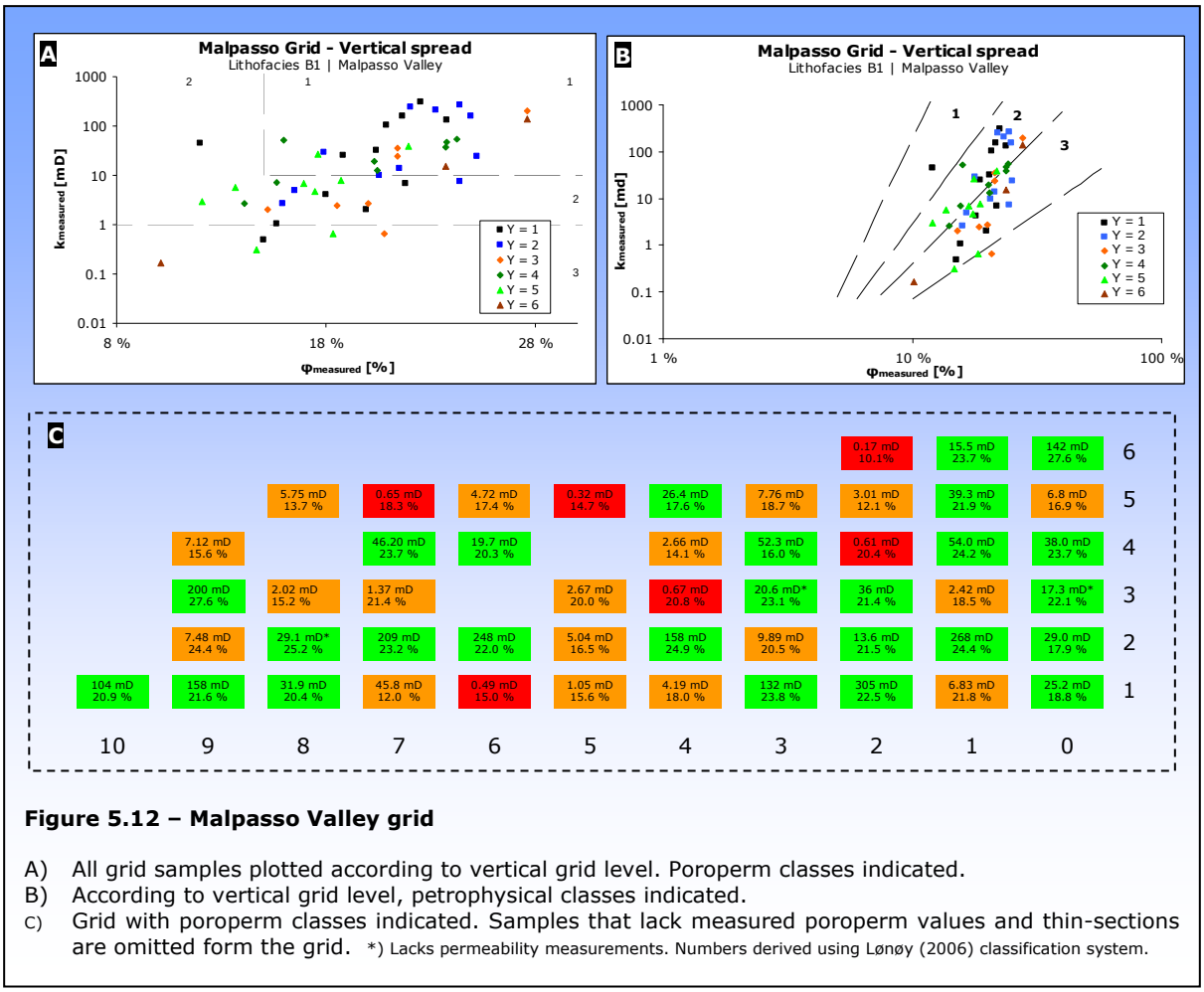

Figure 5.12 – Malpasso Valley grid

A) All grid samples plotted according to vertical grid level. Poroperm classes indicated.
B) According to vertical grid level, petrophysical classes indicated.
C) Grid with poroperm classes indicated. Samples that lack measured poroperm values and thin-sections are omitted form the grid. *) Lacks permeability measurements. Numbers derived using Lønøy (2006) classification system.

Table 5.1A: Permeability values from grid compared with selected populations

	n	GM (k)	AM (ln k)	ΔAM [mD] t-test for ΔAM (α = 0.05)	SD	VA (ln k)	ΔV [mD] F-test for ΔV (α = 0.05)
Grid	**50**	**13.3**		**← 2.59 →**	**1.9**		**← 3.63 →**
All samples	103	7.4	2.0	1.80 **$t>t_\alpha$**	2.5	6.33	15.0 **$F<F_\alpha$**
All MB	99	6.7	1.9	1.99 **$t>t_\alpha$**	2.4	5.81	2.2 **$F<F_\alpha$**
M. supp.	93	8.3	2.1	1.6 **$t>t_\alpha$**	2.3	5.33	1.7 **$F<F_\alpha$**
Malpasso	79	10.9	2.4	1.23 **$t>t_\alpha$**	1.9	3.55	0.08 **$F>F_\alpha$**
C. supp.	6	0.3	-1.3	50.4 **$t<t_\alpha$**	1.6	2.50	1.1 **$F<F_\alpha$**

Table 5.1B: Porosity values from grid compared with selected populations

	n	GM (%)	AM (%)	ΔAM [%] t-test for ΔAM (α = 0.05)	SD	VA (%)	ΔV [%] F-test for ΔV (α = 0.05)
Grid	**52**	**19.3**		**← 19.8 →**	**4**		**← 0.2 →**
All samples	113	17.5	18.6	1.2 **$t>t_\alpha$**	1.4	0.3	0.1 **$F<F_\alpha$**
All MB	109	17.5	18.6	1.2 **$t>t_\alpha$**	1.4	0.3	0.1 **$F<F_\alpha$**
M. supp.	102	17.8	18.8	1 **$t>t_\alpha$**	1.2	0.3	0.1 **$F<F_\alpha$**
Malpasso	85	19.5	19.9	0.1 **$t>t_\alpha$**	0.4	0.2	> 0 **$F>F_\alpha$**
C. supp.	7	13.5	15.1	4.7 **$t>t_\alpha$**	3.3	0.3	0.1 **$F<F_\alpha$**

n	Number of samples in the selected population	All samples	Complete dataset
GM	Geometric mean	All MB	All megabreccia samples
AM	Arithmetic mean	M. supp.	Matrix-supported megabreccias only
SD	Standard deviation	Malpasso	Malpasso samples only (unit M)
VA	Variance	C. supp.	Clast-supported megabreccias only

Malpasso Valley compared to Vico del Gargano quarry samples: Difference in mean arithmetic porosity values (Δ = 5.53 porosity units) (table 5.2A) is statistically significant for $\alpha = 0.005$. Difference in the mean geometric values (Δ = 9.81 mD) (table 5.2B) is statistically significant for $\alpha = 0.025$.

Malpasso clast samples compared to Malpasso matrix samples show a difference in mean arithmetic porosity (Δ = 2.12 porosity units) (table 5.3A) that is not statistically significant for $\alpha = 0.05$. The difference in mean geometric permeability values (Δ = 2.98 mD) (table 5.3B) is neither statistically significant for $\alpha = 0.05$.

Comparison of Vico del Gargano clasts and matrix samples show a difference in mean arithmetic porosity values (Δ = 1.74 porosity units) (table 5.4A) that is not statistically significant for $\alpha = 0.05$. The difference in mean geometric permeability values (Δ = 10.32 mD) (table 5.4B) is statistically significant for $\alpha = 0.025$ but not statistically significant for $\alpha = 0.05$ when outliers (samples #346 and #354) are omitted (table 5.4C).

Difference in mean arithmetic porosity values (Δ = 1.5 porosity units) (table 5.4D) between units B and C is not statistically significant for $\alpha = 0.05$. Neither is the difference in permeability mean geometric values between these two units

Table 5.2 – Malpasso Valley vs. Vico del Gargano Quarry samples

Malpasso vs. Vico: Porosity				
Table 5.2A	Malpasso	Vico	F-test	t-test
n	78	28		
Arithmetic mean	19.7 %	14.17 %		$t > t_{\alpha=0.005}$
Standard deviation	4.14	7.06		
Variance	17.12	49.83	$F > F_{\alpha=0.05}$	
Malpasso vs. Vico: Permeability				
Table 5.2B	Malpasso	Vico	F-test	t-test
n	74	26		
Arithmetic mean	2.4291 mD	0.43088 mD		$t > t_{\alpha=0.025}$
Standard deviation	1.8979	3.9593		
Variance	3.602	15.676	$F > F_{\alpha=0.05}$	
Geometric mean	11.34 mD	1.53 mD		

Table 5.3 – Malpasso Valley results

Malpasso, clasts vs. matrix samples: Porosity				
Table 5.3A	Clast samples	Matrix samples	F-test	t-test
n	14	8		
Arithmetic mean	19.98	17.86		$t < t_{\alpha=0.05}$
Standard deviation	3.62	2.58		
Variance	13.08	6.64	$F < F_{\alpha=0.05}$	
Malpasso, clasts vs. matrix samples: Permeability				
Table 5.3B	Clast samples	Matrix samples	F-test	t-test
n	14	8		
Arithmetic mean	19.9874	1.4618		$t < t_{\alpha=0.05}$
Standard deviation	1.5689	1.7530		
Variance	2.4615	3.0733	$F < F_{\alpha=0.05}$	
Geometric mean	7.29 mD	4.31 mD		

(Δ= 1.08 mD), for α = 0.05 (table 5.4E). Difference in mean arithmetic porosity values between units B and D (Δ = 6.35 porosity units) (table 5.4F) is not statistically significant for α = 0.05, while the difference in mean geometric permeability values (table 5.4G) (Δ = 297.36 mD) is statistically significant for α = 0.0005. Unit C compared with unit D show difference in mean arithmetic porosity values (Δ = 7.85 porosity units) that is statistically significant for α = 0.05 (table 5.4H). The difference in mean geometric permeability values (Δ = 296.28 mD) is statistically significant for α = 0.025 (table 5.4I).

Table 5.4 – Vico del Gargano results

Clast vs. matrix samples: Porosity				
Table 5.4A	Clast samples	Matrix samples	F-test	t-test
n	12	8		
Arithmetic mean	14.41 %	16.15 %		$t < t_{\alpha=0.05}$
Standard deviation	4.60	8.20		
Variance	21.18	67.20	$F > F_{\alpha=0.05}$	
Clast vs. matrix samples: Permeability (F- and t-tests based on ln k values)				
Table 5.4B	Clast samples	Matrix samples	F-test	t-test
n	10	8		
Arithmetic mean	-1.1072	2.3652		$t > t_{\alpha=0.025}$
Standard deviation	3.1116	3.1509		
Variance	9.682	9.9283	$F < F_{\alpha=0.05}$	
Geometric mean	0.33 mD	10.65 mD		
Clast vs. matrix samples: Permeability (F- and t-tests based on ln k values) (samples #346 and #354 omitted).				
Table 5.4C	Clast samples	Matrix samples	F-test	t-test
n	10	6		
Arithmetic mean	-1.1072	0.93184		$t < t_{\alpha=0.05}$
Standard deviation	3.1116	2.0089		
Variance	9.682	4.0356	$F < F_{\alpha=0.05}$	
Geometric mean	0.33 mD	2.54 mD		
Unit B vs. Unit C: Porosity				
Table 5.4D	Clast samples	Matrix samples	F-test	t-test
n	9	15		
Arithmetic mean	14.52	13.02		$t < t_{\alpha=0.05}$
Standard deviation	7.05	7.16		
Variance	49.66	51.28	$F < F_{\alpha=0.05}$	
Unit B vs. Unit C: Permeability				
Table 5.4E	Unit B	Unit C	F-test	t-test
n	8	13		
Arithmetic mean	-1.8637	0.21491		$t < t_{\alpha=0.05}$
Standard deviation	1.9829	3.7357		
Variance (ln)	3.9318	13.956	$F < F_{\alpha=0.05}$	
Geometric mean	0.16 mD	1.24 mD		
Unit B vs. Unit D: Porosity				
Table 5.4F	Unit B	Unit C	F-test	t-test
n	9	3		
Arithmetic mean	14.52	20.87		$t < t_{\alpha=0.05}$
Standard deviation	7.05	4.77		
Variance	49.66	22.77	$F < F_{\alpha=0.05}$	
Unit B vs. Unit D: Permeability				
Table 5.4G	Unit B	Unit D	F-test	t-test
n	8	4		
Arithmetic mean	-1.8637	5.6955		$t > t_{\alpha=0.0005}$
Standard deviation	1.9829	3.7993		
Variance	3.9318	14.435	$F < F_{\alpha=0.05}$	
Geometric mean	0.16 mD	297.52 mD		
Unit C vs. unit D: Porosity				
Table 5.4H	Unit C	Unit D	F-test	t-test
n	15	3		
Arithmetic mean	13.02	20.87		$t > t_{\alpha=0.05}$
Standard deviation	7.16	4.77		
Variance	51.28	22.77	$F < F_{\alpha=0.05}$	
Unit C vs. unit D: Permeability (T- and f-tests based on ln k)				
Table 5.4I	Unit C	Unit D	F-test	t-test
n	13	4		
Arithmetic mean	0.21491	5.6955		$t > t_{\alpha=0.025}$
Standard deviation	3.7357	3.7993		
Variance	13.956	14.435	$F < F_{\alpha=0.05}$	
Geometric mean	1.24 mD	297.52 mD		

THE EFFECT OF DIAGENESIS ON POROPERM SIGNATURES

The present dataset display abundant moldic porosity, produced by the dissolution of grains in the marine-phreatic domain prior to re-sedimentation and re-deposition. These separate vugs increase porosity without contributing to permeability, as they are only interconnected through the interparticle porosity that occupies the areas between the moulds (*e.g.* Lucia, 2007). The effect of touching vugs may increase permeability drastically (*e.g.* Lucia & Ruppel, 1996; Lucia, 2007). Such porosity exists in the present dataset, and is described in the diagenetic history of these sediments. Their effects on poroperm datapoints have been demonstrated. However, it is evident that the effect of separate vugs is reflected to a far greater extent compared to the effect of touching vugs. It may be argued that these to some extent will counter-effect each other, but the net-offset of the datapoints are demonstrated to be towards the influence of separate vugs. This is probably the echo of scale- and directional dependence of touching vugs systems. Hence, larger samles may reflect better this effect than the present database. Several concerns have been addressed on the fact that plug data not adequately describe such fabrics (*i.e.* Lucia 1999, 2007; Honarpou *et.al.* 2003; Byrnes, 2004; Zhang *et.al.*, 2005; Ehrenberg, 2007) and it is a common sense perception that larger samples better capture heterogeneous fabrics. This is important in terms of reservoir description through core- and plug analysis.

Another important take-away from these plots is that the effect of separate vugs apparently decrease as fabrics become increasingly mud-dominated. This reflects the sedimentological observations that are presented in chapter 3, which revealed that separate vugs occur predominantly as moldic pores defined by dissolved grains. The relative grain-dominance of a sample is reflected in the assignment of petrophysical classes and is also in this study reflected by the subdivision of microfacies. When grain-content decreases, the amount of moldic pores decrease accordingly and the effect of these separate vugs subsequently decreases.

6 IMPLICATIONS FOR RESERVOIR CHARACTERIZATION

Carbonate slope megabreccias may form significant reservoirs (*e.g.* Enos & Moore, 1983; Cook & Mullins, 1983; Enos, 1985; Casabianca *et.al.*, 2002) by the introduction of significant volumes of reservoir rocks into the lower-slope to basinal areas. A number of reservoirs produce from slope-deposits (e.g. the Poza Rica Field offshore Mexico (Enos, 1977)), and megabreccia-bearing reservoir levels has been reported from several carbonate fields, although most of them are associated with karst systems (Sun *et.al.*, 1998; Casabianca *et.al.*, 2002). Apulian Platform carbonates form the reservoir unit in several major oil fields in the Val d'Agri area of southern Italy (Shiner *et.al.*, 2004), but no reports or published data on production from slope megabreccia deposits in this area are available. In-house studies by BG International during the mid-1990s identified platform-margin megabreccias as one of several potential reservoir facies (Beckett, 1994; Beckett *et.al.*, 1995, as reported by Casabianca *et.al.*, 2002).

POROSITY AND PERMEABILITY

Porosity of the Monte Sant'Angelo Megabreccias is to a large extent controlled by the diagenetic evolution. Dissolution of grains in the marine-phreatic zone produced secondary porosity. Isopachous calcite cement that precipitated within the same zone obstructed both initial and secondary porosity. Extensive equant calcite cements that precipitated within the meteoric-phreatic zone largely obstructed porosity and is to a large responsible for the relatively low effective porosity values that are displayed by these units. Later stage dissolution by fresh-water may have promoted permeability. It is implied that this later stage diagenetic overprint occurred during uplift, erosion and exposing of these sediments and the effect of this nonfabric-selective porosity should be removed in the assessment of reservoir quality of these deposits.

The petrophysical results have been presented in terms of poroperm classes which, although tempting, must not be directly translated to reservoir properties and quality. Although vital for reservoir characterization and existence, poroperm signatures alone do not provide very useful answers. Reservoir properties are derived from a number of other additional factors such as wettability, saturation, volume, connectivity and play. Poroperm classes may be combined with such other parameters in the assessment of reservoir properties.

Based on poroperm classes, however, the Monte Sant'Angelo Megabreccias display properties that indicate reservoir quality. A majority of datapoints plot within poroperm classes 2 and 3. Matrix-samples produced elevated values compared to corresponding lithoclasts for the northern succession units (BCD). This issue is discussed further in relations to zoning and segmentation of this potential reservoir.

ZONING

The present study has shown that zoning and segmenting of megabreccia intervals occurs at various scales.

Firstly, the Monte Sant'Angelo Megabreccias are confined in time and space depending on 1) accommodation space, 2) sediment production and 3) triggers for re-deposition. Megabreccias were not deposited during periods not meeting these criteria which may have created a segmenting on reservoir scale that may be seen in relations sequence stratigraphy and platform responses (i.e. sediment production).

Secondly, the Monte Sant'Angelo Megabreccias occurs as several stacked, and distinct, levels. In the southern parts, these were on outcrop scale amalgamated and no apparent hinders for fluid flow occurred between them. Unit C of the Vico del Gargano, on the other hand, show the occurrence of dense packstone clinoforms which are expected to obstruct and control the behavior of fluids within the stacked package of megabreccia debris-flow deposits. This effect is well known for siliciclastic reservoirs, where individual parasequences may segment the reservoir into flow units. These are, however generally mappable over long distances and possibly also between individual wells. This enables the mapping and modeling of such baffles. This may not be the case for the Monte Sant'Angelo Megabreccias and equivalent reservoirs. However, it is noted that the slope at this particular spot probably occupied a very narrow zone. The clinoforms may segment the reservoir vertically, but may not contribute much to horizontal (lateral) segmentation.

Thirdly, lithoclasts and matrix display different petrophysical properties and their contacts are distinct. The mapping of fluid behavior across lithoclast-matrix boundaries is important for the overall fluid flow through these sediments.

Samples of lithofacies D1 and C2 display higher porosity and permeability for the matrix than for the corresponding lithoclasts. This probably reflects the provenance area for these materials, which may not have produced reservoir quality rocks. Matrix was probably formed by the disintegration of lithoclasts and incorporation of other facies during transport, and this re-organization of sediments produced fabrics with elevated reservoir qualities which now constitute the matrix to these megabreccia units. It is likely that flow through these deposits would be facilitated mainly through the matrix rather than lithoclasts which in this specific case are more resistant to flow. It is further implied that although lithoclasts have lower permeability, they would still account for a fair amount of total hydrocarbon storage space within these deposits. This poses a significant challenge in the modeling, simulation and production of hydrocarbons that are trapped in reservoirs that are dominated by matrix-supported megabreccia debris-flows.

Unit D display stacked megabreccia debris-flows that are interbedded with proximal turbidites which show elevated poroperm values. This clear differentiation of poroperm signatures within such depositional packages is important information that has impact on reservoir characterization of such deposits. The intra-unit megabreccia bodies are able to store hydrocarbons, but the surrounding turbidite deposits may display much greater ability to transmit fluid-flow. The difference in flow-properties poses a major challenge for reservoir modeling, simulation and production.

LOG RESPONSES AND THE PREDICTION OF PERMEABILITY

Focus on permeability estimation based on porosity data may contribute to the standing challenge of permeability estimation for carbonate reservoirs. Permeability is generally derived from core-data (high resolution) or production tests (low resolution), but may also be derived from electric logs that measure intrusion of drilling fluids to the formation and magnetic resonance logs (MR/NMR). As pointed out by several authors (*e.g.* Lønøy, 2006), the calibration of well-log responses to permeability data from cores works well in reservoirs with a simple and continuous relationship between porosity and permeability such as clean sandstones. It is considered here that the Monte Sant'Angelo Megabreccias does not provide such simple relationships.

Several published studies deal with the estimation of permeability based on well log data for carbonate reservoirs (*e.g.* Ahmed *et.al.*, 1991; Hassall *et.al.*, 2004; Frank *et.al.*, 2005; Sullivan *et.al.*, 2006; Ballosino *et.al.*, 2006; Suat Bagci & Akbas, 2007) and the ongoing research on this subject is one of great importance in the pursuit for cost-efficient, reliable and continuous permeability mapping on reservoir scale.

The data for the present study displays that one-dimensional data are not transferable to larger areas. I.e. no columns of the Malpasso grid of samples are representative for the entire grid. The grid is further not representative for the megabreccias exposed in Vico del Gargano.

Some lithoclasts display preserved internal bedding, and the outlines of these may be derived from dip-meter logs. This may further provide a basis for the calibration of other logging equipments to the signatures of lithoclasts and matrix. This may provide clues as to megabreccia types and depositional model (matrix vs. clast-supported). Image-logs may provide clues as to dominant pore-types and petrophysical classes (*e.g.* Lucia, 2007), and may assists in the mapping of diagenetic impact.

VOLUMES AND PLAY

Volumes depend on the mapping of lateral extent and variations, which has not been performed for the purpose of the present study. Casabianca *et.al.* (2002) published volumetric estimates for the megabreccias of the Maiella Carbonate platform, but the transferability of these numbers to the Apulia slope is questionable and the present data does not support such applications.

It is assumed that the megabreccias are confined to the lower-slope, that they pinch-out upwards (marginwards) and downwards (basinwards) and are overlain by non-reservoir deposits. This may coincide with a 'Tamabra play' (Viniegra & Castillo, 1970; Enos, 1977, 1985, 1988;) which is one of carbonate slope deposits pinch-out up-dip into sealing basinal facies (Horbury *et.al.*, 2005). The discussion on this subjects is speculative. Graziano (2001) states that the Monte Sant'Angelo Megabreccias was mapped with thicknesses of some 200 m in the vicinity of the town of Monte Sant'Angelo, on the southern Gargano. Depending on the lateral extent, this may imply that these debrites may form significant reservoir volumes.

IMPACT OF DIAGENESIS

The effect of diagenesis and the mapping of diagenetic history for carbonate reservoirs are crucial inputs to any decisions be it in the exploration, production or field-development phases. For the Monte Sant'Angelo Megabreccias, late diagenetic alterations of the sediments have significantly lowered the porosity of these sediments. While early diagenesis increases porosity through dissolution of grains, the coinciding marine-phreatic cementation obstructs interparticle porosity. Burial diagenesis have affected the matrix to the megabreccias for the most part, while porosity within lithoclasts has been preserved through early lithification and cementing. This being said, petrophysical analysis of units B and C (Vico del Gargano) indicate that lithoclasts display lower poroperm values compared to the surrounding matrix. As discussed in chapter 5, this effect probably reflects that the margin and upper-slope environments from which the sediments were derived, displayed poor initial reservoir properties. The disintegration of lithoclasts as well as the incorporation of additional sediments in the debris-flows during transport promoted the reservoir properties of the matrix. This has important implications in terms of reservoir characterization, as it is expected that production from such bimodal reservoirs will drain the high-permeability matrix promoting immature water break-trough and encapsulating remaining hydrocarbons that are situated within lithoclasts. Such partial production will to a large extent influence the recovery factor of such reservoir facies.

7 SUMMARY AND CONCLUSIONS

The Monte Sant'Angelo Megabreccias have been investigated through the mapping, description and interpretation of two successions on the Gargano Promontory, Apulia, southern Italy. These were exposed in the Malpasso Valley and the Vico del Gargano quarry, on the southern and northern parts of the Gargano, respectively.

SUMMARY

The two successions were selected based on previously published data, indicating that they represented proximal (Malpasso) and distal (Vico del Gargano) positions relative to the Cretaceous platform margin. These data were largely based on outcrops on the southern Gargano (e.g. Graziano, 2001; *see also figure 2.4)*. The occurrence of clast-supported megabreccias in the northern succession, however, proposes that it may not be directly transferable to the northern parts of the Gargano.

The northern and southern succession displayed important differences in terms of depositional pattern, fabric and petrophysical properties which, along with petrophysical analysis, promoted the subdivision of the two successions into flow units. The southern succession displayed an aggrading package of matrix-supported megabreccias confined to amalgamated, 10-15 m beds. The northern succession display the transition from clast-supported, chaotic megabreccias into prograding, matrix-supported megabreccias that were confined to 5-10 m beds separated by packstone clinoforms, and capped by a channelled package of 1-2 m megabreccia beds interbedded with proximal calciturbidites.

While the matrix-supported megabreccias are interpreted as deposits of debris-flows that were matrix-supported also during transport, the clast-supported debrites are interpreted as grain-flow deposits.

Stratigraphic analysis allowed for the mapping of subfacies that suggests that megabreccias were derived from the marginal and upper-slope environment. This agrees with previously published studies. It is further suggested, based on this dataset, that provenance for the northern and southern megabreccias were different in terms of energy-level and subsequent reservoir quality. This

translates into differences in energy-levels along the eastern margin of the Apulian Platform, agreeing with previously published interpretations.

The Monte Sant'Angelo Megabreccias was triggered by synsedimentary tectonics, but accommodation space controlled their depositional pattern. For the southern succession, faults that dissected the platform margin were interpreted, agreeing with the speculations put forwards by Borgomano (2000). These faults induced the elevated generation of accommodation space. However, high rates of sedimentation in the adjacent carbonate factory matched the available accommodation space and induced the aggrading pattern which is displayed in the southern succession. It is further implied that differentiated subsidence rates during the Cenomanian provoked the differences in accommodation space and generated the synsedimentary tectonic activity that triggered these debrites. In terms of trigger-mechanisms, this study agrees with previously published data concerning these deposits (e.g. Graziano, 2001) as well as other studies related to limestone megabreccias (e.g. Spence & Tucker, 1997).

No indications of siliciclastic input was recorded, which supports previously published interpretations of the geometry of the Cretaceous Apulian Platform.

Diagenetic history of these sediments display a succession of cementation and dissolution that may be described in terms of four major stages and domains; 1) the marine-phreatic zone is characterized by the dissolution of grains and precipitation of an isopachous bladed calcite cement. 2) The meteoric-phreatic zone was characterized by the precipitation of equant calcite cement that constitutes the volumetrically most dominant cement generation in these sediments. 3) Burial diagenesis was characterized by compaction features, and affected the matrix to a greater extent than corresponding lithoclasts, reflecting the lithified fabric of the latter. 4) Uplift and sub-aerial exposure during Tertiary times induced fresh-water leaching and promoted the evolution of a diffuse nonfabric-selective porosity that affected both matrix and lithoclasts.

One hundred and seventeen plug samples with corresponding thin-sections and porosity/permeability measurements formed the petrophysical database. Porosity was estimated based on image analysis, and compared with the corresponding measured values. This displayed a significant scatter, and a clear offset of datapoints indicating that estimated values were significantly lower than the measured values. This is explained by the estimation method failure to include

smaller pores and microporosity. No results relating fabric or thin-section quality to the errors was observed. This bias reflected in permeability estimation and prediction using the Lucia (1983, 1995, 1999, 2007) system. The permeability estimations derived using the system developed by Lønøy (2006) displayed better correlations to measured permeability.

In an attempt to produce good correlations of porosity and permeability, the database was classified according to the systems developed by Choquette & Pray (1970), Lucia (1983, 1995, 1999, 2007) and Lønøy (2006). The subgroups of the Choquette & Pray system coincided with the subdivision of the Lønøy-system for this database. Although these latter systems produced better correlations for porosity and permeability relative to the Lucia-system, all three systems failed to produce adequately correlations. The coefficients of correlations that were obtained by Lønøy (2006) were not reproduced for the present dataset. However, this is seen in relations to the failure of the present database to meet all requirements laid down by Lønøy (2006). Further, the plugs of the present database were larger than those used by Lønøy (2006), and it is suggested that this may reflect in poorer R^2-values.

The majority of megabreccia datapoints plot in poroperm classes 2 and 3 (porosity above 15 %, and permeability above 10 mD), which suggests that they display reservoir quality in terms of porosity and permeability. However, the complete reservoir characterization relies on a number of additional parameters and the present database does not support conclusions on this subject.

The majority of megabreccia datapoints are shifted towards the right in terms of petrophysical classes (Lucia, 1983, 1995, 1999, 2007). This reflects the abundant moldic porosity that these sediments display, and coincide with stratigraphic description and interpretation. The effect of touching vugs is also recognized in the petrophysical data, but not to the extent that might be anticipated from stratigraphical analysis. This apparent deteriorating is subscribed to the failure of plug-scale samples to capture adequately this scale- and directional dependent fabric.

50 samples were gathered from an 11x5 m grid of samples in the southern succession. No vertical trends within this grid were recognized in terms of poroperm classes and petrophysical classes. Statistical analysis reveals that the grid of samples adequately represents the southern succession but fail to capture

the petrophysical properties of the northern succession. This underpinned the need for separately described flow-units.

Important implications for reservoir characterization of these deposits were described. Zoning of these units are expected to occur on different scales. Firstly, the mapped successions display deposits that are confined in time and space by features of the depositional environment that must be fulfilled. This include trigger-mechanisms, sediment production and accommodation space. Secondly, the description of clinoforms in the northern succession (unit C) that from petrophysical analysis indicate low porosity and permeability, may segment this unit into sub-units in terms of flow. Thirdly, the different petrophysical properties of lithoclasts and corresponding matrix may have implications for production and pose challenges for the modelling of such debrites.

The intense heterogeneity of these debrites poses important challenges as to the interpretation of their responses to wireline or LWD logging. It is suggested that dipmeter logs may capture preserved bedding within lithoclasts and potentially provide a basis for calibration. The volumes of these debrites are not mapped for the purpose of this study, but it is indicated that they may form significant reservoirs. Based on previously published studies (*e.g.* Graziano, 2001), it is implied that these debrites may form significant reservoir volumes.

CONCLUSIONS

- Occurrence of clast-supported megabreccias in the Vico del Gargano may not correlate with the established paleogeometry of the Apulian platform margin. A reconsideration of this scheme is called for.
- Within the Monte Sant'Angelo Megabreccias, important differences was mapped in terms of fabric, depositional pattern, depositional mechanisms and petrophysical properties among different megabreccia flow-units as well as among the northern and southern successions.
- The debris-flows and grain-flow were triggered by synsedimentary tectonics, agreeing with previously published data. Their depositional patter was controlled by the accommodation potential.
- The majority of megabreccia datapoints plot in poroperm classes 2 and 3 (porosity above 15 %, and permeability above 10 mD), which suggests that they display reservoir quality in terms of porosity and permeability.
- Petrophysical data reflects the observations of separate vugs. The effect of touching vugs was, however, not recognized to the extent that was anticipated from stratigraphic analysis. This reflects that plug-scale samples may not be suited for description of such fabrics, which is highly scale- and directional dependent. This agrees with previously published concerns on this subject.
- The grid of samples that were gathered from the southern succession provided where representative of this succession. However, it failed to satisfactorily represent the megabreccias exposed in the northern succession. This is underpinned by statistical analysis of the data.
- Porosity and permeability of these debrites suggests reservoir quality. The southern succession displays generally higher values in terms of these petrophysical properties than do the northern succession. The northern succession was characterized by matrix samples displaying elevated values compared to their corresponding lithoclasts. This suggests that reservoir quality of these deposits were induced not by the preserved marginal facies, but probably the disintegration of lithoclasts during transport and reworking of sediments during deposition.

8 REFERENCES CITED

AHMED, U., CRARY, S.F. and COATES, G.R., 1991. Permeability estimation: The various sources and their interrelationships. *SPE paper 19604*.

ARCHIE, G.E., 1952. Classification of carbonate reservoir rocks and petrophysical considerations. *AAPG Bulletin*, **36**, p. 278-298.

AUROUX, C., MASCLE, J., CAMPREDON, R., MASCLE, G. and ROSSI, S., 1985. Cadre géodynamique et évolution récente de la dorsale Apulienne et de ses bordures (reported by Borgomano, 2000). *Giorn.Geol*, **47**, p. 101-127.

BALOSSINO, P., PAMPURI, F., BRUNI, C. and EBZHASAROVA, K., 2006. A new integrated approach to obtain reliable permeability profiles from logs in a carbonate reservoir. *SPE paper 102289*.

BARRON, E.J. and WASHINGTON, W.M., 1982. Cretaceous climate: A comparison of atmospheric simulations with the geologic record. *Palaeogeography, Palaeoclimatology, Palaeoecology*, **40**, p. 103-133.

BATHURST, R.G.C., 1966. Boring algae, micrite envelopes and lithification of molluscan biosparites. *Geological Journal*, **5**, p. 15-32.

BECKETT, D., 1994. Regional hydrocarbon geology and plays of the southern Apennines and Adriatic (reported by Casabianca *et.al.*, 2002). *British Gas International Internal Report*

BECKETT, D., FRETWELL, N., WILKES, M., SELLWOOD, B.W. and WILSON, E., 1995, Sedimentology and diagenesis of the uper cretaceous and early tertiary sequences of the Apulian platform on the Maiella mountain (reported by Casabianca *et.al.*, 2002). *British Gas International/Amoco WEBG/University of Reading Joint Venture Report*.

BERNER, R.A., 1980. Early diagenesis as a theoretical approach. Princeton, *Princeton University Press*, 241 p.

BERNOULLI, D., 1971. Redeposited pelagic sediments in the Jurassic of the Central Mediterranean area (reported by Bosellini *et.al.*, 1993). *Ann. Inst. Geol. Publ. Hung.*, **54**, p. 71-90.

BERNOULLI, D., BERTOTTI, G. and FROITZHEIM, N., 1990. Mesozoic faults and associated sediments in the Australpine-south Alpine passive continental margin. *Mem. Soc. Geol. It.*, **45**, p. 25-38.

BILLI, A., GAMBINI, R., NICOLAI, C. and STORTI, F., 2007, Neogene-quaternary intraforeland transpression along a Mesozoic platform-basin margin: The Gargano fault system, Adria, Italy. *Geosphere*, **3**, p. 1-15.

BOCCALETTI, M., CIARANFI, N., COSENTINO, D., DEIANA, G., GELATI, R., LENTINI, F., MASSARI, F., MORATTI, G., PESCATORE, T. and RICCI LUCCHI, F., 1990. Palinspastic restoration and paleogeographic reconstruction of the Peri-Tyrrhenian area during the Neogene. *Palaeogeography, Palaeoclimatology, Palaeoecology*, **77**, p. 41-50.

BORGOMANO, J.R.F., 2000. The upper cretaceous carbonates of the gargano-murge region, southern Italy: A model of platform-to-basin transition. *AAPG Bulletin*, **84**, p. 1561-1588.

BORGOMANO, J.R.F. and PHILIP, J., 1987. The Rudist carbonate buildups and the gravitary carbonates of the Gargano-Apulian margin (southern Italy, upper Senonian). *Mem. Soc. Geol. It.*, **40**, p. 125-132.

BOSELLINI, A. and MORSILLI, M., 1994. Il lago di varano (Gargano, Puglia Settentrionale): Una nicchia di distacco da frana sottomarina cretacea (reported by Bosellini *et.al.*, 1999). *Univ. Ferrara, Annali (N.S.), Sezione Scienze della Terra*, 5, p. 39-52.

BOSELLINI, A., MORSILLI, M. and NERI, C., 1999. Long-term event stratigraphy of the Apulia platform margin (upper Jurassic to Eocene, Gargano, southern Italy). *Journal of Sedimentary Research*, **69**.

BOSELLINI, A. and NERI, C., 1993. Il margine della piattaforma apula nel gargano meridionale (reported by Bosellini *et.al.*, 1999). *Sci. Terra*, **A**, p. 1-12.

BOSELLINI, A., NERI, C. and LUCIANI, V., 1993. Guida ai carbonati cretaceo-eocenici di scarpata e bacino del gargano (Italia meridionale) (reported by Bosellini *et.al.*, 1999). *Scienze della Terra*, **4**.

BOUMA, A.M., 1962. Sedimentology of some flysch deposits, a graphic approach to facies interpretation., *in* BOUMA, A.M., ed., Hypothetical origin, transport and deposition of turbidites. Amsterdam, *Elsevier*, p. 168.

BRANKMAN, C.M. and AYDIN, A., 2004. Uplift and contractional deformation along a segmented strike-slip fault system: The gargano promontory, southern italy. *Journal of Structural Geology*, 26, p. 807-824.

BUTLER, R.W.H., MAZZOLI, S., CORRADO, S., DE DONATIS, M., SCROCCA, D., DI BUCCI, D., GAMBINI, R., NASO, G., NICOLAI, C., SHINER, P. and ZUCCONI, V., 2004. Applying thick-skinned tectonic models to the Apennine thrust belt of Italy - limitations and implications.: Thrust tectonics and hydrocarbon systems., Memoir 82, *American Association of Petroleum Geologists*, 647-667 p.

CARANNANTE, G., RUBERTI, D., SIMONE, L. and VIGLIOTTI, M., 2007. Cenomanian carbonate depositional settings: Case histories from the central-southern Apennines (Italy). *SEPM Special Publication*, **87**.

CASABIANCA, D., BOSENCE, D. and BECKETT, D., 2002. Reservoir potential of Cretaceous platform-margin breccias, central Italian Appenines. *Journal of Petroleum Geology*, **25**, p. 179-202.

CASTELLARIN, A., 1972. Evoluzione paleotettonica sinsedimentaria del limite tra la ''piattaforma veneta'' e il ''bacino lombardo'', a nord di riva del garda (reported by Bosellini *et.al.*, 1999). *Giornale di Geologia*, **38**, p. 11-212.

CHIAPPINI, M., MELONI, A., BOSCHI, E., FAGGIONI, O., BEVERINI, N., CARMISCIANO, C. and MARSON, I., 2000. Shaded relief magnetic anomaly map of Italy and surrounding marine areas. *Annals of Geophysics*, 43, p. 983-989.

CHOQUETTE, P.W. and PRAY, L.C., 1970. Geological nomenclature and classification of porosity in sedimentary carbonates. *AAPG Bulletin*, **54**, p. 207-250.

CIARANFI, N., PIERI, P. and RICCHETTI, G., 1988. Note alla carta geologica delle murge e del salento (puglia centro-meridionale). *Mem. Soc. Geol. It.*, **41**, p. 449-460.

CONAGHAN, E., MOUNTJOY, E.W., EDGECOMBE, D.R., TALENT, J.A. and OWEN, P.E., 1976. Nubrigyn algal reefs (Devonian), eastern Australia; allochthonous blocks and megabreccias. *GSA Bulletin*, **87**, p. 515-530.

COOK, H.E., MCDANIEL, E., MOUNTJOY, E.W. and PRAY, L.C., 1972. Allochthonous carbonate debris flows at Devonian bank ('reef') margins Alberta, Canada. *Bull. Can. Petr. Geol.*, **20**, p. 439-497.

COOK, H.E. and MULLINS, H.T., 1983. Basin margin environment. *AAPG Memoirs*, **33**, p. 540-617.

CSOMA, A.E., GOLDSTEIN, R.H., MINDSZENTY, A. and SIMONE, L., 2004. Diagenetic salinity cycles and sea level along a major unconformity, Monte Composauro, Italy. *Journal of Sedimentary Research*, **74**, p. 889-903.

D'ARCHIAC, A., 1837. Mémoire sur la formation Crétacée du sud-ouest de la France. *Mémoires de la Société géologique de France*, **2**, p. 189-217.

DAVIS, J., 2002, Statistics and data analysis in Geology. Third Edition.: New York, *Wiley & Sons, Inc.*, 638 p.

DEWEY, J.F., HELMAN, M.L., TURCO, E., HUTTON, D.H.W. and KNOTT, S.D., 1989. Kinematics of the western Mediterranean, *in* COWARD, M.P., DIETRICH, D. and PARK, R.G., eds., Alpine tectonics. London, *Special Publications, Geological Society*, p. 265-283.

DI BUCCI, D., RAVAGLIA, A., SENO, S., TOSCANI, G., FRACASSI, U. and VALENSISE, G., 2006, Seismotectonics of the southern Apennines and Adriatic Foreland: Insights on active regional E-W shear zones from analogue modeling. *Tectonics*, **25**.

DICKSON, J.A.D., 1966. Carbonate identification and genesis as revealed by staining. *Journal of Sedimentary Research*, **36**, p. 491-505.

DICKSON, J.A.D., 1985. Diagenesis of shallow-marine carbonates. *Geological Society, London, Special Publications*, **18**, p. 173-188.

DRZEWIECKI, P.A. and SIMÓ, J.A., 2002. Depositional processes, triggering mechanisms and sediment composition of carbonate gravity flow deposits: Examples from the late Cretaceous of the south-central Pyrenees, Spain. *Sedimentary Geology*, **146**, p. 155-189.

DUNHAM, R.J., 1962. Classification of carbonate rocks according to depositional texture, *in* HAM, W.E., ed., Classification of carbonate rocks, *American Association of Petroleum Geologists*, p. 108-121.

EBERLI, G.P., BERNOULLI, D., SANDERS, D. and VECSEI, A., 1993. From Aggradation to Progradation: The Maiella platform, Abruzzi, Italy, *in* SIMO, T., SCOTT, R.W. and MASSE, J.P., eds., Cretaceous carbonate platforms, *American Association of Petroleum Geology*, p. 213-232.

EBERLI, G.P. and GINSBURG, R.N., 1989. Cenozoic progradation of north-western great Bahama bank, a record of lateral platform growth and sea-level fluctuation, *in* CREVELLO, P.D., WILSON, C.L., SARG, E. and READ, J.E., eds., Controls on carbonate platform and basin development, SEPM Spec. Publ., p. 323-338.

ELLIS, P.M., WILSON, C.L. and LEINFELDER, R.R., 1990, Controls on Upper Jurassic carbonate buildup development in the Lusitanian Basin, Portugal. *IAS Special Publication*, **9**, p. 169-202.

EMBRY, A.F. and KLOVAN, J.E., 1971, A Late Devonian reef tract on northeastern Banks Island, N.W.T. *Bulletin of Canadian Petroleum Geology*, 19, p. 730-781.

ENOS, P., 1977. Tamabra limestone of the Poza Rica Trend, Cretaceous, Mexico. *SEPM Special Publication*, **25**, p. 273-314.

ENOS, P., 1985. Cretaceous debris reservoirs, Poza Rica field, Veracruz, Mexico, *in* ROEHL, P.O. and CHOQUETTE, P.W., eds., Carbonate petroleum reservoirs: New York, *Springer Verlag*.

ENOS, P. and MOORE, C.H., 1983. Fore-reef slope environment. *AAPG Memoirs*, **33**, p. 508-537.

FIELD, M.E., GARDNER, J.M., JENNINGS, A.E. and EDWARDS, B.D., 1982. Earthquake-induced sediment failure on a 0.25 degree slope, Klamath River Delta, California. *Geology*, **10**, p. 542–546.

FINETTI, I., LENTINI, F., CARBONE, S., CATALANO, S. and DEL BEN, A., 1996. Il sistema appennino Meridionale-arco Calabro-Sicilia nel mediterraneo centrale: Studio Geologico-Geofisico (reported by Bosellini *et.al.*, 1999). *Bollettino della Societa Geologica Italiana*, **115**, p. 529-559.

FLÜGEL, E., 2004. Microfacies of carbonate rocks: Berlin, Heidelberg, New York, *Springer-Verlag*, 976 p.

FOLK, R.L., 1959. Practical petrographic classification of limestones. *AAPG Bulletin*, **43**, p. 1-38.

FOLK, R.L., 1962. Spectral subdivision of limestone types, *in* HAM, W.E., ed., Classification of carbonate rocks-a symposium, *American Association of Petroelum Geologists*, p. 62-84.

FRANK, S., 2005. Carbonate rock typing using NMR data: A case study from al Shaheen field, offshore Quatar. *SPE paper 71704*.

FUNICIELLO, R., MONTONE, P., PAROTTO, M., SALVINI, F. and TOZZI, M., 1999. Geodynamical evolution of an intra-orogenic foreland: The Apulia case history (Italy). *Bollettino della Societa Geologica Italiana*, **110**.

GARCIA-MONDEJAR, J., 1990. The Aptian-Albian carbonate episode of the Basque-Cantabrian basin (northern Spain): General characteristics, controls and evolution. *International Association of Sedimentology Special Publication*, **9**, p. 257-290.

GARCIA-MONDEJAR, J. and FERNANDEZ-MENIOLA, P.A., 1993, Sequence stratigraphy and systems tracts of a mixed carbonate and siliciclastic platform-basin setting: The albian of lunada and soba, northern spain. *AAPG Bulletin*, 77, p. 245-275.

GHISETTI, F. and VEZZANI, L., 1999, Depth and modes of Pliocene-Pleistocene crustal extension of the Apennines (Italy). *Terra Nova*, 11, p. 67-72.

GRANDIC, S., BOROMISA-BALAS, E., SUSTERCIC, M. and KOLBAH, S., 1999. Hydrocarbon possibilities in the eastern Adriatic slope zone of Croatian offshore area. *Nafta*, **50**, p. 51-73.

GRAZIANO, R., 1992. Il margine creatacio dell piattaforma carbonatica apula nel Promontorio Garganico: Sedimentologia e stratigrafia sequenziale (reported by Graziano, 2001). *Rend. Accad. Sci. Fis. Mat.*, **59**, p. 173-198.

GRAZIANO, R., 1994. Evoluzione cretacica del sistema "Piattaforma carbonatica apula/bacino est-garganico" Nel promontorio del Gargano. Sedimentologia e stratigrafia sequenziale (reported by Graziano, 2001). *Unpublished doctoral thesis, University of Naples, Italy*.

GRAZIANO, R., 1999. The early cretaceous drowning unconformities of the apulia carbonate platform (Gargano Promontory, Southern Italy): Local fingerprints of global palaeoceanographic events. *Terra Nova*, 11.

GRAZIANO, R., 2000. The Aptian–Albian of the Apulia Carbonate Platform (Gargano promontory, southern Italy): Evidence of palaeoceanographic and tectonic controls on the stratigraphic architecture of the platform margin. *Cretaceous Research*, **21**, p. 107 - 126.

GRAZIANO, R., 2001. The Cretaceous megabreccias of the Gargano Promontory (Apulia, southern Italy): Their stratigraphic and genetic meaning in the evolutionary framework of the Apulia Carbonate Platform. *Terra Nova*, **13**, p. 110-116.

HASSAL, J., FERRARIS, P., AL-RAISI, N.F., BOYD, A. and ALLEN, D.F., 2004. Comparison of permeability predictors from NMR, Formation Image and other logs in a carbonate reservoir. *SPE paper 88683*.

HEATH, K.C., MULLINS, H.T., VAN BUREN, M. and NEWTON, C.R., 1984. Anatomy of a modern open-ocean carbonate slope: Northern Bahama bank. *Sedimentology*, **31**, p. 141-168.

HINE, A.C., LOCKER, S.D., TENDESCO, L.P., MULLINS, H.T., HALLOCK, P., BELKNAP, D.F., GONZALES, J.L., NEUMANN, A.C. and SNYDER, S.W., 1992. Megabreccia shedding from modern, low relief Carbonate Platforms, Nicaraguan Rise. *GSA Bulletin*, **104**, p. 928–943.

HORBURY, A.D., HERNANDEZ, H., OJEDA, A., ITA, G. and ESTRADA, J., 2005. Revitalizing the Poza Rica field: New insights into the Tamabra reservoir and a tale of a paradigm lost. *Search and Discovery Article #20027 (2005), adapted from extended abstract, prepared by the authors for presentation at AAPG International Conference & Exhibition, Cancun, Mexico, October 24-27, 2004.*

HUSINEC, A. and JELASKA, V., 2006. Relative sea-level changes recorded on an isolated carbonate platform: Tithonian to Cenomanian successions, southern Croatia. *Journal of Sedimentary Research*, 76, p. 1120-1136.

IANNONE, A., 1996. Segnalazione di strutture da deformazione sinsedimentaria in una successione carbonatica Cenomaniana, nei pressi di Bari (reported by Graziano, 2001). *Mem. Soc. Geol. It.*, 51, p. 209-215.

JAMES, N.P. and CHOQUETTE, P.W., 1990. Limestones - the meteoric diagenetic environment, *in* MCILREAT, I.A. and MORROW, W., eds., Diagenesis, *Geoscience Canada*, p. 35-73.

JAMES, N.P. and KENDALL, A.C., 1992. Introduction to carbonate and evaporitic facies models: Facies models. Response to sea level change: St. John's, Newfoundland, *Geological Association of Canada*.

JAMES, N.P. and MOUNTJOY, E.W., 1983. Shelf-slope break in fossil carbonate platforms: An overview, *in* STANLEY, D.T. and MOORE, G.T., eds., The shelf-break: Critical interface on continental margins, *Soc. Econ. Paleontol. Miner. Spec. Publ*, p. 189-206.

JELASKA, V., 1973. Paleogeographical and petroleum — geological considerations of the western part of the dinaric carbonate shelf. *Geol. Vjesn.*, **25**, p. 57–64.

KLINKENBERG, L.J., 1941. The permeability of porous media to liquids and gases. *Drilling and Production Practice, American Petroleum Institute*, p. 200-213.

LINDHOLM, R.C. and FINKLEMAN, R.B., 1972. Calcite staining: Semiquantitative determination of ferrous iron. *Journal of Sedimentary Petrology*, **42**, p. 239-242.

LLOYD, C.R., 1982. The Mid-Cretaceous Earth: Paleogeography, ocean circulation and temperature; atmospheric circulation. *Journal of Geology*, **90**, p. 393-413.

LUCIA, F.J., 1983. Petrophysical parameters estimated from visual description of carbonate rocks: A field classification of carbonate pore space. *Journal of Petroleum Technology*, **35**, p. 629–637.

LUCIA, F.J., 1995. Rock-fabric/petrophysical classification of carbonate pore space for reservoir characterization. *AAPG Bulletin*, **79**, p. 1275-1300.

LUCIA, F.J., 1999. Carbonate Reservoir Characterization. New York, *Springer Verlag*.

LUCIA, F.J., 2007. Carbonate Reservoir Characterization: An integrated approach (2nd edition). New York, *Springer Verlag*.

LUCIA, F.J. and RUPPEL, S.C., 1996. Characterization of diagenetically altered carbonate reservoirs, South Cowden Grayburg Reservoir, West Texas. *SPE paper 36650*.

LØNØY, A., 2006. Making sense of carbonate pore systems: Implication for porosity cut-off and STOOIP. *AAPG Bulletin*, **90**, p. 1381-1405.

MARJANAC, T., 1985. Composition and origin of the megabed containing huge clasts: Flysch formation, middle Dalmatia, Yugoslavia (reported by Spence & Tucker, 1997). Int. Assoc. Sedimentol. 6th Eur. Regional Mtg., p. 270-273.

MARSELLA, E., BALLY, A.W., CIPPITELLI, G., D'ARGENIO, B. and PAPPONE, G., 1995. Tectonic history of the Lagonegro domain and southern Apennine thrust belt evolution. *Tectonophysics*, **252**, p. 307-330.

MAURER, F., 2000. Growth mode of middle Triassic carbonate platforms in the western Dolomites (southern Alps, Italy). *Sedimentary Geology*, **134**, p. 275-286.

MENARDI NOGUERA, A. and REA, G., 2000. Deep structure of the Campanian-Lucanian arc (southern Apennine, Italy). *Tectonophysics*, 324, p. 239-265.

MONACO, C., TORTORICI, L. and PALTRINIERI, W., 1998. Structural evolution of the southern Apennines, southern Italy. *Journal of Structural Geology*, **20**, p. 617-638.

MORSILLI, M. and BOSELLINI, A., 1997. Carbonate facies zonation of the Upper Jurassic-lower Cretaceous Apulia Carbonate Platform margin (Gargano Promontory, southern Italy). *Riv. Ital. Paleont. Stratigr.*, **103**, p. 193-206.

MOSTARDINI, F. and MERLINI, S., 1986. Appennino Centro-Meridionale. Sezioni geologiche e proposta di modello strutturale (reported by Graziano, 1999). *Mem. Soc. Geol. It.*, **35**, p. 177-202.

MOUNTJOY, E.W., COOK, H.E., PRAY, L.C. and MCDANIEL, P.N., 1972. Allochthonous carbonate debris flows - world wide indicators of reef complexes, banks or shelf margins: 24th Int. Geol. Congr. Sect., p. 172-190.

MULLINS, H.T., GARDULSKI, A.C. and HINE, A.C., 1986. Catastrophic collapse of the west Florida Carbonate Platform margin. *Geology*, **14**, p. 167–170.

MUTTI, E., BERNOULLI, D., EBERLI, G.P. and VECSEI, A., 1996. Depositional geometries and facies associations in an upper Cretaceous prograding carbonate platform margin (Orfento supersequence, Maiella, Italy). *Journal of Sedimentary Research*, **66**, p. 749-765.

MUTTI, E., LUCCHI, F.R., SEGURET, M. and ZANZUCCHI, G., 1984. Seismoturbidites: A new group of resedimented deposits. *Mar. Geol.*, **55**, p. 103–116.

NAYLOR, M.A., 1978. Slumping and debris-flows in the Palombini Limestone, northern Apennines. *J. Geol. Soc. London*, **135**, p. 247–257.

NAYLOR, M.A., 1981. Debris flow (Olistostromes) and slumping on a distal passive continental margin: The Palombini limestoneshale sequence of the northern Apennines. *Sedimentology*, **28**, p. 837–852.

NICOSIA, U., PETTI, F.M., PERUGINI, G., PORCHETTI, S.D., SACCHI, E., CONTI, M.A., MARIOTTI, N. and ZARATTINI, A., 2007. Dinosaur tracks as paleogeographic constraints: New scenarios for the Cretaceous geography of the Periadriatic region. *Ichnos*, **14**, p. 69 - 90.

PARRISH, J.T., ZIEGLER, A.M. and SCOTESE, C.R., 1982. Rainfall patterns and the distribution of coals and evaporite in the Mesozoic and Cenozoic. *Palaeogeography, Palaeoclimatology, Palaeoecology*, **40**, p. 67-101.

PATACCA, E. and SCANDONE, P., 2001. Late thrust propagation and sedimentary response in the thrust-belt-foredeep system of the southern Apennines (Pliocene-Pleistocene), *in* VAI, G.B. and MARTINI, I.P., eds., Anatomy of an Orogen: The Apennines and the adjacent Mediterranean basins, Kluwer Academic Publishers, p. 401-440.

PHILIP, J., 2003. Peri-Tethyan Neritic carbonate areas: Distribution through time and driving factors. *Palaeogeography, Palaeoclimatology, Palaeoecology*, **196**, p. 19-37.

PHILIP, J. and AIRAUD-CRUMIERE, C., 1991. The demise of the rudist bearing carbonate platforms at the Cenomanian/Turonian boundary: A global control. *Coral Reefs*, **10**, p. 115–125.

PIERI, P., FESTA, V., MORETTI, M. and TROPEANO, M., 1997. Quaternary tectonic activity of the Murge area (Apulian foreland, southern Italy). *Annals of Geophysics*, **40**, p. 1395-1404.

POSAMENTIER, H. and ALLEN, G.P., 1999. Siliciclastic sequence stratigraphy - concepts and applications. SEPM concepts in sedimentology and paleontology, 7: Tulsa, *Society for Sedimentary Geology*, 209 p.

PRAY, L.C. and STEHLI, E., 1962. Allochthonous origin, bone springs 'patch reefs', west Texas (abstract). *Geol. Soc. Am. Spec. Pap.*, **73**, p. 218-219.

RAILSBACK, L.B., 1993. Contrasting styles of chemical compaction in the upper Pennsylvanian Dennis Limestone in the Mid-continent region, USA. *Journal of Sedimentary Petrology*, **63**, p. 61-72.

READ, J.F. and PFEIL, R.W., 1983. Fabric of allochthonous reefal blocks, shady dolomite (lower to middle Cambrian) Virginian Appalachians. *Journal of Sedimentary Petrology*, **53**, p. 761-778.

RENDLE, R.H. and REIJMER, J.J.G., 2002. Quaternary slope development on the western, leeward margin of the Great Bahama Bank. *Mar. Geol.*, **185**, p. 143-164.

RICCHETTI, E., CIARANFI, N., LUPERTO SINNI, E., MONGELLI, F. and PIERI, P., 1988. Geodinamica ed evoluzione sedimentaria e tettonica dell'avampaese Apulo (reported by Bosellini *et.al.*, 1999). *Mem. Soc. Geol. It.*, **41**, p. 57-82.

RICHTER, D.K., GÖTTE, T., GÖTZE, J. and NEUSER, R.D., 2003. Progress in application of Cathodoluminescence (CL) in sedimentary petrology. *Mineralogy and Petrology*, **79**, p. 127-126.

RIGBY, J.K., 1958, Mass movement in Permian rocks at Trans-Pecos, Texas. *Journal of Sedimentary Petrology*, **28**, p. 298-315.

ROSALES, P.A., FERNANDEZ-MENIOLA, P.A. and GARCIA-MONDEJAR, J., 1994. Carbonate depositional sequence development on active fault blocks: The Albian in the Castro Urdiales area, northern Spain. *Sedimentology*, **41**, p. 861–882.

ROSSI, S. and BORSETTI, A.M., 1974. Dati preliminari di stratigrafia e di sismica del mare Ionio settentrionale (reported by Bosellini *et.al.*, 1999). *Mem. Soc. Geol. It.*, **13**, p. 251-259.

SACHPAZI, M., HIRN, A., CLÉMENT, C., HASLINGER, F., LAIGLE, M., KISSLING, E., CHARVIS, P., HELLO, Y., LÉPINE, J., SAPIN, M. and ANSORGE, J., 2000. Western Hellenic subduction and Cephalonia transform: Local earthquakes and plate transport and strain. *Tectonophysics*, **319**, p. 301-319.

SCHLAGER, W., 1991. Depositional bias and environmental change – important factors in sequence stratigraphy. *Sedimentary Geology*, **70**, p. 109-130.

SCHLAGER, W., 2005. Carbonate Sedimentology and Sequence Stratigraphy. *Concepts in Sedimentology and Paleontology, Society for Sedimentary Geology*, **8**, p. 200.

SCHLAGER, W., REIJMER, J.J.G. and DROXLER, A.W., 1994. Highstand Shedding of carbonate platforms. *Journal of Sedimentary Research*, **64**, p. 270-281.

SCHLÜTER, M., STEUBER, T. and PARENTE, M., 2008. Chronostratigraphy of Campaniane-Maastrichtian platform carbonates and rudist associations of Salento (Apulia, Italy). *Cretaceous Research*, **29**, p. 100-114.

SCHOLLE, P.A. and ULMER-SCHOLLE, D.S., 2003. A color guide to the petropgraphy of carbonate rocks. Tulsa, Oklahoma, *AAPG Bulletin*.

SHINER, P., BECCACINI, A. and MAZZOLI, S., 2004. Thin-skinned versus thick-skinned structural models for apulian carbonate reservoirs: Constraints from the Val d'Agri Fields, S Apennines, Italy. *Marine and Petroleum Geology*, **21**, p. 805-827.

SHINN, E.A. and ROBBIN, D.M., **1983**. Mechanical and chemical compaction in fine-grained shallow-water limestones. *Journal of Sedimentary Research*, **53**, p. 595-618.

SIMO, J.A., SCOTT, R.W. and MASSE, J.P., 1993. Cretaceous Carbonate Platforms. *AAPG Memoirs **56***, 1-14 p.

SINNI, E. and BORGOMANO, J.R.F., 1994. Stratigrafia del cretaceo superiore in facies di scarpata di Monte S. Angelo (promontorio del Gargano, Italia Meridionale) (reported by Borgomano, 2000). *Bollettino della Societa Geologica Italiana*, 113, p. 355-382.

SINNI, E.S. and MASSE, J.P., 1987. A platform to basin transition model: The lower Cretaceous carbonates of the Gargano Massif (southern Italy). *Mem. Soc. Geol. It.*, **40**, p. 99-108.

SPENCE, G.H. and TUCKER, M.E., 1997. Genesis of limestone megabreccias and their significance in carbonate sequence stratigraphic models: A review. *Sedimentary Geology*, **112**, p. 163-193.

SUAT BAGCI, A. and AKBAS, C.Y., 2007. Permeability estimation using hydraulic flow units in carbonate reservoirs. *SPE paper 107263*.

SULLIVAN, M.J., BELANGER, D.L., SKALINSKI, M.T., JENKINS, S.D. and DUNN, P., 2006. Permeability from production logs - method and application. *SPE paper 102894*.

SUN, Q.S., ESTEBAN, M., PURDY, E.G. and WILSON, J.L., 1998. Worldwide carbonate fields database (reported by Casabianca *et.al.*, 2002). *Carbonates International Report*, 4, p. 679-697 & Synthesis.

TIBERTI, M.M., ORLANDO, L., DI BUCCI, D., BERNABINI, M. and PAROTTO, M., 2005. Regional gravity anomaly map and crustal model of the central-southern Apennines (Italy). *Journal of Geodynamics*, **40**, p. 73-91.

TONDI, E., PICCARDI, L., CACON, S., KONTNY, B. and CELLO, G., 2005. Structural and time constraints for dextral shear along the seismogenic Mattinata fault (Gargano, southern Italy). *Journal of Geodynamics*, **40**, p. 134-152.

TUCKER, M.E., 1993. Carbonate diagenesis and sequence stratigraphy. *Sedimentology Review*, **1**, p. 51-72.

VINIEGRA, F. and CASTILLO-TEJERO, C., 1970. Golden Lane Fields, Veracruz, Mexico, *in* HALBOUTY, M.T., ed., Geology of Giant Petroleum Fields, *AAPG Memoirs*, p. 309-325.

VLAHOVIC, I., TISLJAR, J., VELIC, I. and MATICEC, D., 2005. Evolution of the Adriatic Carbonate Platform: Palaeogeography, main events and depositional dynamics. *Palaeogeography, Palaeoclimatology, Palaeoecology*, **220**, p. 333–360.

VON MORLOT, A., 1847. Ueber Dolomite and seine kuenstliche Darstellung aus Kalkstein. *Haidinger Natawiss Abhsndl*, **1**, p. 305-315.

WRIGHT, V.P. and BURCHETTE, T.P. 1996. Shallow-water carbonate environments, *in* READING, H.G., ed., Sedimentary environments: Processes, facies, stratigraphy. Oxford, *Blackwell*.

ZAPPATERRA, E., 1990. Carbonate paleogeographic sequences of the Periadriatic region. *Bollettino della Societa Geologica Italiana*, **109**, p. 5-20.

ZAPPATERRA, E., 1994. Source-rock distribution model of the Periadriatic region. *AAPG Bulletin*, **78**, p. 333-354.

ZOLOTUKHIN, A.B. and URSIN, J.R., 2000. Introduction to petroleum reservoir engineering. Kristiansand, *Norwegian Academic Press*.

APPENDIX

A1 METHODS

The present database of petrophysical measurements were derived from plug samples collected from the two outcrops; Malpasso Valley and Vico del Gargano quarry.

Poroperm values were obtained for the available plugs through standard laboratory methods. A selected number of plug samples were measured in-house, while the bulk of samples were measured externally, by Reslab AS.

The database of sample thin-sections was utilized in the estimation of porosity and permeability. For porosity estimation, the software Photoshop CS2™ by Adobe® was utilized. This software were also utilized for image enhancement.

For the estimation of permeability from porosity values, the two systems of Lucia (1983, 1995, 1999, 2007) and Lønøy (2006) where used. The system developed by Choquette & Pray (1970) was not utilized, although it is noted that this system is a widely used classification system, especially amongst petroleum geologists.

This section presents the technical description of the laboratory methods and estimation methods, as well as briefly introducing the evolution of the digital topography model and image enhancement methods.

POROSITY

A rock's porosity, or fluid-storage capacity, is the void part of the rock's total volume unoccupied by particles or cement. *Absolute porosity* is defined as the ratio of the total void volume, V_{Pa}, to the bulk volume V_B of a rock sample, irrespective of whether the voids are interconnected or not, while the *effective* porosity is defined as the ratio of the total volume of interconnected voids, V_P, to the bulk volume of the sample (equation A1.1) (*e.g.* Zolotukhin & Ursin, 2000).

$$\phi \overset{def}{=} \frac{V_{Pa}}{V_B} = \frac{V_B - V_M}{V_B}$$

Equation A1.1

V_{Pa} = Total pore volume
V_B = Bulk volume (total sample volume)
V_M = Matrix volume

IN-HOUSE POROSITY MEASUREMENTS

Porosity was measured on selected plug samples using the following method:

Plug samples weighed when dry and when saturated to 100 % brine saturation. The difference in weight yields the volume of pore space within the plug, when the density of the brine is known. Divided on the bulk volume of the sample (measured), the effective porosity is calculated (equation A1.1).

Uncertainties related to this method lies mainly in the weighing process, but also to some extent in the saturation of the samples.

Uncertainties lie in;

- Dimensions of plugs. Standard deviations and accuracies were available for plug dimension measuring-equipment.
- Weighing of plugs. Standard deviations and accuracies for equipment were available and are mapped.
- Vacuum-related uncertainties. The vacuum induced was sufficient, and minimizes this uncertainty factor.
- Saturation. A possibility exists that plugs may not have been 100% saturated with brine. Due to sufficient vacuum, this uncertainty factor was minimized.
- Plug sample irregularities. Some plugs were not evenly sided. This effect was noticeable, and must account for some uncertainty. However, techniques were used to overcome this uncertainty factor. Among these were the triple measuring of plug dimensions, using average values which should minimize this uncertainty factor.
- Large pores cut by plug wall. Some plugs displayed large pores and cavities that were cut by plug wall. The method relies on 100% saturation of plugs while weighing. Such large pores may not have capillary properties sufficient to withhold brine. A solution was developed, and plugs were wrapped in plastic tape to contain water. This solution is believed to minimize this uncertainty factor, but this still accounts for a large portion of the mapped uncertainty related to this method.

PERMEABILITY

The permeability of a porous medium is the medium's capability to transmit fluids through its network of interconnected pores. Permeability is thus related to the effective porosity (connected pores) of the porous medium and all factors affecting the latter will also affect the former.

Permeability may be regarded as a constant property of a porous medium only if the flow through the medium is of a single phase. This is the *absolute* permeability. However, when more than one fluid is introduced to the same medium, the *effective* permeability of each fluid will vary strongly with respect to its relative saturation. One fluid will hinder the free flow of the other fluid causing the effective permeability of the two to be drastically reduced compared to the absolute permeability. The ratio of a porous media's effective permeability to a particular fluid versus its absolute permeability is termed the *relative* permeability to that fluid.

$$q = -\frac{K \cdot A}{\mu}\frac{\Delta p}{\Delta x}$$

Note: The negative component of the original Darcy Equation serves mainly as a mathematical correction to the negative pressure gradient in the x-direction (*Δp drops as* Δx increases). For the purpose of this study, this formality is disregarded as the absolute value for Δp/Δx is used.

Equation A1.2
Darcy Equation in generalized form for linear, horizontal flow of an incompressible fluid.

q	Fluid flow rate [cm^3/s]
Δp	Pressure gradient across porous medium during flow [atm]
A	Cross-sectional area of the porous medium in the flow-transverse direction [cm^2]
Δx	Length of porous medium in flow-parallel direction [cm]
K	Absolute permeability [D]
μ	Viscosity [cp]

The permeability, *k*, appears in the Darcy equation as a proportionality coefficient rather than an established physical parameter. The quantitative definition of permeability as a physical unit can be derived by rearranging equation A1.2. This implies that a unit permeability is the permeability of a porous medium whose unit proportion, with a unit length (1 cm) and unit cross-sectional area (1 cm^2), is able to transmit – under a unit pressure differential (1 atm) – a fluid of a unit viscosity (1 cp) at a unit rate (1 cm^3/s). This permeability unit is termed *darcy* (1 D) and is generally referred to in millidarcies (mD).

KLINKENBERG EFFECT

A gas flowing at relatively low pressures through a porous medium tends to behave like an inviscid fluid, due to negligible friction against the pore-channel

walls. The flow velocity at the walls is non-zero and the bulk flow velocity is effectively higher than might be expected for a liquid or a high-pressure gas. This causes gas permeability at low mean pressures to display erroneously high values compared to the same sample's liquid (absolute) permeability. This phenomenon is known as the *Klinkenberg Effect* (Klinkenberg, 1941). The Darcy Equation assumes a Newtonian fluid behaviour, and the Klinkenberg Effect requires an appropriate correction to be made (Zolothukin & Ursin, 2000).

IN-HOUSE PERMEABILITY MEASUREMENTS

Permeability is defined through the Darcy equation, and the methods used to calculate this parameter relies on the fact that the flow-rate is a function of the pressure gradient (equation A1.2). In the setup used (fig A1.1), production-end pressure was kept constant at atmospheric pressure leaving only changes in injection-end pressure to define changes in the pressure gradient. The remaining parameters; permeability, viscosity, production-end pressure and plug length and area, were kept constant throughout the process. Flow-rates and corresponding pressure gradients were plotted, and a linear relationship was derived. The slope of this line represents the remaining parameters of the Darcy equation, and permeability was calculated based on three or more measurements for each plug sample.

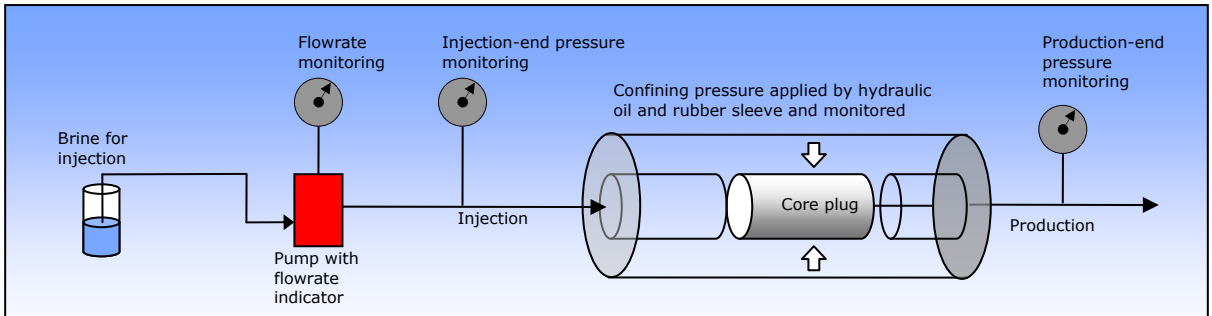

Figure A1.1 - In-house permeability measurement setup

Uncertainties lie in;

- Pump accuracy and flow-rate consistency throughout the process. This was measured separately for the pump used for these measurements, and measured flow rate showed no significant deviation from calculated flow rate.
- Pressure-control during permeability measurements. Standard deviations and accuracies were available for the equipment used for pressure-control.

- Plug lengths. Standard deviations and accuracies were available for plug dimension measuring-equipment.

Accuracy of in-house permeability measurements were approximately 5 %. For measurements and uncertainty calculations, see appendix 2.

EXTERNAL POROSITY AND PERMEABILITY MEASUREMENTS

Gas permeability was determined by flowing nitrogen gas through the samples at steady-state conditions, recording the flow rate and pressure drop over the sample. 20 Bar confinement pressure was applied. The gas permeability was corrected for the Klinkenberg effect (*see section A1.2.1.2*). For permeabilities below 2.0 mD, the following correction algorithm was used: $K = 0.68 \times Kn2^{1.06}$. For permeabilities above 2.0 mD, an iteration loop was used.

Uncertainties related to the porosity measurements were reported to be ± 0.5%. Uncertainties related to permeability measurements were reported to be max 5% in the 100 mD area, and somewhat higher in the areas below 1 mD.

The above information was provided by Olav Bryberg, Reslab AS, September 2007. Further information on the specifications of this method may be obtained by contacting Reslab AS.

ESTIMATION OF POROSITY

Porosity was estimated from epoxy-stained thin-sections using Adobe™ Photoshop CS2 on digital photos of the sections. High-resolution 2X magnification images using the Spot camera, as well as high-resolution scans of thin-sections were obtained. These digital images formed the basis for porosity estimation.

Visible pore-space was selected using the *magic wand* tool in combination with the *select similar* feature. The *histogram* tool gives the accurate number of pixels in the selected area. Divided by the total amount of pixels in the image an estimate of the pore area fraction is obtained. This was performed on each whole-sections scan. In addition, this method was performed on a number of 2X magnified sub-sections from each thin-section. These results were compared to the whole-section porosity. For permeability estimation, porosity estimations from whole-section scans were used where available, and mean values from 2X sub-sections were used where the former were unavailable.

ESTIMATION OF PERMEABILITY

Permeability was estimated using the systems developed by Lucia (1983, 1995, 1999, 2007) and Lønøy (2006). For the Lucia-system, interparticle porosity fraction was determined using porosity estimation methods and used for the prediction of permeability. For the Lønøy-system, measured values of porosity were utilized. For extended introductions to these systems, read the publications of Lønøy (2006) and Lucia (2007). See also chapters 3 and 4 of this study.

DIGITAL TOPOGRAPHY MODEL

Several photos were taken and digitally stitched together forming panorama overviews of different parts of the Vico del Gargano quarry outcrop from several different angles. GPS positions along with elevation data were recorded along the edges of the quarry using a handheld GPS. The points were imported to RMS as XYZ-data and used to create a framework for the topographic model. Additional points were manually digitized in Irap RMS using the GPS-measurements as a framework, to form the basis for mapping of the surface that forms the topographic model.

A surface was then draped across the altered set of XYZ-points, and further edited using the contour-editing feature in Irap RMS. The resulting topographic surface was compared with photos of the area until a sufficient correlation between the two was reached (fig A1.2A).

Based on the field work and photos, selected horizons were interpreted and plotted on the topographic surface as points. Figure A1.2B show one of these surfaces activated for demonstrational purposes.

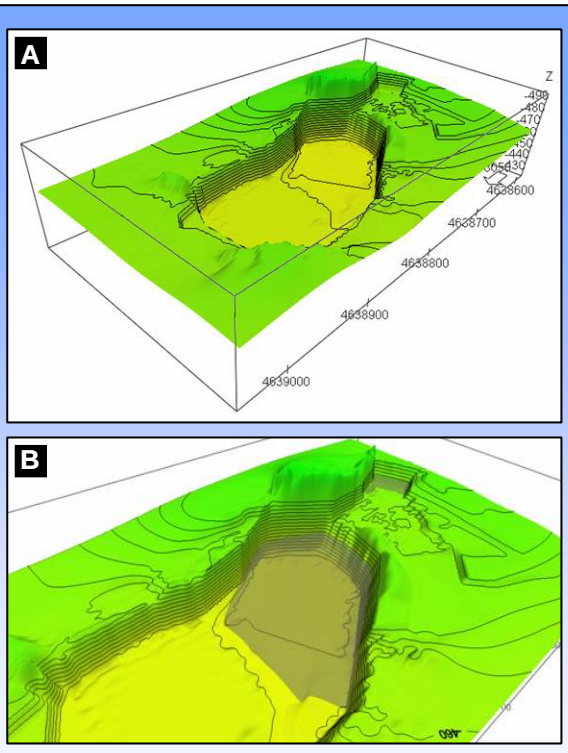

Figure A1.2 – Topographic model

Topographic model of Vico del Gargano quarry, screenshots from Irap RMS™.

A) Model overview looking SE.
B) One unit visualized (transparent grey surface).

IMAGE ENHANCEMENT

Image enhancement methods were developed and used on digital photos. The software used for the image enhancement was Photoshop™ CS2, by Adobe®.

An example is presented to visualize these methods (figure A1.3). The original image (A) display megabreccias on the eastern wall of the Malpasso Valley outcrop. Some clasts are visible as scattered slightly darker grey areas on the rock face.

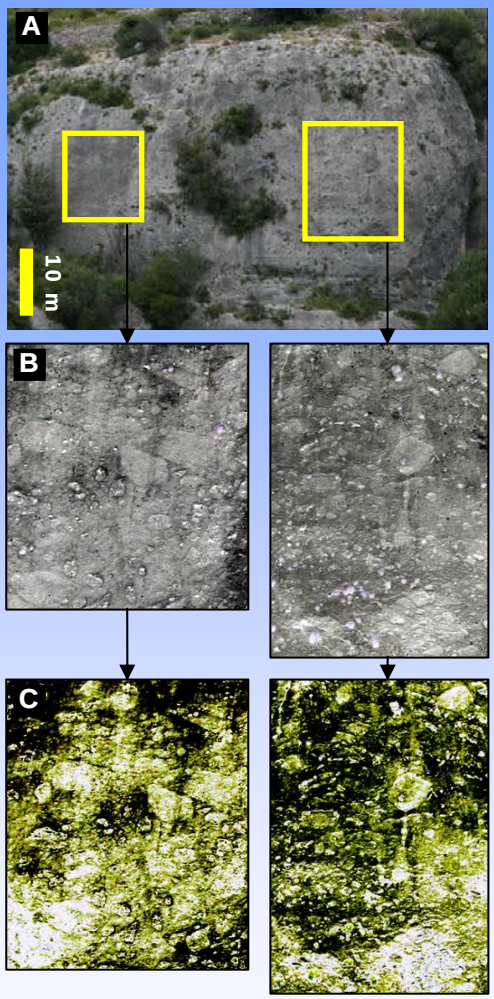

Figure A1.3 – Image enhancement

A) High resolution photo used for method development and description, from the eastern wall of the Malpasso Valley. Photo: Pr. Mike Talbot, UiB. Sections used for enhancement indicated.
B) Result after inverting and automatically adjusting levels and colours.
C) Result after adding colour gradient.

Although some clasts are visible prior to enhancement, it is evident that the image does not sufficiently exhibit the details of the complex geological deposit which it contains.

Inverting proved to be a valuable and simple method, turning dark areas light and vice versa. This method utilized an automated feature of the software and requires no advanced technical knowledge. This may also be applied using a number of other image-editing software. In the example displayed in figure A1.3B, levels, colours and contrast are automatically adjusted by the software to a best-fit of the contents. A further, and slightly more advanced method, is to adjust curves for each RGB channel to enhance contrasts in the image. A colour gradient may be added for increased visibility (figure A1.3C).

A2 IN-HOUSE LABORATORY MEASUREMENTS

Poroperm values from 26 samples were measured in-house using methods further described in appendix 1. This section presents selected highlights from the laboratory journal.

Tables A2.1 and A2.2 presents porosity and permeability measurements, respectively. Uncertainties are provided by equipment standards for measured values, and calculated based on these for calculated values. Reverse permeability was measured on selected plugs.

The following remarks correspond to remark-indications in both tables:

1) Length and diameter measurements were performed 3 times for irregular plugs, and mean length was used for further calculations.
2) Plastic tape was wrapped around plugs with large pores cut by plug wall, to prevent water from seeping out prior to weighing. Weight of tape is included in further calculations on those plugs, theoretically yielding slightly elevated uncertainties.
3) Flowrates provided by pump was ml/h. These values are re-calculated to Darcy-compatibility (ml/s).
4) Pressure provided by pressure-control equipment in bars. These values are re-calculated to Darcy-compatibility (atm).
5) Slope of linear trend based on pressure/flow-rate plots. See appendix 1 for further description of method.

POROSITY MEASUREMENTS

Table A2.1 – In-house porosity measurements. Laboratory journal.

	Plug dimensions						
Plug #	Length (measurements) [cm] [1)]	Length (mean) [cm]	Diameter (measurements) [cm] [1)]	Diameter (mean) [cm]	Flow area (short-end area) [cm^2]	Weight before saturation [g]	Weight before saturation including plastic [g] [2)]
45	5.09 ± 0.002	5.090 ± 0.010	3.69 ± 0.002	3.690 ± 0.010	10.694 ± 0.058	111.06 ± 0.01	N/A ± 0.01
63	5.09 ± 0.002	5.090 ± 0.010	3.69 ± 0.002	3.690 ± 0.010	10.694 ± 0.058	111.7 ± 0.01	N/A ± 0.01
82A	4.174 ± 0.002 4.056 ± 0.002 4.094 ± 0.002	4.108 ± 0.068	3.996 ± 0.002 4.022 ± 0.002 4.051 ± 0.002	4.023 ± 0.032	12.711 ± 0.201	114.10 ± 0.01	N/A ± 0.01
82B	4.298 ± 0.002 4.3 ± 0.002 4.254 ± 0.002	4.284 ± 0.027	4.021 ± 0.002 4.029 ± 0.002 4.058 ± 0.002	4.036 ± 0.021	12.794 ± 0.135	114.66 ± 0.01	N/A ± 0.01
83	7.646 ± 0.002 7.734 ± 0.002 7.688 ± 0.002	7.689 ± 0.051	4.917 ± 0.002 4.935 ± 0.002 4.911 ± 0.002	4.921 ± 0.014	19.019 ± 0.107	306.79 ± 0.01	308.05 ± 0.01
100A	2.496 ± 0.002 2.545 ± 0.002 2.528 ± 0.002	2.523 ± 0.028	3.716 ± 0.002 3.758 ± 0.002 3.765 ± 0.002	3.746 ± 0.028	11.023 ± 0.166	58.48 ± 0.01	58.72 ± 0.01
100B	4.718 ± 0.002 4.7 ± 0.002 4.686 ± 0.002	4.701 ± 0.018	3.744 ± 0.002 3.766 ± 0.002 3.75 ± 0.002	3.753 ± 0.013	11.064 ± 0.075	109.25 ± 0.01	109.66 ± 0.01
101A	2.514 ± 0.002 2.489 ± 0.002 2.495 ± 0.002	2.499 ± 0.014	3.725 ± 0.002 3.745 ± 0.002 3.735 ± 0.002	3.735 ± 0.012	10.956 ± 0.068	60.39 ± 0.01	60.69 ± 0.01
101B	6.835 ± 0.002 6.824 ± 0.002 6.822 ± 0.002	6.827 ± 0.008	3.746 ± 0.002 3.76 ± 0.002 3.72 ± 0.002	3.742 ± 0.023	10.998 ± 0.136	167.92 ± 0.01	168.68 ± 0.01
102	6.800 ± 0.002 6.831 ± 0.002 6.815 ± 0.002	6.815 ± 0.018	3.766 ± 0.002 3.739 ± 0.002 3.746 ± 0.002	3.750 ± 0.016	11.047 ± 0.092	161.27 ± 0.01	162.21 ± 0.01
105A	2.72 ± 0.002 2.636 ± 0.002 2.628 ± 0.002	2.661 ± 0.053	3.728 ± 0.002 3.728 ± 0.002 3.73 ± 0.002	3.729 ± 0.001	10.919 ± 0.007	61.25 ± 0.01	61.55 ± 0.01
105B	6.148 ± 0.002 6.124 ± 0.002 6.14 ± 0.002	6.137 ± 0.014	3.726 ± 0.002 3.744 ± 0.002 3.746 ± 0.002	3.739 ± 0.012	10.978 ± 0.068	151.26 ± 0.01	151.97 ± 0.01
106A	2.082 ± 0.002 2.09 ± 0.002 2.111 ± 0.002	2.094 ± 0.017	3.752 ± 0.002 3.734 ± 0.002 3.726 ± 0.002	3.737 ± 0.015	10.970 ± 0.088	52.55 ± 0.01	52.73 ± 0.01
106B	5.166 ± 0.002 5.09 ± 0.002 5.084 ± 0.002	5.113 ± 0.047	3.734 ± 0.002 3.724 ± 0.002 3.734 ± 0.002	3.731 ± 0.006	10.931 ± 0.034	128.41 ± 0.01	128.76 ± 0.01
108A	2.138 ± 0.002 2.122 ± 0.002 2.13 ± 0.002	2.130 ± 0.009	3.721 ± 0.002 3.758 ± 0.002 3.766 ± 0.002	3.748 ± 0.026	11.035 ± 0.153	47.95 ± 0.01	N/A ± 0.01
108B	5.082 ± 0.002 5.032 ± 0.002 4.98 ± 0.002	5.031 ± 0.059	3.714 ± 0.002 3.726 ± 0.002 3.739 ± 0.002	3.726 ± 0.014	10.906 ± 0.084	110.59 ± 0.01	111.16 ± 0.01
112A	4.622 ± 0.002 4.594 ± 0.002 4.59 ± 0.002	4.602 ± 0.018	3.73 ± 0.002 3.724 ± 0.002 3.748 ± 0.002	3.734 ± 0.014	10.951 ± 0.081	112.94 ± 0.01	N/A ± 0.01
112B	5.952 ± 0.002 5.96 ± 0.002 5.982 ± 0.002	5.965 ± 0.017	3.754 ± 0.002 3.76 ± 0.002 3.748 ± 0.002	3.754 ± 0.007	11.068 ± 0.041	147.38 ± 0.01	N/A ± 0.01
318	6.128 ± 0.002 6.189 ± 0.002 6.100 ± 0.002	6.139 ± 0.051	3.772 ± 0.002 3.768 ± 0.002 3.783 ± 0.002	3.774 ± 0.009	11.188 ± 0.051	148.79 ± 0.01	149.21 ± 0.01
326	7.995 ± 0.002 7.971 ± 0.002 7.972 ± 0.002	7.979 ± 0.014	3.780 ± 0.002 3.751 ± 0.002 3.748 ± 0.002	3.760 ± 0.018	11.102 ± 0.109	218.9 ± 0.01	219.77 ± 0.01
328	5.618 ± 0.002 5.590 ± 0.002 5.608 ± 0.002	5.605 ± 0.016	3.776 ± 0.002 3.734 ± 0.002 3.760 ± 0.002	3.757 ± 0.024	11.084 ± 0.143	157.7 ± 0.01	N/A ± 0.01
341	6.660 ± 0.002 6.626 ± 0.002 6.654 ± 0.002	6.647 ± 0.020	3.770 ± 0.002 3.780 ± 0.002 3.776 ± 0.002	3.775 ± 0.006	11.194 ± 0.034	193.26 ± 0.01	N/A ± 0.01
343	8.348 ± 0.002 8.350 ± 0.002 8.352 ± 0.002	8.350 ± 0.002	3.764 ± 0.002 3.790 ± 0.002 3.762 ± 0.002	3.772 ± 0.016	11.175 ± 0.096	207.22 ± 0.01	208.15 ± 0.01
353A	4.772 ± 0.002 4.772 ± 0.002 4.748 ± 0.002	4.764 ± 0.014	3.744 ± 0.002 3.766 ± 0.002 3.726 ± 0.002	3.745 ± 0.023	11.017 ± 0.136	119.08 ± 0.01	N/A ± 0.01
353B	5.321 ± 0.002 5.336 ± 0.002 5.3 ± 0.002	5.319 ± 0.021	3.776 ± 0.002 3.754 ± 0.002 3.79 ± 0.002	3.773 ± 0.021	11.183 ± 0.123	163.73 ± 0.01	164.46 ± 0.01
354	4.03 ± 0.002 4.045 ± 0.002 4.049 ± 0.002	4.041 ± 0.011	3.779 ± 0.002 3.73 ± 0.002 3.76 ± 0.002	3.756 ± 0.028	11.082 ± 0.167	92.93 ± 0.01	N/A ± 0.01

→ **Table A2.1 (continued)**

	Weighing (continued)		*Volumes*			*Results*
Plug #	Weight after saturation [g]	Weight, injected water [g]	Volume, injected water [cm^3]	Bulk Volume [cm^3]	Pore volume [cm^3]	Effective porosity [%]
45	122.73 ± 0.01	11.67 ± 0.02	11.11 ± 0.02	54.43 ± 0.13	11.11 ± 0.02	**20.42 % ± 0.06 %**
63	123.94 ± 0.01	12.24 ± 0.02	11.66 ± 0.02	54.43 ± 0.13	11.66 ± 0.02	**21.42 % ± 0.06 %**
82A	124.28 ± 0.01	10.18 ± 0.02	9.70 ± 0.02	52.22 ± 0.89	9.70 ± 0.02	**18.57 % ± 0.32 %**
82B	126.95 ± 0.01	12.29 ± 0.02	11.70 ± 0.02	54.81 ± 0.37	11.70 ± 0.02	**21.36 % ± 0.15 %**
83	324.65 ± 0.01	16.6 ± 0.02	15.81 ± 0.02	146.25 ± 0.99	15.81 ± 0.02	**10.81 % ± 0.07 %**
100A	65.26 ± 0.01	6.54 ± 0.02	6.23 ± 0.02	27.81 ± 0.33	6.23 ± 0.02	**22.40 % ± 0.27 %**
100B	121.79 ± 0.01	12.13 ± 0.02	11.55 ± 0.02	52.02 ± 0.22	11.55 ± 0.02	**22.21 % ± 0.10 %**
101A	66 ± 0.01	5.31 ± 0.02	5.06 ± 0.02	27.38 ± 0.16	5.06 ± 0.02	**18.47 % ± 0.13 %**
101B	182.58 ± 0.01	13.9 ± 0.02	13.24 ± 0.02	75.08 ± 0.25	13.24 ± 0.02	**17.63 % ± 0.06 %**
102	179.23 ± 0.01	17.02 ± 0.02	16.21 ± 0.02	75.29 ± 0.25	16.21 ± 0.02	**21.53 % ± 0.08 %**
105A	68.74 ± 0.01	7.19 ± 0.02	6.85 ± 0.02	29.06 ± 0.58	6.85 ± 0.02	**23.56 % ± 0.48 %**
105B	164.41 ± 0.01	12.44 ± 0.02	11.85 ± 0.02	67.38 ± 0.18	11.85 ± 0.02	**17.58 % ± 0.06 %**
106A	56.44 ± 0.01	3.71 ± 0.02	3.53 ± 0.02	22.98 ± 0.19	3.53 ± 0.02	**15.38 % ± 0.15 %**
106B	137.38 ± 0.01	8.62 ± 0.02	8.21 ± 0.02	55.89 ± 0.52	8.21 ± 0.02	**14.69 % ± 0.14 %**
108A	53.55 ± 0.01	5.60 ± 0.02	5.33 ± 0.02	23.50 ± 0.13	5.33 ± 0.02	**22.69 % ± 0.15 %**
108B	126.46 ± 0.01	15.87 ± 0.02	15.11 ± 0.02	54.87 ± 0.65	15.11 ± 0.02	**27.55 % ± 0.33 %**
112A	121.87 ± 0.01	8.93 ± 0.02	8.50 ± 0.02	50.39 ± 0.22	8.50 ± 0.02	**16.88 % ± 0.08 %**
112B	158.88 ± 0.01	11.50 ± 0.02	10.95 ± 0.02	66.02 ± 0.20	10.95 ± 0.02	**16.59 % ± 0.06 %**
318	163.52 ± 0.01	14.31 ± 0.02	13.63 ± 0.02	68.69 ± 0.58	13.63 ± 0.02	**19.84 % ± 0.17 %**
326	227.44 ± 0.01	7.67 ± 0.02	7.30 ± 0.02	88.58 ± 0.27	7.30 ± 0.02	**8.25 % ± 0.03 %**
328	161.66 ± 0.01	3.96 ± 0.02	3.77 ± 0.02	62.13 ± 0.27	3.77 ± 0.02	**6.07 % ± 0.04 %**
341	196.03 ± 0.01	2.77 ± 0.02	2.64 ± 0.02	74.41 ± 0.23	2.64 ± 0.02	**3.55 % ± 0.03 %**
343	225.45 ± 0.01	17.3 ± 0.02	16.48 ± 0.02	93.31 ± 0.20	16.48 ± 0.02	**17.66 % ± 0.04 %**
353A	127.37 ± 0.01	8.29 ± 0.02	7.90 ± 0.02	52.49 ± 0.22	7.90 ± 0.02	**15.04 % ± 0.07 %**
353B	175.56 ± 0.01	11.1 ± 0.02	10.57 ± 0.02	59.48 ± 0.28	10.57 ± 0.02	**17.77 % ± 0.09 %**
354	103.07 ± 0.01	10.14 ± 0.02	9.66 ± 0.02	44.79 ± 0.21	9.66 ± 0.02	**21.56 % ± 0.11 %**

PERMEABILITY MEASUREMENTS

Table A2.2 – In-house permeability measurements

	Measured values for Darcy input				*Result*	*Reverse permeability measurements*		
Plug #	Pump flowrate [ml/h]	Darcy flowrate [ml/s] [3]	Injection-end pressure [atm] [4]	Slope [unit-less] [5]	**Absolute permeability [mD]**	Darcy flowrate [ml/s] [3]	Injection-end pressure [atm] [4]	Absolute reverse permeability [mD]
45	150	0.042 ± 0.001	2.17 ± 0.02					
	300	0.083 ± 0.001	3.82 ± 0.02					
	400	0.111 ± 0.001	4.97 ± 0.02	0.0248	**12.9 ± 0.6**			
63	150	0.042 ± 0.001	1.03 ± 0.02					
	350	0.097 ± 0.001	2.18 ± 0.02					
	450	0.125 ± 0.001	2.84 ± 0.02	0.0461	**23.9 ± 1.2**			
83	50	0.014 ± 0.001	6.18 ± 0.02					
	75	0.021 ± 0.001	9.10 ± 0.02					
	100	0.028 ± 0.001	13.38 ± 0.02	0.0019	**0.8 ± 0.2**			
100A	100	0.028 ± 0.001	1.97 ± 0.02					
	200	0.056 ± 0.001	3.73 ± 0.02					
	300	0.083 ± 0.001	5.61 ± 0.02	0.0153	**3.8 ± 0.3**			
100B	100	0.028 ± 0.001	1.35 ± 0.02					
	200	0.056 ± 0.001	2.34 ± 0.02					
	300	0.083 ± 0.001	3.36 ± 0.02	0.0277	**12.8 ± 0.8**			
101B	100	0.028 ± 0.001	2.38 ± 0.02			0.028 ± 0.001	2.94 ± 0.02	
	150	0.042 ± 0.001	3.54 ± 0.02			0.042 ± 0.001	4.19 ± 0.02	
	200	0.056 ± 0.001	4.74 ± 0.02	0.0118	**8.0 ± 0.8**	0.056 ± 0.001	5.37 ± 0.02	7.7 ± 0.8
105A	200	0.056 ± 0.001	0.72 ± 0.02					
	300	0.083 ± 0.001	1.09 ± 0.02					
	400	0.111 ± 0.001	1.38 ± 0.02	0.0837	**22.2 ± 2.1**			
105B	100	0.028 ± 0.001	5.79 ± 0.02			0.028 ± 0.001	7.30 ± 0.02	
	150	0.042 ± 0.001	8.64 ± 0.02			0.042 ± 0.001	10.37 ± 0.02	
	200	0.056 ± 0.001	11.94 ± 0.02	0.0045	**2.7 ± 0.3**	0.056 ± 0.001	13.84 ± 0.02	2.6 ± 0.3
106A	50	0.014 ± 0.001	8.54 ± 0.02					
	75	0.021 ± 0.001	12.68 ± 0.02					
	100	0.028 ± 0.001	17.29 ± 0.02	0.0016	**0.3 ± 0.1**			
108B	100	0.028 ± 0.001	0.40 ± 0.02			0.028 ± 0.001	0.43 ± 0.02	
	250	0.069 ± 0.001	0.96 ± 0.02			0.069 ± 0.001	1.05 ± 0.02	
	490	0.136 ± 0.001	1.87 ± 0.02	0.0741	**37.3 ± 2.6**	0.136 ± 0.001	2.03 ± 0.02	34.3 ± 2.5
112A	50	0.014 ± 0.001	4.36 ± 0.02			0.014 ± 0.001	4.01 ± 0.02	
	100	0.028 ± 0.001	8.63 ± 0.02			0.028 ± 0.001	8.25 ± 0.02	
	150	0.042 ± 0.001	12.53 ± 0.02	0.0034	**1.6 ± 0.2**	0.042 ± 0.001	12.49 ± 0.02	1.5 ± 0.2
112B	100	0.028 ± 0.001	1.92 ± 0.02			0.028 ± 0.001	2.28 ± 0.02	
	150	0.042 ± 0.001	2.86 ± 0.02			0.042 ± 0.001	3.33 ± 0.02	
	200	0.056 ± 0.001	3.87 ± 0.02	0.0143	**8.4 ± 0.8**	0.056 ± 0.001	4.36 ± 0.02	7.9 ± 0.8
318	10	0.003 ± 0.001	8.96 ± 0.02					
	15	0.004 ± 0.001	10.24 ± 0.02					
	20	0.006 ± 0.001	13.92 ± 0.02	0.0005	**0.3 ± 0.2**			
326	20	0.006 ± 0.001	10.83 ± 0.02					
	25	0.007 ± 0.001	14.80 ± 0.02					
	30	0.008 ± 0.001	17.17 ± 0.02	0.0004	**0.3 ± 0.2**			
328	5	0.001 ± 0.001	8.11 ± 0.02					
	12	0.003 ± 0.001	17.02 ± 0.02					
	9	0.003 ± 0.001	13.38 ± 0.02	0.0002	**0.1 ± 0.2**			
343	100	0.028 ± 0.001	3.53 ± 0.02					
	150	0.042 ± 0.001	5.49 ± 0.02					
	220	0.061 ± 0.001	8.39 ± 0.02	0.0069	**5.6 ± 0.5**			
353A	25	0.007 ± 0.001	4.69 ± 0.02					
	50	0.014 ± 0.001	9.75 ± 0.02					
	75	0.021 ± 0.001	14.63 ± 0.02	0.0014	**0.7 ± 0.2**			
353B	150	0.042 ± 0.001	3.11 ± 0.02			0.042 ± 0.001	6.38 ± 0.02	
	200	0.056 ± 0.001	5.01 ± 0.02			0.056 ± 0.001	8.57 ± 0.02	
	250	0.070 ± 0.001	6.12 ± 0.02	0.0090	**4.7 ± 0.5**	0.070 ± 0.001	9.32 ± 0.02	4.5 ± 0.5
354	300	0.083 ± 0.001	0.22 ± 0.02					
	400	0.111 ± 0.001	0.27 ± 0.02					
	490	0.136 ± 0.001	0.33 ± 0.02	0.4840	**192.4 ± 37.4**			

FIXED VALUES AND FORMULAS

Brine density (ρ_{brine}): 1.05 g/cm^3

Brine viscosity (μ_{brine}): 1.09 cp

Darcy and porosity equations are presented in Appendix 1.

Equation A2.1 was used to calculate uncertainties in permeability measurements.

Equation A2.1: Absolute permeability uncertainty

$$\Delta k_{abs} = \sqrt{\left(\frac{\mu_{brine} L}{A \Delta P} \Delta q\right)^2 + \left(\frac{\mu_{brine} q}{A \Delta P} \Delta L\right)^2 + \left(\frac{q \mu_{brine} L}{A^2 \Delta P} \Delta A\right)^2 + \left(\frac{q \mu_{brine} L}{A P^2} \Delta(\Delta P)\right)^2}$$

A3 LIMITATIONS AND SUGGESTIONS FOR FUTURE CONTRIBUTIONS

Some limitations that have acted on this study should be addressed and accounted for. Firstly, the database from which the presented results are derived is not sufficiently large enough to produce reliable results in terms of petrophysical and sedimentological data. Secondly, this study, along with other similar studies, also suffers from the strict time-restraints that are put upon master-theses submissions. Thirdly, the thin-sections that were produced for the purpose of this study were severely delayed and displayed low qualities. These thin-sections were vital components of the present database, and errors related to thin-section qualities have impacted on the final results.

The time restraints also introduce limitations in relations to the combination of sedimentology and petroleum engineering that is attempted in this study. Ideally, all samples in the present database should be measured using both described laboratory methods and subsequently more efforts should be put into the method comparison, as it is assumed that method-related factor have impacts on the results. However, inasmuch as petroleum engineering and petroleum geology are related, and should be combined, in terms of hydrocarbon exploration and –production, master studies generally do not span these two areas. An important feature is the wettability of the samples, which in turn control secondary vital parameters such as relative permeability. The samples in the present dataset origin from outcrops, and they are assumed to be strongly water-wet by the effect of exposure. Most carbonate reservoirs are, on the contrary, oil-wet and this may have important impacts on the flow of hydrocarbons through these rocks.

The investigation of structural geology, fracturing and their relations to fluid flow facilitation should also be addressed. These areas have not been investigated for the purpose of the present study.

This study probably raises more questions than it answers, spanning from uncertainties related to the depositional environment and histories to uncertainties in petrophysical properties and the measurements and estimations of the former. It is evident that reliability of the results would benefit from the expansion of the database and this should be stressed by future contributors. Some suggestions for future contributions are proposed here:

Additional localities should be investigated and sampled to contribute to the variety and size of the dataset. The apparent differences in terms of depositional mechanism, sequence stratigraphy and petrophysical properties should be explored through the expansion of the database and incorporation of additional localities. The paleogeographic situation of these deposits is unclear, and the presence of clast-supported megabreccias in the Vico del Gargano area raises the need for a re-evaluation of the Cenomanian paleogeography with respect to the eastern margin of the Apulian Platform as it appears on the northern Gargano. For reservoir exploration and field-development related scenarios, the detailed mapping of the margin relative to the slope deposits is important as reefs and shoals of the margin may represent the main reservoir while slope-deposits in many cases are explored as potential secondary discoveries. The expansion of the present database may form the foundation for reservoir modelling of megabreccia-bearing slope deposits, which may contribute to the overall understanding of these deposits. Also, the effect of lithoclasts on formation evaluation well-logging signals should be explored and modelled in order to predict the log-responses that may be related to such reservoirs.

On the petroleum engineering side, further investigation of the plug samples that make up the present dataset should be undertaken in order to map important petrophysical properties related to wettability and saturation-profiles. The mapping of poretypes and porosity-relations may also be further investigated using more advanced methods such as MR-scanning.

On the geophysical side, the mapping of velocities and synthetic seismic modelling of the Monte Sant’Angelo Megabreccias may contribute to the increased understanding of the response of such deposits and their appearance on seismic data.